AD669440

RESEARCH REPORT
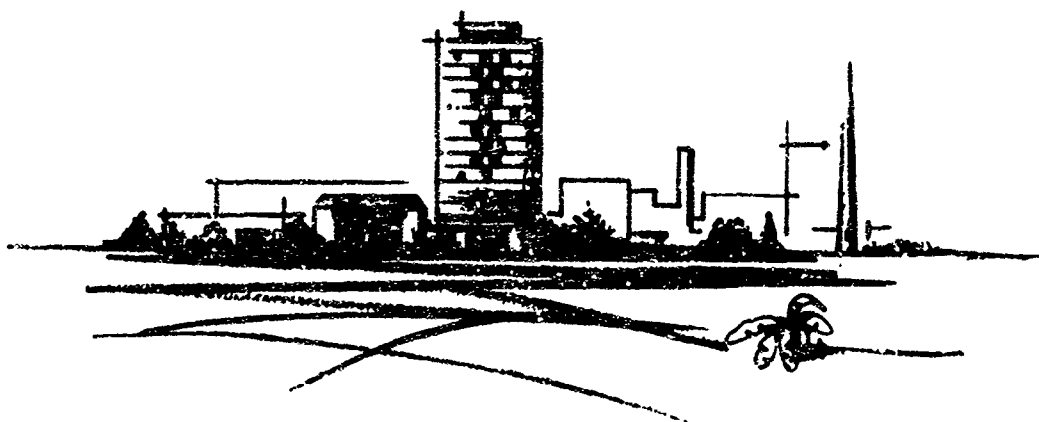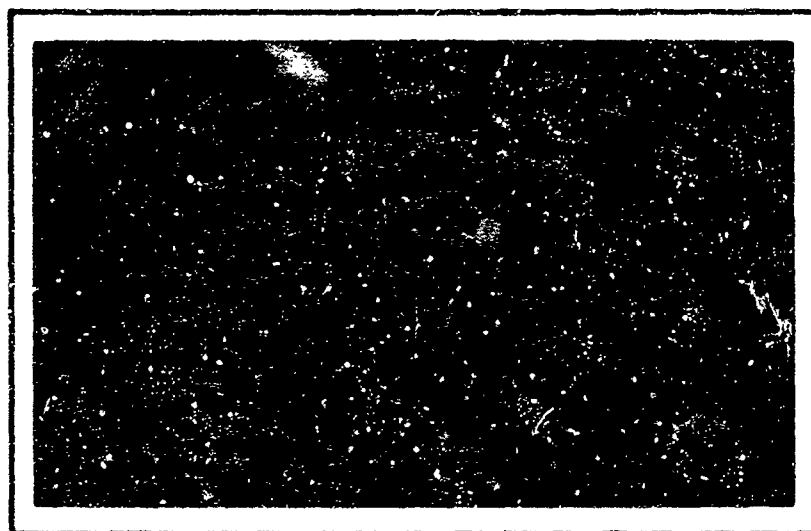
BATTELLE MEMORIAL INSTITUTE

COLUMBUS LABORATORIES

D D C

MAY 29 1968

RECEIVED

C
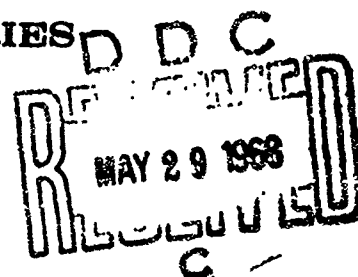
132

SUMMARY REPORT

on

SPALL FRACTURE AND DYNAMIC
RESPONSE OF MATERIALS

Contract No. DA-49-083 OSA-3176

Report No. BAT-197A-4-3

March 21, 1968

J. H. Oscarson
K. F. Graff

Sponsored by

Advanced Research Projects Agency
ARPA Order No. 197

BATTELLE MEMORIAL INSTITUTE
Columbus Laboratories
505 King Avenue
Columbus, Ohio 43201

Battelle-DEFENDER

May 21, 1968

Director
Advanced Research Projects Agency
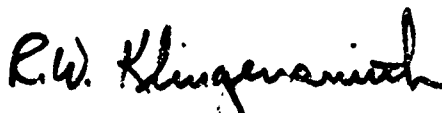The Pentagon
Washington, D.C.   20301

Attention Capt. H. H. Ward, III (USN)
           Room 3D 155

Dear Sir:

Enclosed are three copies of the unclassified report entitled
"Spall Fracture and Dynamic Response of Materials", BAT-197A-4-3,
prepared by J. H. Oscarson and K. F. Graff. This report is a review of
the literature relating to spall fracture phenomena and includes a
discussion of material response to shock loading. The report was pre-
pared as part of the spall study initiated under Task 4 of the Battelle
DEFENDER project, Contract No. DA-49-083 OSA-3176, ARPA Order No. 197.

We will welcome any comments or questions regarding this study.

Very truly yours,

R. W. Klingensmith
Project Director
Battelle-DEFENDER

RWK:lls

Enclosures

cc: Mr. C. E. McLain (3)
     Mr. F. A. Koether (1)

ACKNOWLEDGMENT

ABSTRACT

        A review of the literature on spall fracture and dynamic response of
materials is presented. Current theories underlying large amplitude wave prop-
agation and spall fracture under conditions of uniaxial strain are described in
detail. Relevant features of elastic, plastic, and shock wave phenomena are
reviewed, and the effects of subsidiary properties on the material response are
considered, including strain rate, temperature, finite strain, work hardening,
and the Bauschinger effect.

TABLE OF CONTENTS

LIST OF FIGURES

LIST OF FIGURES
(Continued)

LIST OF FIGURES
(Continued)

SPALL FRACTURE AND DYNAMIC RESPONSE OF MATERIALS

by

J. H. Oscarson
K. F. Graff

INTRODUCTION

This report presents a review of the literature on spall fracture and dynamic response of materials. Since the purpose of the review is to provide background and direction for an experimental and analytical spall study presently being conducted at Battelle-Columbus Laboratories (BCL), the greatest emphasis is given to those topics most closely related to this study. With this constraint, most of the subject matter will be devoted to a detailed description of the current theories underlying large amplitude wave propagation and spall fracture under conditions of uniaxial strain.

Fundamental to the study of spallation phenomena is the determination of stress history at the spall plane. However, the stress condition in the interior of the material cannot be measured directly, but must be inferred from measurements of free surface motions of the target material and solution of the stress wave propagation problem. It is necessary, as a prelude to solution of the stress wave problem, to know the dynamic properties of the material—that is, the constitutive relation of the material.

The purpose of the appendices is to review the relevant features of elastic, plastic, and shock wave phenomena. Prime attention is directed to a review of elastic-plastic stress wave theory with the intent of relating experimental measurements of rear surface motion to the gross features of the interior stress history. It will be found, however, that the detailed analysis of the stress history is too complex for simple analysis and must await computer investigation.

The effects of a number of subsidiary properties on the material response will also be considered. These will include the effects of strain rate, temperature, finite strain, work hardening, and the Bauschinger effect. Some assessment of these effects is necessary if the spall study data are to be interpreted unobscured by unknown complexities of material response.

Unfortunately, detailed knowledge of dynamic material properties is scant, so that it is only possible to estimate the consequences of a number of the material effects. It shoul. be noted that dynamic material properties is currently the subject of intense research.

The early time response of a plate subjected to lateral impulsive loading takes the form of a compressive dilatational stress wave propagating through the thickness. If the induced stresses are greater than the elastic limit of the material, the peak stress of the wave will be attained and propagate behind a higher velocity elastic precursor wave. Thus, at the strain rates of interest $(10^6 - 10^7/\text{sec})$, the unstressed material will first experience an almost instantaneous rise to the stress corresponding to the elastic limit. It will remain at this stress for some finite time, and then experience another rapid rise to the peak stress. Details of the unloading will depend in large part on how the impulsive load was generated, i.e., contact explosive or flying plate impact.

When the front of the waveform reaches the stress-free rear surface of the plate, it reflects as a tensile wave and propagates into the compressed material associated with that part of the wave which has yet to be reflected. If the total duration of the incoming compressive pulse is sufficiently short, there will be a plane at some finite distance from, and parallel to, the rear surface, for which the net stress first becomes tensile. (Here, net stress refers to the sum of the compressive stress associated with the incoming wave and the tensile stress associated with the reflected wave.) If the stress and pulse duration are sufficiently large, the material may fracture (spall) at or near this plane. Appendices A, B, C, D, and E describe all the events leading up to conditions sufficient for spall.

"General Physical Features of Plastic Flow and Fracture" provides a brief and very elementary review of the physics and mechanics of flow and fracture from a primarily micromechanical point of view. It is included in this report so that those readers unfamiliar with these concepts might acquire some background for the topics discussed in subsequent sections.

"Spall" is a detailed statement of the current knowledge regarding spall fracture. This includes a discussion of the factors affecting spall, as well as the means by which these factors and their effects are used to predict spall.

The final section is a brief summary of conclusions drawn from the review of literature on spall.

Appendices A, B, C, D, and E present a detailed discussion of large amplitude wave propagation and constitutive relations of materials, the major emphasis being given to metals.

DISCUSSION

General Physical Features of Plastic
Flow and Fracture

Observations generally descriptive of material behavior in standard
tensile or compressive tests (i.e., quasi-static loading and uniaxial stress
states) are sufficiently numerous and well-developed to serve as a background
for understanding the physical nature of stress wave propagation and spallation
in uniaxial strain. Furthermore, the existence and operation of many of the
basic mechanisms are only quantitatively modified by changes in loading condi-
tions. Thus, before proceeding to detailed discussions on material response and
spall, a brief review of the essential physical features of flow and fracture
appears to be in order.

Physics and Mechanics of Plastic Flow

Composition of Metals. Metallic elements consist of atoms in an
ordered arrangement, called a lattice, at equilibrium under their mutual forces.
Typical crystallographic arrangements are body-centered cubic (BCC) and face-
centered cubic (FCC) as shown in Figure 1.

FCC   BCC   (DF 193)
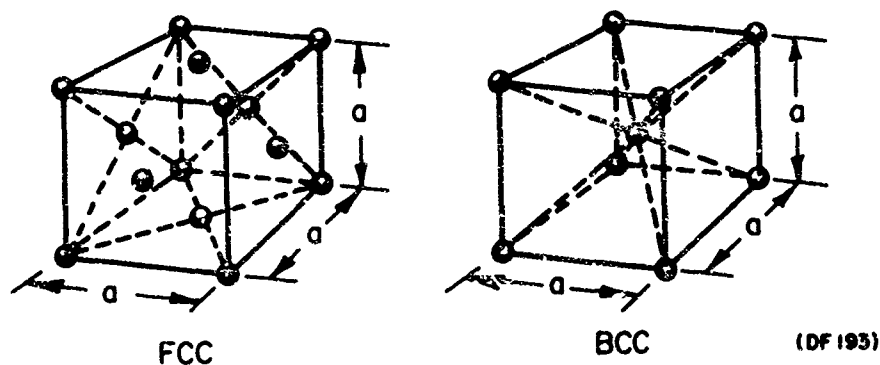
FIGURE 1.   BODY-CENTERED AND FACE-CENTERED LATTICE
            ARRANGEMENTS

These figures represent only a small portion of the total possible lattice arrangements. However, over 70 percent of metals and alloys crystallize in the above or in a hexagonal system.

A pure and perfect metallic specimen would consist of an uninterrupted repetition of the particular lattice arrangement of the metal. However, typically, as a liquid metal solidifies from a melt, a variety of defects are formed. The simplest defect, called a vacancy, occurs when an atom is missing from the lattice. An extra atom wedged in the lattice between the normal atomic sites may also occur; this is termed an interstitial atom. Impurity atoms may replace a regular lattice atom or be accommodated within the lattice as an interstitial impurity. Such defects, involving only one atom, are called point defects. Line defects are the next level of lattice imperfection. The incomplete translation of one part of the lattice relative to the other, designated as a dislocation, is an example.

Surface defects within the crystal may also exist. Thus, across a surface defect, the crystal structure may undergo a change of orientation. An example would be the boundary which occurs when the crystallographic structure forms a mirror image of itself as shown in Figure 2.

As a metal solidifies from a melt, crystals grow from many nuclei on cooling so that the resultant solid consists of many grains of metal, each grain composed of the crystal lattice. Since the grains will be misoriented relative to one another, grain boundaries are formed where some compromise of lattice
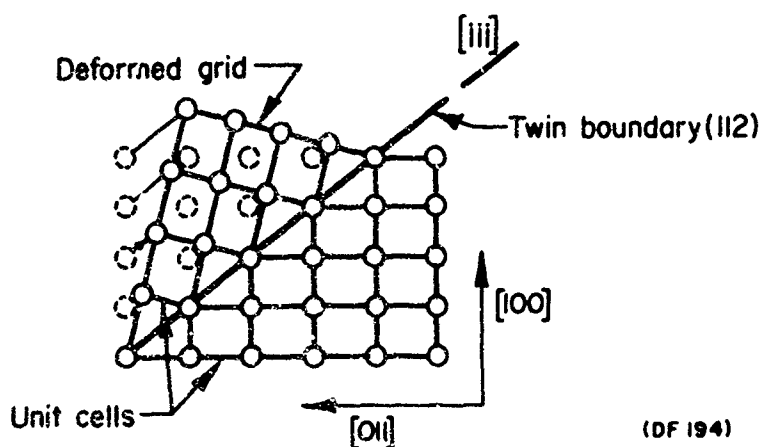
FIGURE 2. TWIN BOUNDARY WITHIN A CRYSTAL

position occurs. In fact, if the relative misorientation between grains is large, the boundary may be considered a thin transition layer of high disorder with amorphous rather than crystalline properties. The situation is schematically illustrated in Figure 3.

Microscopic Deformation of Metals. In the case of small loads applied to a perfect crystal, small distortions will occur in the crystal lattice as the atoms seek new equilibrium positions in response to the applied forces. If the lattice is perfect, enormous forces are required to rupture the atomic bonds-- as shown by tests on perfect crystals. Once the loads are removed, the atoms return to their original positions and the material thus exhibits "perfect elasticity". The case for polycrystals is similar except the loads necessary to produce some irreversible changes in the lattice structure are much smaller; therefore, polycrystals are also capable of exhibiting perfect elasticity, but to a lesser extent.

The case of permanent changes in the lattice structure caused by loads greater than considered above will now be considered. The fundamental mechanisms of permanent or plastic deformation within a crystal are the generation and motion of dislocations. The two basic dislocation types are screw dislocation and edge dislocation. In a screw dislocation, relative shifting of the crystallographic planes has occurred, but this has not propagated through the entire crystal and, in fact, terminates along the screw dislocation line. The edge dislocation, which is simpler to visualize, is the result of an extra half plane of atoms being "pushed" into the lattice.

(DF 195)
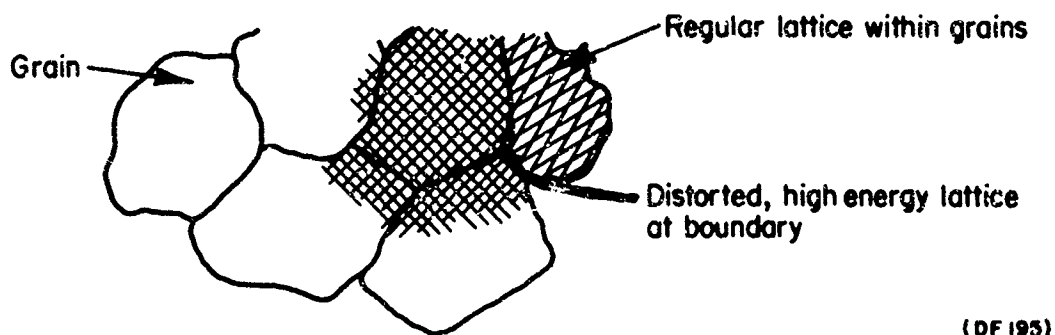
FIGURE 3. GRAINS AND GRAIN BOUNDARIES IN A POLYCRYSTAL

In either type of dislocation, a plane or a portion of a plane of atoms has glided with respect to an adjacent plane, and after the gliding motion, the geometric pattern of the crystal has again come back into registry.

In all types of deformation considered, the lattice undergoes some distortion in the vicinity of the crystal fault; consequently, the lattice possesses additional strain energy and is therefore in a higher energy state than without the fault. Nevertheless, the essential lattice structure is only locally distorted by the presence of a dislocation and the identifying features of the crystal are, in the main, retained.

Macroscopic Deformation of Metals. The microscopic deformation of metals manifests itself macroscopically as plastic flow and deformation. That is, microscopic dislocations translate as plastic deformations of the crystal or polycrystal. Although an annealed crystal will contain a large number of dislocations per unit volume (10^5 to 10^8 per cubic centimeter), the magnitudes of macroscopically observed plastic strains are not solely attributable to the gliding of these existing dislocations. It is known that the dislocation density increases with the start of plastic deformation. Although the description of these multiplication mechanisms is beyond the scope of this review, both the theoretical basis for their operation and X-ray evidence of their existence have been established. Thus, flow takes place due to relative motion of various dislocation glide planes. The number of operative glide planes tends to greatly increase due to multiplication mechanisms as flow progresses, resulting in macroscopic plastic deformation.

Physics and Mechanics of Fracture

Fracture in most materials requires the contribution of two usually distinct mechanisms; crack or void nucleation and crack growth or propagation. Since the operation and characteristics of both mechanisms are highly dependent on the inelastic behavior modes of the material, the discussion to follow will consider separately the fracture of perfectly-brittle materials, semibrittle materials, and ductile materials.*

---

* Principal sources for this discussion are References 1, 2, 3, and 4, page 35.

Perfectly-Brittle Materials

Under certain conditions, e.g., low temperatures, both amorphous
materials and some metals will behave in a semibrittle or ideally brittle fashion.
(Fracture of materials falling in the semibrittle category are discussed in a
subsequent section.) Those materials belonging to the latter category, which have
been studied most extensively, are the inorganic glasses. Materials such as
ceramics have received less attention.

Crack Nucleation. The discrepancy between the theoretical cohesive
strength (5-10% of E*) and the experimentally determined tensile strength is
attributed to stress concentrations at the tips of randomly distributed microcracks
on the surface or in the volume of the material. For uniformly stressed material,
the most severe (longest) crack propagates through the material in a direction
perpendicular to the maximum principal normal stress, and thus causes failure at
relatively low applied stress. While these microcracks have never been micro-
scopically observed, order-of-magnitude increases in the strength of glass specimens
with a surface layer etched off have been obtained. In the case of glass, the
severe surface cracks which cause failure are attributed to mechanical damage
introduced in processing or handling.

Crack Propagation. In uniaxial tension, the stress, σ_o, necessary to
propagate an elliptical crack of length 2C (with major axis normal to σ_o) was
derived by Griffith: [1]

$$\sigma_o = \sqrt{\frac{2\alpha E}{\pi C}} , \tag{1}$$

where α = specific surface energy. When this equation is satisfied, the crack
begins to propagate across the plane of maximum tension. As the crack elongates,
the stress concentration at its tip increases, thereby accelerating the motion

---

*Young's Modulus.

of the tip to maximum velocities as high as the Rayleigh wave velocity. As long as σ_o is maintained on the specimen, the crack will continue to move at steady-state velocity unless it hits an obstacle (hard region) or forks.

Materials with crack nucleation and propagation characteristics like those described above exhibit pronounced size effects in their tensile strengths, i.e., large specimens are weaker than small. This is due to the fact that the probability of a specimen containing a severe crack increases with size.

The simple considerations introduced above have been extended to more elaborate analyses; these include biaxial and triaxial stress fields and statistical approaches relating flaw densities and distributions to strength.

Semibrittle Materials

Some body-centered cubic metals (BCC), such as low-carbon steel and tungsten, and glassy materials, such as inorganic glasses and polymers, will deform plastically or viscously at high temperatures or low strain rates, but at low temperatures or high strain rates they will fracture in a semibrittle manner. In both crack nucleation and propagation, striking differences can be found between semibrittle fracture and the perfectly-brittle fracture. Another factor which contributes to the ductile/semibrittle fracture mode transition of these materials is the presence of a high triaxial tensile stress. In the poly-crystalline materials, the fractures are usually transcrystalline (cleavage of individual crystals), although some semibrittle fracture is of the intercrystalline variety (brittle separation along grain boundaries).

Crack Nucleation. The main difference between perfectly-brittle and semibrittle fracture in the glassy materials is that, in the latter case, some plastic deformation may precede or accompany failure. The mechanism for crack nucleation is the same as that discussed earlier. In metals, however, cracks are preceded and can be nucleated by inhomogeneous plastic deformation on a microscopic scale, i.e., slip and twinning.

Crack nucleation by slip can be caused by an edge dislocation pile-up at a strong obstacle such as a high or medium angle grain boundary (see Figure 4) or a pile-up in the form of a low angle boundary (see Figure 5). In both cases, the concentrated stress becomes equal to the theoretical strength of the material, and as long as the stress does not relax too rapidly, the cracks will continue to grow. An interesting aspect of the grain boundary pile-up mechanism is that the crack nucleation stress is grain-size dependent. This is due to the fact that more dislocations, and hence greater stress concentrations, will occur in larger grained materials. Pile-ups in the form of low-angle boundaries are common to hexagonal metals and single crystals of ionic compounds, such as magnesium oxide. (See Figure 5.)

A sketch of the mechanism of crack nucleation by the interaction of deformation twins is shown in Figure 6. This mechanism, found in BCC crystals, requires higher stresses than those needed for dislocation pile-ups. Only a few intersections of this type will result in crack nucleation, since the stresses are easily relieved.

Crack Propagation. Once defects (cracks) have been introduced by the flow of crystalline material, the occurrence of semibrittle or ductile fracture will be governed by whether or not an elastic-plastic crack propagation condition is satisfied. Such a condition was given by Orowan[1] as

$$\sigma_o = \frac{2_p E}{\pi C} , \tag{2}$$

where p = the work of plastic deformation per unit increase in crack area. This is just the Griffith equation with p substituted for α. In general, however, p will not be constant.

Observed from a microscopic point of view, it is probable that a flow-nucleated crack in a single crystal would be of sufficient length to satisfy the Griffith brittle crack propagation criterion. In a polycrystalline material however, a cleavage crack will usually be stopped by a grain boundary between grains with greatly differing cleavage planes. Once the crack is stopped, plastic deformation at its tip serves to blunt it, thus creating the necessity for additional crack propagation energy. For this reason, the term "p" in Orowan's equation is much higher than the corresponding "α" term in Griffith's equation.
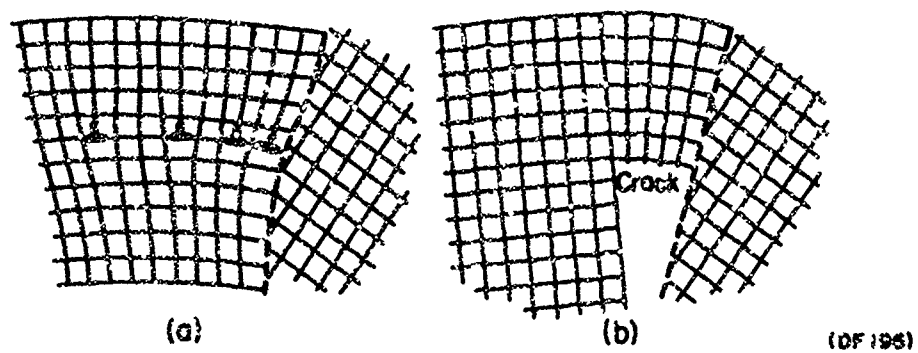
FIGURE 4. FORMATION OF A CRACK BY FUSING TOGETHER OF DISLOCATIONS AT THE TIP OF A PILE-UP
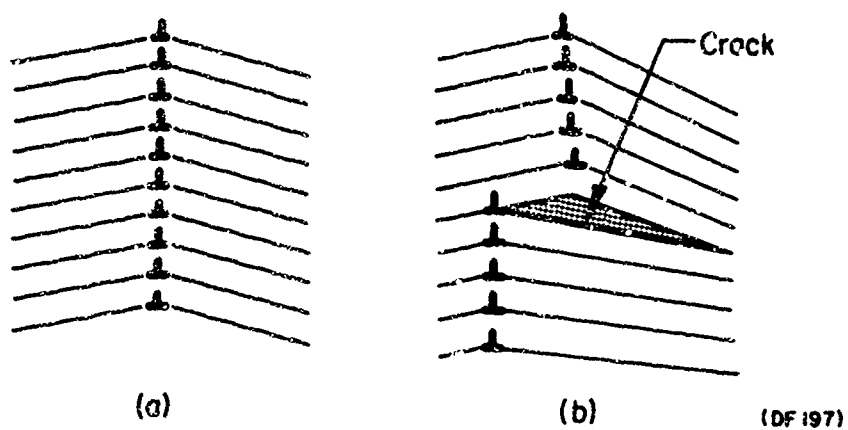
FIGURE 5. FORMATION OF A MICROCRACK BY SHEAR OF PART OF A TILT BOUNDARY
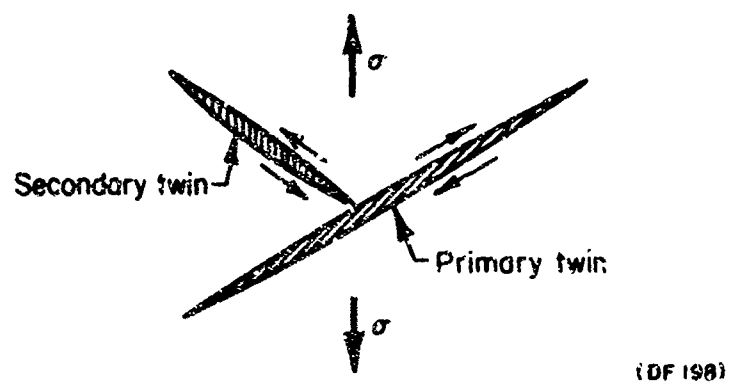
FIGURE 6. CRACK NUCLEATION BY THE INTERSECTION OF TWO DEFORMATION TWINS

As was the case for crack nucleation in polycrystalline materials, grain size plays an important role in crack propagation. The improved resistance to semibrittle fracture of fine-grained materials is due not only to the fact that cracks are more difficult to nucleate, but also that they are more difficult to propagate.

Intercrystalline semibrittle fracture is nucleated and propagated in the grain boundaries. It is due either to some form of grain boundary embrittlement or a thin film of a brittle phase separating at the grain boundary.

Ductile Materials

Materials such as some FFC (face-centered cubic) metals do not undergo a ductile/semibrittle fracture mode transition. In a standard tension test, these materials develop voids or ductile cracks under the influence of triaxial tension in the center of the necked region. These voids subsequently grow in size and number and coalesce as the load is maintained or increased. The fine structure of the fracture surface at the center of a completely separated specimen shows that the voids grow to such an extent that the material between them ruptures (shear failure) rather than cleaves.

Crack Nucleation. The origin of the voids which grow to cause ductile fracture is attributed to either stress concentrations in the grain boundaries due to impurities or inclusions, fracture of perfectly-brittle elements (such as pearlite in steel), or excessive localized strain concentrations in bands of heavy deformation.

Crack Propagation. Crack propagation, or more descriptively, void growth, proceeds according to the manner in which the crack was nucleated. Thus, if the cracks were initiated by failure of brittle elements, they would become blunted and turn into holes. The growth and coalescence of the holes would depend on the amount of further plastic strain and the magnitude of the transverse stress. On the other hand, if the cracks were formed along grain boundaries or bands of heavy deformation, the cavity acts as a notch to concentrate stress in planes

oriented at 30 to 40 degrees to the tensile axis. Large amounts of plastic flow occur in this region, forming a heavy concentration of voids in the shear band, and the weakened region then splits open.

Spall

This section is devoted to a detailed statement of the current knowledge of spall fracture. For reasons of readability and conceptual clarity, the results of the various investigators are presented in an integrated [5] rather than sequential [6] manner. In this format, topics such as spall models and degrees of spall are discussed separately. Particular emphasis is placed on those results most closely related to spallation in uniaxial strain caused by plate-slap impact, i.e., rectangular pulses. Furthermore, the closely related and at least equally important problem of determining material response prior to spall will receive only cursory attention, since this has been considered in detail in Appendices A to E.

The Degrees of Spall

The most general definition of spall is given in terms of its cause; namely, material failure due to the interaction of two or more rarefaction waves. The failure itself may range from cracks, detectable only by microscopic examination, to sublimation or disintegration of part of the material. The latter type of failure is referred to as ultimate or cohesive spall; the former type represents a lower limit to a different and less drastic failure mode called ductile spall. In addition, materials which exhibit a pressure-induced phase transformation may fail in an intermediate mode known as phase transformation spall. Since both ultimate and phase transformation spall occur at relatively high stress levels compared to ductile spall, and since they have received only a small amount of experimental or theoretical attention, they will be mentioned only briefly in this study. The major emphasis will be placed on the more practically interesting failure mechanism known as ductile spall.

Ultimate or Cohesive Spall. This mode of spall has been observed by a few investigators, most notably McQueen and Marsh.[7] By generating short duration pulses with an explosively-driven flyer plate, and assuming hydrodynamic material response, the ultimate strength of single-crystal and polycrystalline copper was found to be in excess of 150 kbar. The distinguishing feature of the observed failure mode was that the material literally disintegrated or sublimed, in contrast to the behavior at lower spall thresholds where flaw-related mechanisms such as crack nucleation and propagation are prominent. It is interesting to note the rather favorable comparison between the experimentally obtained ultimate spall threshold and the static theoretical strength of the material derived from consideration of the interatomic forces in a crystal. Using the equation for the theoretical, static cohesive of $.05E - .10E$, and assuming a modulus of 18×10^6 psi for copper, the strength is found to lie between 62 and 125 kbar.

Phase-Transformation Spall. This mode of failure occurs only in materials which exhibit a pressure-induced phase transformation. It has been observed in Armco iron by Erkman[8] and Moss and Glass.[9] Both of these investigations used plate-slap impact techniques to induce stresses in excess of the phase-transformation pressure (130 kbar), thereby creating a characteristic double plastic shock wave structure. The phase-transformation spall threshold, which is the negative of the phase-transformation pressure, does not represent a point of change in failure mechanism, but rather marks a point of change in the appearance of the spall surface. This change is attributed to the phase transformation. As induced pressures are increased through the phase-transformation pressure, the spall plane takes on a characteristically smooth appearance, although the failure mechanism remains one of crack nucleation and propagation. Phase-transformation spall has also been observed in steel by Novikov and others,[10] and in iron and steel by Ivanov and others;[11] both studies used contact high explosives to induce the required pressures.

Ductile Spall. Low-pressure or ductile spall involves the same basic mechanisms, i.e., crack nucleation and propagation, that are associated with lower strain-rate failure. Three separate levels of ductile spall have been recognized and classified according to the severity of damage. In order of increasing damage they are; incipient, intermediate and complete.

The incipient spall threshold is defined as that combination of stress and time (pulse duration) below which no damage to the specimen would be visible. In order to determine the visibility of failure, it is necessary to section, polish, and etch the specimen and perform a metallographic examination at about 100 x magnification. The large number of parameters influencing the spall threshold precludes a general description of the appearance of the fractured region, although it can be stated that several usually transgranular microcracks or voids with dimensions on the order of a grain diameter would be evident. Also, the cracks would be generally parallel and would lie in a fairly narrow band parallel to the free surface of the specimen. Photomicrographs illustrating the appearance of incipient spall in 6061-T6 aluminum and copper are given in References 12 and 13, respectively.

If the tensile stress and/or pulse duration is greater than that required for incipient spall, the degree of damage is correspondingly greater; i.e., the cracks are more numerous and larger, and some are joined together. A criterion for quantitative determination of the degree of damage has been suggested by Herrmann of Sandia, who proposed that the damaged specimens, including the spall plane, be cut into tensile members and pulled apart in a tension testing machine.[13] In this way, a quantitative measure of the degree of damage is provided by the residual strength of the tensile member. As the tensile stress and/or pulse duration is increased beyond the incipient spall threshold values, the degree of damage to the specimen increases and, hence, its residual strength decreases. At some point, however, the residual strength of the specimens ceases to decrease with increase in the severity of loading. The tensile stress and pulse duration corresponding to this point are said to define the intermediate spall threshold.

If a specimen is subjected to a tensile pulse of sufficient magnitude and/or duration in excess of the intermediate spall threshold values, the damage will be so great that a fairly intact piece of material will separate or be detached from the specimen. The combination of stress and pulse duration at which this occurs is known as the complete spall threshold. This threshold is of greater practical importance than the others and has, historically, been the object of the greatest study, e.g., Hopkinson, Kolsky, Rinehart. Obviously, the residual

strength of the material above this threshold is zero, and a complete characterization of the three ductile spall thresholds in terms of residual strength would appear as shown in Figure 7.
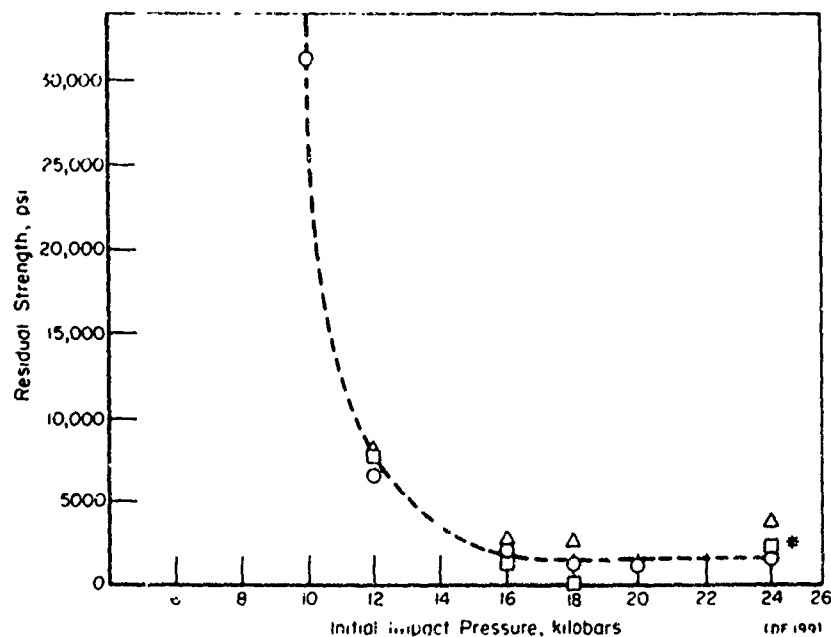
FIGURE 7.   RESIDUAL STRENGTH OF TARGETS USING 1.5 μs SQUARE PULSES

* The 24-kbar data were obtained with a grooved target.
  Edge effects prevented complete separation at 22 kbar.

Photomicrographs illustrating the appearance of the fracture zone in copper at the three ductile spall thresholds are given in Reference 13.

Some of the more recent investigators of the complete spall threshold have used specimen configurations specifically designed to eliminate the influence of edge effects and shear failure, which necessarily enter into the complete spall of a standard plate specimen. By using tapered plugs fitted into plates of similar material, Smith[13] obtained complete spall thresholds for copper which were lower than those obtained with standard specimens. When a scheme such as this is employed, however, care must be taken to ensure that uniaxial strain conditions are maintained while the material is in tension. If this is not done, the different stress states occurring in compression and tension must be accounted for in the solution of the wave propagation equations. Glass and others,[14]

experimenting with single crystals of copper, used cylindrical specimens of L/D > 1
embedded in copper plates. They observed rather severe necking in the region of
the specimen adjacent to the spall zone, indicating a stress state similar to that
prevailing in a standard tensile test, i.e., uniaxial stress.

Parameters Influencing Ductile Spall Thresholds

A sufficient amount of experimental and theoretical evidence has now been
gathered to support the assertion that the "critical normal fracture stress"
criterion for spall must be at least extended, if not totally revised. This
criterion, which states that a material will spall instantaneously and completely
when a unique critical value of normal tensile stress is attained, has yielded
erroneous and even contradictory predictions of spall in several instances. Indica-
tions are that a realistic spall criterion must include at least one, if not several
more parameters to account for the anomalies in experimentally observed spall
behavior. In this section, those parameters which have been found to affect spall
behavior will be enumerated and discussed, with reference to specific experiments.

Time-Related Parameters. One of the first indications that a critical
normal fracture stress did not constitute an adequate spall criterion was the
disparity, both in numbers and sizes, between predicted and measured scabs in
multiple-spall experiments. In his experiments with several metals and glass
subjected to explosively induced pressures, Broberg[15] attributed these discrepancies
to the noninstantaneous fracture behavior of ductile materials. If a material which
is subjected to a triangular compressive pulse does not spall instantaneously when
the net reflected tension reaches a critical value, then the magnitude of the pulse
available to cause additional spalling upon reflection from the first spalled
surface is reduced.

In a later article,[16] reporting on experiments done with granite and
lucite, Broberg explained the spall delay time in terms of the mechanisms associated
with fracture at lower strain rates, i.e., crack nucleation and propagation. Thus,
the stress-dependent fracture delay time decreases with increasing stress, not
only because more cracks are nucleated, but also because the acceleration of the
crack tips increases. Similarly, ductile materials require more time to fracture

than brittle materials because stresses are relieved not only by fracture, but also by flow. Ductility limits the magnitude of stress concentrations and causes the tips of cracks to become blunt, thereby retarding both the velocity and the acceleration of crack propagation.

Results of plate-slap tests provide additional evidence for the necessity of including a time-related parameter in the spall criterion. Butcher and others[17] point out that, for the same material, the difference between the spall threshold stress generated by contact explosives (triangular pulses) and the spall threshold stress obtained by plate-slap impact (rectangular pulses) indicates a time dependence for spall failure. In the cases where a strict comparison was possible, the explosively induced spall threshold stress was always greater than the plate-slap spall threshold.

In plate-slap experiments on 6061-T6 aluminum, Blincow and Keller[18] observed that the flyer velocity required to cause incipient spall decreased with increasing flyer thickness in an approximately linear manner. Since impact velocity can be directly related to stress, and flyer thickness can be similarly related to pulse duration, a definite time dependence of spall is implied. Another interesting observation made by these investigators was that the thickness or extent of the spalled region increased with decreasing impact velocity (above the incipient spall threshold). This phenomenon can also be attributed to a time-dependent spall mechanism by recognizing that for a given pulse width, if the stress is greater than that required for spall, the material will fail more quickly than it would at the threshold value of stress. Due to this more rapid spall at higher stress levels, the remainder of the tension wave reflects sooner from the spalled surface as a compressive wave to prevent additional fracturing near the original spall. Also, since the width of the pulse that is transmitted across the spall plane prior to spall is less than that at lower stress levels, the material between the impact surface and the spall plane is less likely to experience subsequent fracture (multiple spall).

Other investigators have found evidence for time-dependent spall in experiments with copper. In his plate-slap experiments, Smith[13] found that the required tensile stress decreased with increasing pulse duration for all ductile spall thresholds. Of additional interest in this reference are several photo-micrographs illustrating spall damage for different combinations of stress and pulse

duration. These pictures show increasing damage, i.e., larger cracks and voids, for the case when stress is held constant and pulse duration increased and the case when pulse duration is kept constant and stress is increased.

Glass and others[14] used contact explosives to study the fracture of copper single-crystals. These authors point to the presence of a necked-down region adjacent to the spall zone as definite proof that the material does not fracture instantaneously.

Not all investigators explicitly introduce time as a parameter with which to augment a spall criterion. Al'Tshuler and others[19] attribute the difference between explosive and plate-slap spall threshold stresses to the different tensile strain rates corresponding to these loadings. It is interesting to note that, contrary to the results of the comparison made by Butcher,[17] they found the spall threshold stress for copper obtained by plate-slap impact to be more than twice the explosively induced threshold stress. They estimate the strain rates as 10^5 sec $^{-1}$ for explosive loading and 10^7 sec $^{-1}$ for plate slap.

Whiteman[20] has introduced tensile-stress unloading rate to account for the nonunique spall threshold stresses which he measured in aluminum, mild steel, brass, and copper by plate-slap impact techniques. Plausibility of the results is indicated to the extent that curves of spall stress versus this stress rate generally show spall stress approaching the theoretical strength at the highest stress rates. In addition, the trends of the curves appear to be consistent with theoretical considerations. If it is assumed that cracks are nucleated by dis-location pile-ups at grain boundaries, then the stress necessary to initiate fracture must increase with increasing stress rate (and, hence, shorter load-application times) to give the dislocations sufficient velocity to reach the boundary. More discussion of the stress-rate dependent spall criterion will be given in the section devoted exclusively to spall models (pages 23-32).

Other Parameters. In contrast to time-related effects, evidence pertaining to the influence of other parameters on ductile spall thresholds is comparatively meager. Furthermore, some of this evidence is not only rather tenuous, but contradictory as well. For the sake of completeness, however, results pertaining to the influence of all parameters (other than time, of course) will be presented here.

The previously discussed discrepancies observed in multiple-spall experiments evoked an explanation other than that of a time-dependent spall mechanism. Rinehart[21] felt that the discrepancies could be explained by the fact that not all spall planes experienced the same peak compressive stress before going into tension. In other words, the critical normal fracture stress of a material depends on the transient compressive stress immediately preceding tension. To the extent that explosively generated pulses can be controlled, and their shapes accurately described, Rinehart's suspicions are borne out by the experiments of Buchanan and James[22] with mild steel. Varying the magnitude of the precompression pulse by using specimens of different thicknesses, they found that the critical normal fracture stress increased in an approximately linear manner with increasing precompression. In particular, the tensile stress required to cause spall increased by about 50 percent when the magnitude (peak stress) of the preceding compressive pulse was tripled. However, n these experiments, the rate of stress application also increased with increasing peak stress so that the precompression explanation of the observed effect is not unique.

More work should be done to determine what effects the compression phase of the stress-time history has on the spall behavior of materials, if for no other reason than the fact that crack nucleation, which is dependent on shear stresses rather than normal stresses, can occur in the compressive as well as the tensile phase. In both phases, the stress states are nonhydrostatic. Note that the trend of the results described above, i.e., increasing strength with increasing pre-compression, runs contrary to what would be expected if increased precompression implied a greater amount of crack nucleation.

The influence of ambient temperature on spall thresholds is another area warranting further investigation. For the rather extensive range of temperatures they considered, O'Brien and Davis[23] found no change in the fracture stress of high-purity polycr, italline aluminum subjected to explosive loads. In contrast to this are the results obtained by Penning and others[12] from plate-slap tests on lucite. With a very limited number of tests, covering only a small temperature range, they found that the fracture stress increased with increasing temperature.

It appears that neither of the above-mentioned investigators accounted for the influence of temperature on the equation-of-state, and consequently, on

the wave propagation. Obviously, this type of effort must accompany, if not pre-
cede, any investigation into the effect of ambient temperature on spall thresholds.

The results of a study done by Piacesi and Watt[24] show that yield
strength can play a double role in the spallation phenomenon. In addition to
affecting the shape of the stress pulse and, therefore, the stress-time history
at the spall plane, the yield strength of a material influences the amount of
bulge at the rear surface of a specimen that has not completely spalled. Thus,
with specimens not designed to be free of edge effects and shear failure, such as
described previously, yield strength would influence both the intermediate and
complete spall thresholds.

In this study, the effect of yield strength on rear surface bulge was
demonstrated experimentally by impacting 7075-T6 aluminum targets at various
temperatures (and, consequently, different yield strengths) with 1/4-inch-diameter
aluminum spheres. The bulge distance versus impact velocity curves for 7075-T6
aluminum at 500° F and 7075-0 aluminum at 72° F, which have equal yield strengths,
were approximately identical. This result indicated that temperature did not
affect spall, in agreement with the conclusions of O'Brien[23] discussed previously.
Thus, the results obtained in tests at lower temperatures, i.e., smaller bulge
distances for all impact velocities, could justifiably be attributed to the
influence of yield strength alone.

The necessity for investigating the influence on spallation of micro-
scopic material properties, such as structure and composition, has been recognized,
and some work has been done. In the study previously mentioned,[23] O'Brien and
Davis found that the fracture stress remained constant for aluminum single crystals
at various orientations, zone-refined polycrystalline aluminum, polycrystalline
aluminum rods that had been cold worked to various textures, and 2024 aluminum-
copper alloy in the hardened and solution-treated condition. Although the ap-
pearance of the spall was influenced by the ductility of the specimens, the
conclusion reached was that the structural defect causing failure was present in
an as-grown crystal or was caused by the precompression shock.

In their experiments with lead, aluminum, and copper, subjected to
explosive loads, Vitman and others[25] found spall threshold stresses to be
insensitive to alloying.

The structural parameter that has been found to have the greatest influence on spallation is the material form (i.e., bar or plate). Using plate-slap techniques to study spallation in copper, Plauson and others[26] found that the spall stresses for annealed bar sp-cimens (grains aligned normal to the specimen faces) were more than twice the stresses for plate specimens (grains aligned parallel to the specimen faces). In addition, the spall stresses of the plate specimens were found to be relatively insensitive to material condition (i.e., annealed, 1/4 hard, or hard).

The individual cracks constituting the entire spall zone were observed to be of a transgranular nature in both the bar and plate specimens, but the gross appearance of the spall differed greatly. In the plate material, the individual fractures were cleavage fractures which showed little attendant grain deformation, while in the bar material, shear fractures and large amounts of grain deformation were observed. In both bars and plates, the gross spall formed on a plane perpendicular to the direction of impact. However, the individual cracks were oriented in the direction of grain alignment.

Similar, but less quantitative results on the effect of grain alignment in copper have been obtained by Smith.[13] This reference contains excellent photomicrographs which illustrate the marked differences in the appearance of the spall zones in bar and plate specimens.

In a series of plate-slap experiments on 6061-T6 aluminum plate stock, Butcher[27] found that the critical values of stress and pulse duration required for crack nucleation were insensitive to the angle between the impact velocity vector and the plane of grain elongation and impurity stratification. Crack propagation, on the other hand, was found to be extremely sensitive to this orientation. Cracks usually propagated in the plane of weakness, i.e., grain elongation and impurity stratification, regardless of the plane's orientation. Thus, when this plane was parallel to the direction of impact, little propagation was noticed because the tension normal to this plane is neither uniform nor of maximum magnitude. In this orientation, evidence of massive plastic flow was found in the area of the spall zone.

It appears that the increased spall strength of specimens in which grain elongation is parallel to the direction of impact is due to the fact that cracks nucleated in these specimens are not aligned perpendicular to the direction of maximum tension and, thus, do not propagate as readily nor coalesce as easily as cracks aligned parallel to the spall plane. Since incipient spall involves very ~~~ ~~ack propagation, the insensitivity of this threshold to grain alignment. ~ ~ed by Butcher, is not surprising. Blincow and Keller [18] also repo~ e incipient spall threshold of 6061-T6 aluminum is the same for both pl~ ~nd bar specimens, but certainly more data is needed.

These observations, and the remarks made previously in connection with the effect of precompression, indicate that significant progress toward understanding the spallation phenomenon must necessarily involve a deeper understanding of the roles played by the basic fracture mechanisms.

Spall Models

Except for very simple pulse shapes, analytical predictions of spall (i.e., thickness and number) are handled most efficiently by a computer in conjunction with wave propagation calculations. The critical normal fracture stress spall criterion, being the simplest and requiring the least data, is presently being used in several codes and requires no further discussion. The more sophisticated models, incorporating such parameters as time, rate, temperature, and thus requiring more experimental data, are at various stages of development. Some have had successful, if limited, application and verification, while others remain at the purely conceptual stage. With one exception, which will be discussed separately, all of these spall models are phenomenological in nature; e.g., spall stress is related to time, rate, etc., by experimentally determined constants which characterize the spall behavior of the material. The explanatory model, based on the principle of bond rupture, represents an attempt to predict spall behavior from consideration of the physical mechanisms actually involved.

Phenomenological Spall Models. Aside from being a numerical application of a particular spall criterion, a spall model should also have the capability to predict the spall behavior of a material subjected to a pulse of arbitrary shape. Thus, if an experimentally determined relationship between fracture delay time

and constant applied tensile stress is known, the spall model must contain some statement as to how this information is to be used when the material is subjected to a variable stress. Penning and others[12] suggest that the spall delay time of a material under variable tensile stress is cumulative, i.e., the material will spall at that time, τ, given by

$$\int_0^\tau \frac{dt}{t_s} = 1 \; ; \tag{3}$$

where $t_s = t_s (\sigma)$ is the delay time versus constant tensile stress relationship.

To see this more clearly, consider the sketch of the stress-time history, $\sigma = \sigma (t)$, shown in Figure 8.
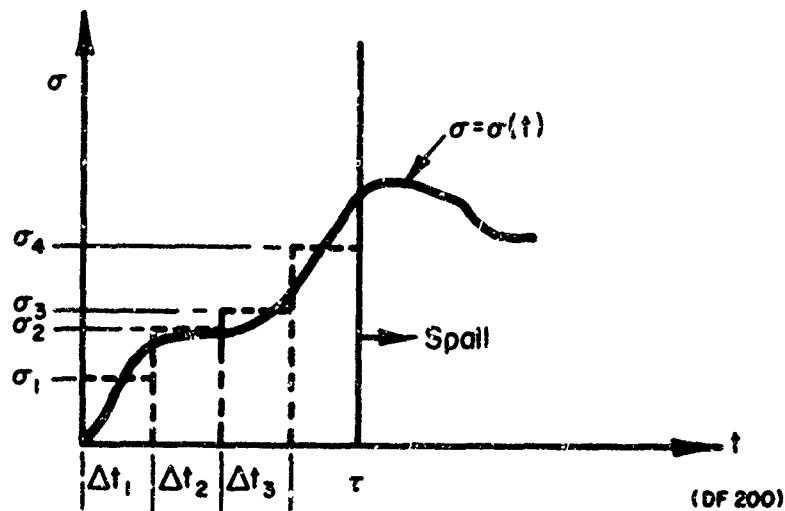
FIGURE 8. ASSUMED TENSILE STRESS TIME-HISTORY
AT THE SPALL PLANE

At time $t = \tau$, spall occurs, i.e.,

$$\frac{\Delta t_1}{t_s(\sigma_1)} + \frac{\Delta t_2}{t_s(\sigma_2)} + \frac{\Delta t_3}{t_s(\sigma_3)} + \frac{\Delta t_4}{t_s(\sigma_4)} = 1. \tag{4}$$

It can be seen that spall does not occur until the percent of damage associated with the individual approximating pulses (σ_n, Δt_n) accumulates to 100 percent.

The obvious shortcoming of this scheme is that the effect of previous stressing is not included in the t_s versus σ relationship. For each time increment, Δt_n, the corresponding delay time, t_s (σ_n), is based on σ_n being applied instantaneously, with no previous stress present. From these considerations, it would appear that the τ obtained by this method would be too large.

Butcher and others[17] have utilized the cumulative method to obtain closed form expressions for τ. By considering only triangular pulses, and assuming a definite functional relationship between t_s and σ, they were able to integrate Equation 3 and solve for τ in terms of a material spatial coordinate, the shock velocity, and parameters characterizing the pulse shape and the t_s versus σ relationship.

Tuler and Butcher[28] incorporated the cumulative spall model into an elastic-plastic-wave propagation code. They used a t_s versus σ relationship of the form

$$t_s = k(\sigma - \sigma_o)^{-\lambda} ; \tag{5}$$

where k and λ are positive constants and σ_o represents the minimum tensile stress required for failure, regardless of time duration.

Predictions made with this model were compared to spall data for 1100 aluminum which had been subjected to explosively induced pulses.

More fundamental difficulties are encountered when the spall delay time versus applied tensile stress relationship is examined. Two of the more common forms of this relationship are given by

$$t_s = \lambda e^{-\mu\sigma} \quad \text{(References 29 and 30),} \tag{6}$$

$$t_s = \alpha\sigma^\beta \quad \text{(Reference 31);} \tag{7}$$

where λ, μ, α, and β are constants.

Equation 6 represents not only the experimentally observed behavior of a wide variety of materials when t_s is relatively large (milliseconds and above),

but has been derived by Waldorf[30] from theoretical considerations and shown to hold for al' values of t_s. In this theory, which will be discussed subsequently in more detail (see page 28), the constants λ and μ are identified with such physical parameters as sublimation energy, Boltzmann's constant, absolute temperature inside the shock, and the lattice vibrational frequency.

Equation 7 merely represents a fit to data gathered for several materials, most of which were ablators and plastics.

Regardless of the form of the delay time versus constant applied-stress relationship, the difficulty of applying the relationship to the prediction of spall when a material is subjected to unsteady tensile stress is one of logical contradiction. When the stress causing spall is not large compared to the dynamic yield stress, the hydrodynamic interpretation of material response is not justified. Elastic-plastic wave-propagation calculations show that the stress-time history at the spall plane is very unsteady due to the complicated interaction of the unloading compressive wave and the elastic-plastic rarefaction from the free surface. Thus, data describing a spall threshold in terms of stress and pulse duration necessarily imply that the fine structure of the actual stress-time history at the spall plane is unimportant, and that spall can be characterized in terms of an equivalent rectangular pulse. This equivalent rectangular pulse can be obtained in various ways. In his experiments with copper, Smith[13] completely neglected the effect of the elastic precursor. Others[12] have performed sophisticated calculations of the stress-time history at the spall plane, and then they appear to have "eyeballed" an equivalent rectangular pulse with which to describe the spall threshold.

From these considerations, it must be concluded that the only consistent way to predict the spall behavior of a material subjected to an arbitrary finely-structured pulse, from this type of data, is to idealize the actual pulse in a manner identical to that which was used to obtain the data. From a physical standpoint, a more desirable approach would be to introduce additional parameters to characterize the actual shape of the spall-threshold pulse. Again, since fracture may be considered basically a mechanism of energy transfer, it may be

more realistic to describe spall in terms of total mechanical energy introduced
to the spall plane. A spall criterion based on this concept would have the form

$$k = \int_0^\tau \sigma v dt \; ; \tag{8}$$

where

k = an empirically determined constant in units of energy per
unit area,

τ = time at which spall occurs,

σ = instantaneous net tensile stress at the spall plane,

v = instantaneous net particle velocity at the spall plane,

t = the length of time for which the spall plane has been
in tension.

If only rectangular pulses are considered, and if linear elastic material approximations are made, i.e., $\sigma = \rho c v$, then this equation can be integrated to yield

$$\tau = t_s = k\rho c \sigma^{-2} \; . \tag{9}$$

Note the formal similarity to Equation 7 which represents a fit to experimental
data. Equation 7 also involves a negative exponent, although it is of different
magnitude.

A spall model based on the criterion of stress-rate-dependent spall
stress has been used successfully by Breed and others[32] at Los Alamos Scientific
Laboratories (LASL). These investigators found that Whiteman's[20] data, relating
spall stress to the tensile stress unloading rate for aluminum and copper, could
be put in the computationally convenient form of

$$\sigma_s = A + B \left(\frac{\partial \sigma}{\partial x}\right)^{1/2} \; ; \tag{10}$$

where

σ_s = spall stress,

$\frac{\partial \sigma}{\partial x}$ = instantaneous net tensile-stress unloading gradient at spall plane,

A,B = experimentally determined constants.

Using this model in the LASL hydrodynamic SIN code, the damage done to
a 2.5 cm thick aluminum block, subjected to the contact explosion of a 10 cm

block of composition B-3, was predicted to be 10 spalls in 23 µs. A radiograph of an actual test specimen taken at 25 µs showed 11 ± 1 spalled layers. Close agreement between predictions of the code and experimental results was also found for the case of a copper-aluminum-copper sandwich subjected to plate-slap impact.

These results illustrate how successful a phenomenological spall model can be, provided that consistency is maintained between the analysis of test data and analytical predictions of material behavior based on this data. Since it is now generally accepted that the hydrodynamic material approximation yields erroneous results, except at extremely high pressures, a more physically satisfying approach would be to incorporate this spall model into a code for elastic-plastic stress wave calculations.

Explanatory Spall Model. The spall model developed by Waldorf[30] is based on the fundamental physical criterion that atomic bonds must be broken in order for fracture to occur. By using this criterion in conjunction with several material idealizations, Waldorf was able to derive a relationship between spall delay time, t_s, and applied tensile stress, σ_o, for homogeneous materials, i.e., single crystals. This relationship is then extended and modified to describe the fracture of materials in which crack propagation plays an important role, i.e., polycrystalline materials. The essential features involved in the development of these relationships are outlined in this section.

For a microscopically homogeneous, isotropic, and flawless material loaded in uniaxial strain with the bonds parallel to the applied stress carrying the entire load, the rate at which bonds are broken can be written as

$$\frac{dn}{dt} = -nP_b ; \tag{11}$$

where

  n = the number of unbroken bonds per unit area perpendicular to
       the stress,
  P_b = the probability of an atomic bond rupturing per unit time.
       (This is a function of the applied stress and temperature.)

Now assuming that the atoms move about their equilibrium positions in the lattice with a Maxwellian velocity distribution in the direction of the applied stress, and defining bond rupture as occurring when an atom has traveled a distance equal to the equilibrium spacing, δ_o, the rupture probability, P_b, is derived as

$$P_b = \omega e^{-E/kt} ; \tag{12}$$

where

  ω = the vibrational frequency of the lattice,

  k = Boltzmann's constant,

  T = absolute temperature,

  E = the energy per bond with which the atoms are bound into the lattice.

In the unstressed state, the binding energy, E, is equal to E_o, which is approximately the sublimation energy.

The dependence of E on applied stress, σ_o, is found by assuming that E varies linearly with lattice spacing, δ, and by using an average value of bulk modulus to relate σ_o to δ. By further assuming that fracture occurs at a time equal to the mean lifetime of the bonds and that, during this time, the number of unbroken bonds may be averaged to a constant value, the E versus σ_o relationship becomes

$$E = E_o - \frac{\delta_o \alpha \sigma_o}{n_o} ; \tag{13}$$

where

  $\alpha = \dfrac{e}{e-1}$;

  n_o = number of bonds per unit area in the unstressed state.

Now Equation 11 can be integrated to yield

$$\ln \frac{n}{n_o} = \omega \int_o^\tau \exp\left[-\frac{E_o - \dfrac{\delta_o \alpha}{n_o}\sigma_o(t)}{KT} \right] dt. \tag{14}$$

Since fracture occurs when $n = o$, the delay time, t_s, versus applied stress, σ_o, relationship becomes

$$1 = \omega \int_o^{t_s} \exp\left[-\frac{E_o - \dfrac{\delta_o \alpha}{n_o}\sigma_o(t)}{KT} \right] dt. \tag{15}$$

When σ_o is constant, this reduces to

$$t_s = \frac{1}{\omega} \exp \left[\frac{E_o - \frac{\delta_o \alpha}{n_o} \sigma_o}{KT} \right] . \tag{16}$$

A less approximate approach would be to relate E and δ by the Morse potential function, i.e.,

$$E = E_o \left[e^{-2a(\delta_o - \delta)} - 2e^{-a(\delta - \delta_o)} \right] ; \tag{17}$$

where a is a constant such that $E = o$ when $\delta = 2\delta_o$, i.e., the atoms become unbound when forced apart by an amount δ_o. Then, using an average value of effective modulus in uniaxial strain, $\overline{E}$, it can be written that

$$\frac{\delta - \delta_o}{\delta_o} = \frac{\sigma_o}{\overline{E}} \tag{18}$$

and

$$E = E_o \left[e^{-2a\delta_o \sigma_o / \overline{E}} - 2e^{-a\delta_o \sigma_o / \overline{E}} \right] . \tag{19}$$

This expression could then be used in place of Equation 13 in the solution to the bond breaking equation, i.e., the t_s versus σ_o relationship.

The fracture of polycrystalline materials involves plastic flow and crack propagation, so that the relationships previously derived must be modified to account for nonhomogeneous rates of bond rupture. Waldorf's material model assumes a distribution of microcracks which grow until they join to form a continuous fracture surface. The lengths and spacing of the cracks, which are assumed to be nucleated by the usual mechanisms, are assumed to be about the same as the grain diameter, so that each crack must roughly double its length for fracture to occur. It is assumed further that crack widths are about equal to the thickness of the grain boundaries, i.e., 10 atoms.

The time required for neighboring cracks to coalesce, and hence the delay time for fracture, t_s, is given by

$$t_s = \frac{b}{v} ; \tag{20}$$

where

        v = the crack propagation velocity (this is a function of the applied stress),

        b = one-half the mean tip-to-tip spacing of the cracks.

In order to find the relationship between crack-propagation velocity and applied stress, it is assumed that the variation of tensile stress with distance from the crack tip is described by a step function. Thus, for a distance d_o from the crack tip, the stress is constant and equal to the maximum value of concentrated stress at the crack tip. At distances from the crack tip greater than d_o, the stress is constant and equal to the applied stress, σ_o.

Now, by assuming that the stress level in the region d_o of stress concentration is so large that fracture will occur across the width d_o in a time very small compared to fracture anywhere else, and considering the grains to be perfect homogeneous crystals, it may be concluded that the crack tip moves across the distance d_o in the time t_s' required for a homogeneous material to fracture under the concentrated stress. As the crack propagates, this process repeats, so that the propagation velocity may be written as

$$v = \frac{d_o}{t_s'} ; \qquad (21)$$

where t_s' is the delay time for fracture in homogeneous materials subjected to constant applied stress.

Expressing d_o and b in terms of the grain diameter, Y, and the grain boundary thickness, c, and making a correction for plastic flow, the equations for propagation velocity and, hence, fracture-delay time may be obtained in terms of the applied stress and atomic characteristics of the material. For a constant value of applied stress, the delay time versus stress relationship becomes

$$1 = \frac{\alpha}{2} \frac{1}{B\sigma_o Q} e^{\left(\frac{2}{\alpha}\right)\left(B\sigma_o Q\right)} \left[1 - e^{-\frac{1}{2} BA \frac{1}{\alpha} e^{\left(\frac{2}{e} B\sigma_o Q\right)} \sigma_o t_s} \right] ; \qquad (22)$$

where

$A = \omega e^{-E_o/Kt}$,

$B = \dfrac{\delta_o \alpha}{n_o KT}$,

$Q = \left(\dfrac{Y}{c}\right)^{\frac{1}{2}}$,

Y = grain diameter,

c = grain boundary thickness.

Since the crack-propagation velocity cannot exceed the velocity of sound in the material, c_s, the minimum value of delay time, occurring at high stress levels, would be given by

$$t_s = \frac{b}{c_s} .$$ (23)

As a partial experimental verification of his theory, Waldorf cites the agreement between his predictions and stress-fracture delay-time data obtained by other investigators for homogeneous plastics and metals at relatively low values of applied stress and long time durations, i.e., quasi-static strengths.

Louie and others[33] attempted to test the validity of Waldorf's theory by conducting crack-propagation experiments with plastics and polycrystalline aluminum. By applying quasi-static tensile forces perpendicular to the line of small surface cracks, they found that the cracks widened prior to a sudden increase in length. This circumstance made it difficult to measure the crack velocities accurately and correlate them with the applied tensile stresses. Nevertheless, their results showed no indication that crack velocity is an exponential function of applied stress, as predicted by Waldorf's theory. In addition, photographs showed that the propagation was accompanied by considerable plastic flow at the crack tips. From these observations, it was concluded that omission of plastic flow effects in the Waldorf equation is a serious omission, since this flow can appreciably alter the effective stress at the crack tips under suitable conditions. This phenomenon will also modify the temperature dependence of the strength of the material on the _a priori_ determined parameters of the theory.

From these considerations, it would appear that the Waldorf model in its present form is applicable only to very brittle materials. It should be noted, however, that stress wave propagation in uniaxial strain inhibits plastic flow due to the triaxiality of the stress state and the high strain rates. Thus, the results of the crack-propagation study done by Louie and others do not prove conclusively that the Waldorf model is unsuited to the prediction of spall in ductile materials. Experimental verification of the Waldorf theory for the stress levels and pulse durations associated with plate-slap impact spallation has yet to be provided.

SUMMARY

Three major categories of spall fracture in materials have been identified. In the order of decreasing associated stress levels, they are; ultimate or cohesive spall, phase transformation spall, and ductile or low-pressure spall. Low-pressure spall has been further subdivided into complete spall, intermediate spall, and incipient spall. These low-pressure spall thresholds mentioned here are also listed in order of decreasing associated stress level. Damage done to materials at the low-pressure spall thresholds varies from separation of large parts of the material at the complete spall threshold to microcrack formation at the incipient spall threshold.

Several investigators have found that other parameters, in addition to a unique value of tensile stress at the spall plane, are necessary to the formulation of an adequate spall criterion. Parameters that have been found experimentally or offered in the way of conjecture as influencing the spall behavior of materials are; tensile pulse duration at the spall plane, strain and stress rates as the spall plane is loaded in tension, spatial stress gradients representing the unloading of the spall plane from a maximum value of tension, precompression of the material at the spall plane, ambient temperature, yield strength, and metallurgical characteristics such as grain orientation.

Spall models which would appear to have some feasibility for the prediction of spall at intermediate stress levels are neither abundant nor verified. Four basically different types of models exist: the Cumulative model, the Energy model, the Stress-Rate model, and the Bond-Breaking model. The first three of these models are of a phenomenological or empirical nature, while the last represents an attempt to describe time-dependent fracture in terms of processes taking place at the atomic level of activity.

The cumulative model purports to predict the spall due to an arbitrarily shaped pulse by combining previously obtained rectangular pulse data in a cumulative manner. Thus, if the relationship between spall delay time and constant applied tensile stress is known for all values of stress, the arbitrary pulse in question can be approximated by a series of rectangular pulses whose time durations can be compared with the data. The ratio of the duration of the approximating

pulse to the spall delay time corresponding to that stress level is calculated for each approximating pulse consecutively and added to the sum of those calculated previously. Spall occurs when the accumulated sum of these ratios is equal to unity.

The Energy model conceived at Battelle is based on the criterion that the mechanical energy supplied to the spall plane up to the time of fracture is invariant. Thus, spall would be predicted to occur at the time. τ, when the following equation is satisfied:

$$K = \int_0^\tau \sigma_s V_s dt \; ; \tag{24}$$

where

$\sigma_s = \sigma_s(t)$ = net tensile stress at the spall plane,

$V_s = V_s(t)$ = net particle velocity at the spall plane,

K = the invariant spall energy in units of energy per unit area.

The Stress-Rate model uses the criterion that the tensile strength of a material is dependent on its tensile unloading characteristics, i.e., stress rate or stress gradient. For a given material, a locus of tensile stress versus corresponding stress-rate (or gradient) points, dividing spall and "no spall", can be determined empirically. To predict spall due to an arbitrary pulse, tensile stresses and stress rates are calculated and compared with the critical values lying on the locus.

The Bond-Breaking model represents an attempt to predict spall from physical, rather than phenomenological considerations. For a microscopically homogeneous material, i.e., a single crystal, the relationship between time required for fracture and applied tensile stress is found by integrating an equation expressing the rate at which atomic bonds are broken as a function of stress. Using this relationship to determine an expression for crack-propagation velocity in terms of stress, and assuming a typical size and distribution of microcracks, a delay time versus applied stress relationship is found for polycrystalline materials. Since the delay time versus applied stress relations are derived from physical considerations, the constants in the equations represent physical characteristics of the material rather than the empirical "black boxes" of the preceding models. Some of the material constants that are required are the vibrational frequency of the lattice, the sublimation energy, and grain size.

REFERENCES

1. McClintock, F., and Argon, A., Mechanical Behavior of Materials, Addison-Wesley, Reading, Massachusetts (1966), 770 pp.

2. Progress in Material Science 12, Edited by Chalmers and King, Pergamon Press, New York (1963), "The Fracture of Metals", (Low, J.).

3. Fundamental Phenomena in the Materials Sciences 4, Edited by Bonis, Duga, and Gilman, Plenum Press, New York (1967), "The Microstructural Aspects of Tensile Fracture", (McMahon, C., Jr.).

4. Gilman, J., "Physical Nature of Plastic Flow and Fracture", paper presented at Proceedings of the Second Symposium on Naval Structural Mechanics: Plasticity, Pergamon Press, London, England (1960), pp. 43-99.

5. Herrman, W., "Stress Wave Propagation and Spallation in Uniaxial Strain", Sandia Corporation, Albuquerque, New Mexico, ASD-TDR-62-399, 1962.

6. Rieder, Z., "Survey of Spallation Literature", Republic Aviation Corporation, Farmingdale, New York, SWR-TM-60-3, November 1959, Air Force Special Weapons Center, Kirtland AFB, New Mexico, Contract No. AF 29(601)-1777.

7. McQueen, R. and Marsh, S., "Ultimate Yield Strength of Copper", Journal of Applied Physics, Vol. 33, No. 2, pp. 654-665 (February 1962).

8. Erkman, J., "Smooth Spalls and the Polymorphism of Iron", Journal of Applied Physics, Vol. 32, No. 5, pp. 939-944 (May 1961).

9. Moss, G. and Glass, C., "Fracture of Fe With Stress Waves", Ballistic Research Laboratories, Aberdeen Proving Ground, Maryland Report No. 1289, 85 pp., July 1965.

10. Novikov, S., Divnov, I. and Ivanov, A., "Failure of Steel, Aluminum and Copper Under Explosive Shock Loading", The Physics of Metals and Metallography, Vol. 21, No. 4, pp. 122-128 (1966).

11. Ivanov, A., Novikov, S. and Tarasov, Yu., "Fragmentation Phenomena in Iron and Steel Caused by Explosive Shock Wave Interactions", Soviet Physics-Solid State, Vol. 4, No. 1, pp. 177-185 (July 1962).

12. Penning, J., Jr., Young, D. and Prindle, J., "Negative Equation of State and Spall Criteria", The Boeing Company, Seattle, Washington, RTD-TDR-63-3039, September 1963.

13. Smith, J., "Three Low-Pressure Spall Thresholds in Copper", paper presented at Symposium on the Dynamic Behavior of Materials, ASTM (1963)

14. Glass, C. M., Golaski, S. K., Misey, J. J. and Moss, G. L., "Fracture of Single Crystals Under Explosive Loading", paper presented at Symposium on the Dynamic Behavior of Materials, ASTM, pp. 287-305 (1963).

REFERENCES (Continued)

15. Broberg, K., "Studies on Scabbing of Solids Under Explosive Attack", Journal of Applied Mechanics, Vol. 22, pp. 317-323 (September 1955).

16. Broberg, K., "Some Aspects of the Mechanism of Scabbing", paper presented at International Symposium on Stress Wave Propagation in Materials, Edited by Davids, Interscience Publishers, Inc., New York (1960).

17. Butcher, B., Barker, L., Munson, D. and Lundergan, C., "Influence of Stress History on Time-Dependent Spa   "'etals", AIAA Journal, Vol. 2, No. 6, pp. 977-990 (June 1964).

18. Blincow, D. and Keller, D., "Experiments on the Mechanism of Spall", paper presented at Symposium on the Dynamic Behavior of Materials, ASTM (1963).

19. Al'Tshuler, L., Novikov, S. and Divnov, I., "The Relationship Between the Critical Breaking Stresses and the Time of Failure as a Result of the Explosive Stressing of Metals", Soviet Physics-Doklady, Vol. 11, No. 1, pp. 79-82 (July 1966).

20. Whiteman, P., "Preliminary Report on the Effect of Stress Rate on the Dynamic Fracture of Steel, Brass and Aluminum", Atomic Weapons Research Establishment, Aldermaston, Berkshire, Great Britain, Undex 445, S.W.A.N. No. 10/61 (December 1962).

21. Rinehart, J., "Practical Countermeasures for the Prevention of Spallation", Colorado School of Mines, Golden, Colorado, AFSWC-TR-60-7 (February 1960).

22. Buchanan, J. and James, H., "Measurement of High Intensity Stress Pulses", British Journal of Applied Physics, Vol. 10, pp. 290-295 (June 1959).

23. Response of Metals to High Velocity Deformation, Interscience Publishers, Inc., New York (1961), "On the Fracture of Solids Under Impulsive Loading Conditions", (O'Brien, J. and Davis, R.), Vol. 9, pp. 371-388.

24. Piacesi, R. and Watt, J., "A Study of the Role of Mechanical-Strength Properties on the Phenomena of Spallation", Naval Ordnance Laboratory, Silver Spring, Maryland, NOLTR 66-42, Ballistic Research Report 157, 26 pp. (January 1966).

25. Vitman, F., Ivanov, M. and Joffe, B., "Tensile Strength of Ductile Metals Under Sudden Load", The Physics of Metals and Metallography, Vol. 13, No. 5, pp. 717-723 (1964).

26. Plauson, R., Grimsley, J. and Solem, A., "Spall Studies in Copper", Naval Ordnance Laboratory, Silver Spring, Maryland, NOLTR 61-121, Preprint (December 1961).

REFERENCES (Continued)

27. Butcher, B. M., "Spallation in 6061-T6 Aluminum", Sandia Corporation, Albuquerque, New Mexico, SC-DC-66-2448, 1966.

28. Tuler, F. R. and Butcher, B. M., "A Criterion for the Time Dependence of Dynamic Fracture", to be published in the International Journal of Fracture Mechanics.

29. Hsiao, C., "Time Dependent Fracture", paper presented in Proceedings of Symposium on Structural Dynamics Under High Impulse Loading, ASD-TDR-63-140, pp. 325-355 (May 1963).

30. Wagner, M., Waldorf, W., and Louie, N., "Determination of Hugoniot Equations-of-State for Polymers and Re-Entry Vehicle Materials and Investigations of Fracture Phenomena", Aerojet-General Corporation, Downey, California, AFSWC-TDR-62-66, Vol. 1, August 1962.

31. Morgan, D., Averell, J., et al, "Optimizing Re-Entry Vehicle Materials to a High-Altitude Nuclear Effect", AVCO Corporation, Wilmington, Massachusetts, RTD-TDR-63-3018, August 1963.

32. Breed, B., Mader, C., and Venable, D., "Dynamic Tensile Strength Characteristics of Several Metals", Los Alamos Scientific Laboratory, University of California, Los Alamos, New Mexico.

33. Louie, N., Andersen, W., and Wagner, M., "Experimental Fracture Studies and Equation-of-State Measurements", Aerojet-General Corporation, Downey, California, RTD TDR-63-3102, March 1964, Contract No. AF 29(601)-5382.

APPENDIX A

BASIC PRINCIPLES OF C^ /TINUUM THEORY

BASIC PRINCIPLES OF CONTINUUM THEORY

The fundamental principles of continuum theory are restated briefly in this Appendix. Although it is possible to present these principles in their general tensorial form, this would only tend to obscure the fundamental simplicity of the postulates. These are

> CONSERVATION OF MASS,
> CONSERVATION OF MOMENTUM,
> CONSERVATION OF MOMENT-OF-MOMENTUM,
> CONSERVATION OF ENERGY.

If thermodynamic effects are included in a continuum formulation, to the above must be added the

> PRINCIPLE OF ENTROPY.

In addition, the basic concepts of

> STRESS, STRAIN

must be included.

The above postulates pertain to all media and do not contain the distinguishing characteristics of a particular material. There must be included, therefore, a material characterizing relation in the form of a

> CONSTITUTIVE EQUATION

that relates the basic state variables (e.g., stress, internal energy, and temperature).

It is to this basic equation, descriptive of a material and its relation to the stress wave propagation problem, that attention is directed in the following appendices. The various postulates are given mathematical formulations convenient to the applications at hand.

APPENDIX B

ELASTIC WAVES

APPENDIX B

ELASTIC WAVES

When the propagation of plane compressional waves in an infinite, isotropic, elastic medium is considered, the previously stated postulates yield the equation of motion:

$$(\lambda + 2\mu) \frac{\partial^2 u}{\partial x^2} = \rho \frac{\partial^2 u}{\partial t^2} ; \qquad (B-1)$$

where u is displacement in the x direction, and λ, μ are material moduli (the Lamé constants). The constitutive equation is Hooke's Law, given as

$$\sigma_{ij} = \lambda \epsilon_{kk} \delta_{ij} + 2\mu \epsilon_{ij} ; \qquad (B-2)$$

where σ_{ij} is the stress, ϵ_{ij} the strain, and δ_{ij} the Kronecker delta, and the summation convention for repeated subscripts is utilized. The strain and displacements are related by the infinitesimal strain expression,

$$\epsilon_{ij} = \frac{1}{2} (u_{i,j} + u_{j,i}) . \qquad (B-3)$$

The stated case of propagation represents motion under conditions of one-dimensional strain. Thus, by replacing index notation with coordinate subscripts, one has

$$\epsilon_{xx} = \frac{\partial u}{\partial x} , \ \epsilon_{yy} = \epsilon_{zz} = 0 ,$$

$$\sigma_{xx} = (\lambda + 2\mu)\epsilon_{xx} , \ \sigma_{yy} = \sigma_{zz} = \lambda \epsilon_{xx} . \qquad (B-4)$$

The governing equation of motion (Equation B-1) is the wave equation, having the general solution

$$u = f(x + c_1 t) + g(x - c_1 t) , \qquad (B-5)$$

where $c_1 = [(\lambda + 2\mu)/\rho]^{\frac{1}{2}}$ is the dilatation velocity. The solution indicates that a given wave shape propagates undistorted with distance and at a constant velocity, c_1, as shown in Figure B-1.

FIGURE B-1. UNDISTORTED STRESS-PULSE PROPAGATION

The reflection of an elastic wave from a free boundary results in tension waves reflecting as compressive waves, and incoming compressive waves reflecting as tension waves. This latter phenomenon is the basic mechanism of spall fracture, both in the elastic and inelastic regimes.

Although the character of elastic waves is altered by interaction with boundaries, the waves do not interact with themselves. That is, leftward- and rightward-propagating elastic stress waves may encounter and pass through one another without consequent alteration of their wave shapes or propagation directions. During the duration of their encounter, the resulting stress and displacement fields will merely be the superposition of the individual fields. It will be found that the simple reflection and interaction behavior reviewed here for elastic waves does not hold for elastoplastic waves.

Finally, it is useful to review propagation of elastic waves in thin, straight rods, since many studies of dynamic material properties use this geometry. The bar geometry, which is the simplest case, is assumed to represent a one-dimensional stress situation and has the governing equation

$$E \frac{\partial^2 u}{\partial x^2} = \rho \frac{\partial^2 u}{\partial t^2} , \qquad (B-6)$$

where E is Young's modulus and is related to the previously given Lamé constant by $\lambda = E\nu/(1 + \nu)(1 - 2\nu)$. Only the σ_{xx} stress is nonzero, with all other stresses assumed zero; then

$$\sigma_{xx} = E\epsilon_{xx} , \quad \epsilon_{xx} = \partial u/\partial x . \qquad (B-7)$$

There are nonzero lateral strains, but since the inertia associated with the resultant motions is neglected, the remaining strain expressions are not required.

The governing equation is also the wave equation predicting constancy of wave shape. The propagation velocity is given as $c_B = \sqrt{E/\rho}$, and is somewhat less than the one-dimensional strain-wave velocity. For example, in steel, $c_1 = 22.4 \times 10^4$ in/sec and $c_B = 20 \times 10^4$ in/sec. This decreased velocity for the bar case may be interpreted as a result of relaxation of lateral constraints. For elastic-plastic waves, the plastic wave velocities are drastically different between one-dimensional stress and strain cases, whereas the velocities given above show only a slight di_ rence for the elastic case.

APPENDIX C

SHOCK WAVES

APPENDIX C

SHOCK WAVES

The preceding discussion of elastic waves represents wave propagation at very low stress regimes (of the order 10^4 psi). Under conditions of extremely high impulsive stress (pressures of the order 10^6 psi), shock waves develop and propagate in a material in a manner similar to the fluid dynamics situation. Thus, there is a propagating single wave front across which the material variables, such as density, stress, velocity, and energy, undergo large changes in short distances. Also, it becomes reasonable to consider the solid as behaving like a compressible fluid, described by an equation-of-state in the form $P = P(v)$, where v is the specific volume. Consequently, shock wave propagation, as in the case of elastic waves, has inherent simplifying features (simplified equation-of-state versus linear elastic behavior) permitting ready solution to the stress wave problem, at least for the one-dimensional strain case.

The theory of shock wave propagation, again in contrast to the elastic-plastic case, has been reviewed extensively. (See, for example, References C-1 and C-2.) As a result, only one or two major aspects of the theory, useful for later comparisons with the elastic-plastic case, will be reviewed here.

Consider a shock wave propagating, as shown in Figure C-1.

$$U = \text{shock velocity}$$

$$
\begin{array}{c|c}
P_1, \ \rho_1 & P_o, \ \rho_o \\
u_1, \ E_1 & E_o
\end{array}
$$

FIGURE C-1. PROPAGATING SHOCK FRONT

The conservation of mass, momentum, and energy-equations applied across the shock front are, respectively:

$$\rho_o U = \rho_1 (U - u_1), \qquad \text{(a)}$$

$$P_1 - P_o = \rho_o U u_1, \qquad \text{(b)}$$

$$p_1 u_1 = \frac{\rho_o U u_1^2}{2} + \rho_o U(E_1 - E_o). \qquad (c) \qquad (C-1)$$

According to these equations, velocities, densities, pressures, and energies are discontinuous across the shock front, but they are related as given above. There is a total of eight parameters in the three equations above (ρ_o, ρ_1, p_o, p_1, U, u_1, E_o, E_1). If it is assumed that E_o, ρ_o, and p_o are known, three equations in five unknowns remain. By eliminating U and u_1 between two of the equations, the equation can be reduced to

$$E_1 - E_o = 1/2 \left(\frac{1}{\rho_o} - \frac{1}{\rho_1} \right) (p_1 + p_o) . \qquad (C-2)$$

This establishes the states (E_1, ρ_1, p_1) that can be reached by a shock transition from an initial state (E_o, ρ_o, p_o). By elimination of the particle velocity, u_1, from the mass and momentum equations above, an equation for the shock velocity becomes

$$U = \frac{1}{\rho_o} [(p_1 - p_o)/(v_o - v_1)]^{\frac{1}{2}} ; \qquad (C-3)$$

where $v_o = 1/\rho_1$ and $v_1 = 1/\rho_1$ are the specific volumes.

When a plane shock wave arrives at a free surface, the shock pressure, p_r is reduced to zero by a rarefaction wave from the free surface. Both the arriving compression and reflected rarefaction waves impart particle velocities to the free surface. The total free surface motion, u_f, is given by

$$u_f = u_c + u_r ; \qquad (C-4)$$

where u_c and u_r are the compression and rarefaction particle velocities, respectively. Experiments have shown that $u_c \cong u_r$. Hence, from Equation C-4, it is concluded that the particle velocity, u, is equal to one-half the free surface velocity,

$$u = \frac{1}{2} u_f . \qquad (C-5)$$

Experimental measurements enable one to obtain the shock velocity and free surface velocity. These results, coupled with the conservation equations, are sufficient to determine the equation-of-state for the material. As an example, consider the results obtained from an experiment on Armco iron.[C-3] Measurements indicated that

$$
\begin{aligned}
\rho_o &= 7.87 \text{ g/cc,} \\
U &= 6.06 \times 10^5 \text{ cm/sec,} \\
u_f &= 2.786 \times 10^5 \text{ cm/sec,} \\
p_o &= 1 \times 10^9 \text{ dynes/cm}^2 \text{ .}
\end{aligned} \tag{C-6}
$$

From Equation C-5,

$$
u = 1.393 \times 10^5 \text{ cm/sec .} \tag{C-7}
$$

By substituting in Equation C-1 (b) and solving for p_1, one obtains

$$
p_1 = 665 \times 10^9 \text{ dynes/cm}^2 = 665 \text{ kbar .} \tag{C-8}
$$

To obtain the specific volume v_1, the above data is substituted in Equation C-3 and solved by v_1, giving

$$
v_1 = 0.09787 \text{ gram/cm}^3 \text{ .} \tag{C-9}
$$

Consequently, $v_1/v_o = 0.77$, indicating that the iron was compressed to 77% of its original volume.

The results of a series of experiments at differing shock pressures constitute a Hugoniot equation-of-state curve which relates pressure to specific volume. A typical result for copper is shown in Figure C-2.

Because of permanent deformations and heat generation that occurs during the shock transition, the Hugoniot is neither an adiabatic nor an isothermal curve. It is, instead, a dynamic compressibility curve representing an irreversible process; that is, $S_1 - S_o > 0$. However, more detailed thermodynamic considerations show that dS is small, and that it is a reasonable

approximation to consider the process as isentropic (i.e., constant entropy). This approximation, which is useful at shock pressure, will also be used in the elastic-plastic wave process.
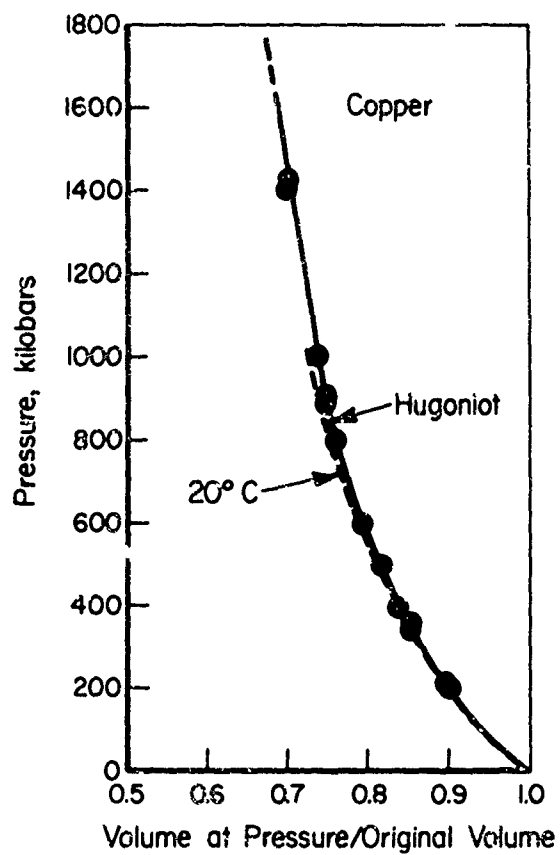
FIGURE C-2. HUGONIOT CURVE FOR COPPER[C-3]

APPENDIX C

REFERENCES

C-1. Solid State Physics, Academic Press, New York (1958), "Compression of Solids by Strong Shock Waves", (Rice, M. H., McQueen, R. G., and Walsh, J. M.).

C-2. Response of Metals to High Velocity Deformation, Edited by Shewmon and Zackay, Interscience Publishing Company, New York (1960), (Dwell, G. E.), pp. 165-203.

C-3. Zukas, E. G., "Shock Wave Strengthening", Metal Engineering Quarterly, pp. 1-20 (May 1966).

APPENDIX D

ELASTIC-PLASTIC WAVE PROPAGATION

APPENDIX D

ELASTIC-PLASTIC WAVE PROPAGATION

The past sections have reviewed briefly the basic principles of continuum theory and some of the major features of elastic and shock wave propagation. The cases of wave propagation considered represented extremes in terms of stress levels, with elastic waves corresponding to wave propagation at low stress levels and shock waves corresponding to extremely high stress levels. It was noted that at either extreme, various assumptions tending to simplify the propagation problem became reasonable. The present case of elastic-plastic waves represents the intermediate case of stress level.

At intermediate stress levels, the inherent ability of solid materials to support significant shear stresses makes the assumption of ideal fluid behavior used in shock analysis a less accurate one. Thus, neglecting material rigidity, which represents a realistic assumption at extremely high stresses, becomes less plausible at intermediate stress levels and must be replaced by a more accurate model of the material.

In this section, the theory of plasticity will be applied to the derivation of the governing equations for stress wave propagation under conditions of one-dimensional strain. A number of complicating subsidiary effects, known to exist in some materials, will be neglected in this preliminary review of theory, but will be considered in later sections. Attention will, instead, be focused on the major features of wave propagation and the governing equations.

The Longitudinal Stress-Strain Relationship

In this section, the essential features of stress-strain curves resulting from quasi-static, uniaxial-stress test conditions will be reviewed, as well as the idealized forms used for mathematical analysis. The construction of the elastic-plastic stress-strain relations corresponding to conditions of uniaxial strain will then be given.

Stress-Strain Relations Under Uniaxial Stress

Representative results of stress-strain curves obtained for various materials under quasi-static, isothermal, uniaxial tensile-stress conditions are shown in Figure D-1.
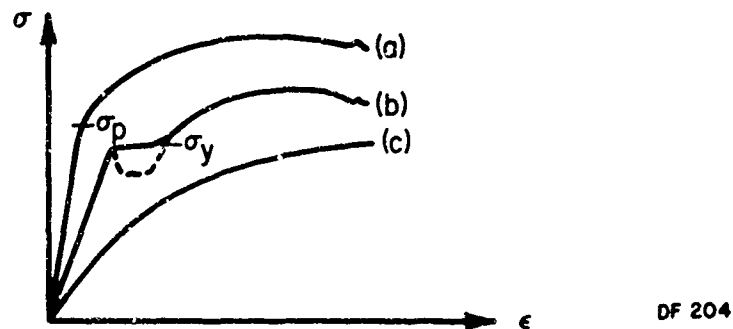
FIGURE D-1. TYPICAL STRESS-STRAIN CURVES FOR VARIOUS MATERIALS

The curves are not meant to represent any specific material, but, instead, to illustrate a number of properties. Thus, material (a) is a linear elastic material until the proportional limit, σ_p, is reached. Beyond σ_p, the material deforms plastically. The increasing stress with strain, however, indicates that work-hardening is occurring. Material (b) possesses a definite yield point, σ_y. In some cases, a lower yield point exists, as indicated by the dotted line. Material (c) has no well-defined, proportional limit. Of course, such material behavior represents the macroscopic response of the material and is a consequence of the microscopic deformation processes reviewed earlier in this report.

The behavior described above is a result of a continually increasing load. If the specimen is unloaded, reverse loaded, or load cycled during a test, responses as depicted in Figure D-2 are possible.

FIGURE D-2. TYPICAL LOAD CYCLING AND REVERSE LOADING CURVE

Thus, the material has been loaded beyond its yield point, and then unloaded (a). Upon reloading, a small hysteresis loop is formed. Both unloading and loading are elastic until, in the latter case, the load reaches the original unloading value, (b), at which yieldin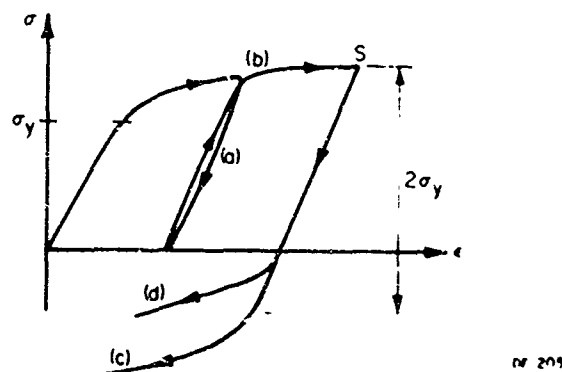g again occurs. If, at a later stage, unloading and then reverse loading occurs, reverse yielding takes place approximately at (c), which is the magnitude of the maximum stress attained less twice the yield stress, σ_y. However, reverse yielding may occur at a somewhat lesser value, (d), in which case the material is said to exhibit the Bauschinger effect.

A detailed mathematical representation of the actual stress-strain curve is generally too complicated for use in analysis. Hence, simplifications are often adopted which, although approximating the actual stress-strain relations, greatly reduce the complexity of the mathematical representation. Figure D-3 shows a number of idealized curves.
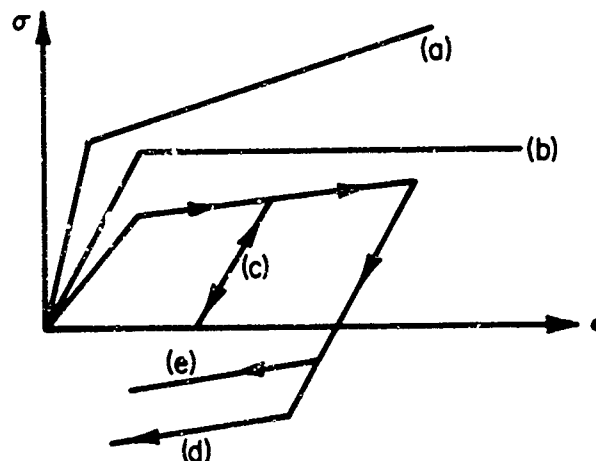
DF 206

FIGURE D-3. MATHEMATICAL IDEALIZATIONS OF STRESS-STRAIN CURVES

In Figure D-3, (a) is a bilinear representation of an elastic-plastic material with work hardening; (b) is an elastic, perfectly-plastic material. The lower curve is an idealization of several aspects of unloading and reverse loading. Thus, the small hysteresis loop which occurs during load cycling has been neglected, (c). Reverse yielding is shown at (d), and a representation of the Bauschinger effect is indicated by (e).

The stress-strain relations, discussed in the foregoing, have been based on engineering stress and strain defined as

$$\sigma = \frac{P}{A} \, , \quad \epsilon = \frac{L - L_o}{L_o} \, . \tag{D-1}$$

However, these definitions are often replaced by true stress and true strain definitions, given as

$$\bar{\sigma} = \frac{P}{\bar{A}} \, , \quad \bar{\epsilon} = \ln \frac{L}{L_o} \, ; \tag{D-2}$$

where $\bar{A}$ represents the instantaneous cross-sectional area, and L is the current length. The relationships between the true stresses and strains and the engineering counterparts* are given by

$$\sigma = \frac{\bar{\sigma}}{1 + \epsilon} \, , \quad \bar{\epsilon} = \ln(1 + \epsilon) \, . \tag{D-3}$$

Stress-Strain Relations for Uniaxial Strain

The governing equations of elastic-plastic wave propagation for conditions of one-dimensional strain require the appropriate stress-strain relations. These will be derived in this section using plasticity theory and the quasi-static, stress-strain relations from uniaxial stress conditions. The basic concepts of plasticity theory will be reviewed briefly before developing the stress-strain relations using the Fowles procedure.[D-1]

Plasticity Theory. When a material is loaded, permanent deformation occurs as stresses exceed certain limits characteristic of the material, including its past loading history. Unloading allows a degree of elastic recovery. In plasticity theory, a basic assumption is made that there exists a scalar function, $f(\sigma_{ij}, \epsilon_{ij}^{P}, \kappa)$, called a yield function, which depends on the state of stress and strain and the history of loading. This function characterizes

---

* In the work that follows, the engineering definition is used.

the yielding of the material under any possible combination of stresses. Here, σ_{ij} is the stress state, e_{ij}^P is the plastic strain, and $\varkappa$ is a parameter representing the previous loading history. The equation, $f = 0$, represents a closed surface in the stress space. No change in plastic deformation occurs when $f < 0$. Plastic deformation only occurs for $f = 0$. No meaning is associated with $f > 0$, provided the material properties are independent of strain rate.

Yield functions of complete generality, containing the parameters indicated above and successfully describing all aspects of plastic deformation of materials, have not been developed. However, many materials may be adequately described by simplified forms of the yield function. Thus, if the plastic deformation characteristics of a material are isotropic and work-hardening effects are neglected, it is reasonable to assume that plastic yielding can depend only on the magnitudes of the three principal applied stresses, σ_1, σ_2, σ_3, and not on their directions. Hence, a yield function of the form[D-2]

$$f(J_1, J_2, J_3) = 0 \tag{D-4}$$

may be assumed, where J_i is the invariant in each of the first three stress tensors given by

$$J_1 = \sigma_1 + \sigma_2 + \sigma_3, \quad J_2 = -(\sigma_1\sigma_2 + \sigma_2\sigma_3 + \sigma_3\sigma_1),$$

$$J_3 = \sigma_1\sigma_2\sigma_3 . \tag{D-5}$$

However, experimental observations have indicated that plastic yielding is quite insensitive to hydrostatic stress. By introducing the deviatoric principal stresses, σ_1', σ_2', σ_3', defined as

$$\sigma_1' = \sigma_1 - \frac{1}{3}(\sigma_1 + \sigma_2 + \sigma_3),$$

$$\sigma_2' = \sigma_2 - \frac{1}{3}(\sigma_1 + \sigma_2 + \sigma_3), \quad \sigma_3' = \sigma_3 - \frac{1}{3}(\sigma_1 + \sigma_2 + \sigma_3), \tag{D-6}$$

and noting that $J_1' = \sigma_1' + \sigma_2' + \sigma_3' = 0$, the general form of the plastic yield criteria may be reduced to

$$f(J_2', J_3') = 0 . \tag{D-7}$$

Many specific forms of yield criteria have been suggested over the years. However, most of these have attributed some influence to hydrostatic stress and, thus, have not been in accord with experimental observations. The two simplest criteria not having this fault were those suggested by Tresca (1864) and von Mises (1913). The Tresca criterion states that yielding occurs when the maximum shear stress reaches a certain value; thus,

$$\sigma_1 - \sigma_3 = \text{constant} \qquad \text{(D-8)}$$

where $\sigma_1 \geq \sigma_2 \geq \sigma_3$. The above may be expressed in terms of J_2', J_3', but the results are somewhat cumbersome. [D-3]

The von Mises criterion does not involve the function J_3', but states that yielding occurs when J_2' reaches a critical value, given as

$$\sigma_{ij}' \, \sigma_{ij}' = \sigma_1'^2 + \sigma_2'^2 + \sigma_3'^2 = \text{constant}; \qquad \text{(D-9)}$$

where the deviatoric stress tensor, σ_{ij}', is defined in terms of σ_{ij} by

$$\sigma_{ij}' = \sigma_{ij} - \sigma\delta_{ij} . \qquad \text{(D-10)}$$

Both models describe elastic, perfectly-plastic behavior. For most metals, it is found that the von Mises criterion fits experimental data more closely, although the Tresca condition is simpler to use in theoretical applications. This difficulty is sometimes resolved by using the Tresca condition with an empirical adjustment factor intended to minimize the differences between the two results. Fortunately, in the one-dimensional situations to be considered, both criteria reduce to the same result.

The two major mathematical formulations of plasticity are identified as plastic deformation theory (also known as total strain theory) and plastic flow theory (also known as incremental theory). Although the deformation theory finds application in some problems involving continuous loading, it yields anomalous predictions under conditions of cyclic or reverse loading. The plastic flow theory, which relates increments of strain to increments of stress at any given state of stress and strain, has generally found the widest acceptance and application and is utilized in the present review.

In the elastic region, the relation between stress and strain is given by Hooke's Law. In incremental tensor form, this is

$$d\varepsilon_{ij}^{e} = \frac{d\sigma_{ij}'}{2\mu} + \frac{1 - 2\nu}{E} \delta_{ij} d\sigma \; ; \tag{D-11}$$

where $d\sigma_{ij}'$ is the deviatoric stress increment defined as

$$d\sigma_{ij}' = d\sigma_{ij} - d\sigma \; , \tag{D-12}$$

and $d\sigma = d\sigma_{ii}/3$ is the hydrostatic component. Compressive stresses and strains are taken as positive.

When the material is strained beyond the yield point, the total strain increment, $d\varepsilon_{ij}$, at a given state of strain is comprised of an elastic and a plastic portion given as

$$d\varepsilon_{ij} = d\varepsilon_{ij}^{e} + d\varepsilon_{ij}^{P} \; . \tag{D-13}$$

Hence, at a given stress-strain state, the increment of plastic work, dW_{p}, will be given as

$$dW_{p} = \sigma_{ij} \, d\varepsilon_{ij}^{p} \; . \tag{D-14}$$

The von Mises yield criterion has the form

$$Y(W_{p}) = \left(\frac{3}{2}\right)^{\frac{1}{2}} (\sigma_{ij}' \, \sigma_{ij}')^{\frac{1}{2}} \; , \tag{D-15}$$

where Y is the yield stress in simple tension. Since Y may change as a result of work hardening (i.e., plastic work, W_{p}), this is accounted for by the functional form $Y(W_{p})$, and is illustrated in Figure D-4.
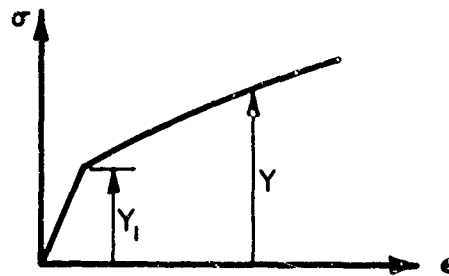
FIGURE D-4.   CHANGE OF YIELD POINT AS A RESULT OF PLASTIC WORK

Y_1 = initial yield point

Y = increasing value of yield point
as a result of plastic work.

Finally, it was previously pointed out that plastic deformation was observed to be insensitive to hydrostatic pressure. This observation is stated mathematically by requiring no permanent volumetric change due to plastic deformation; it is given as

$$de^p_{ii} =$$

(D-16)

The fundamental relations of elastic-plastic theory, mentioned above, will now be specialized to one-dimensional stress and one-dimensional strain situations.

One-Dimensional Stress. The one-dimensional stress situation corresponding to uniaxial tension and compression test conditions is approximately achieved during longitudinal wave propagation in rods. This phenomenon will be developed briefly here. To distinguish between later one-dimensional strain results, the direction of stress will be taken here as the s direction. Then, the incremental elastic stress-strain relations, Equation D-11, become

$$de^e_s = \frac{d\sigma'_s}{2\mu} + \frac{(1 - 2\nu)}{3E}\, d\sigma = \frac{d\sigma_s}{E} .$$

(D-17)

The von Mises yield criterion (Equation D-15) reduces to $\sigma_s = Y(W_p)$. The expression for the increment of plastic work, dW_p, reduces to

$$dW_p = Y\, de^p_s ;$$

(D-18)

where $d\epsilon_s^p = d\epsilon_s - d\epsilon_s^e$. If there is no work hardening, Y = constant, and $dY = 0$ for the added strain increment. Consequently, $d\epsilon_s = 0$. For the more general case of work hardening (i.e., $dY \neq 0$), $d\epsilon_s^e = dY/E$ so that Equation D-18 becomes

$$dW_p = Y[d\epsilon_s - d\sigma_s/E] = Y[d\epsilon_s - dY/E]. \qquad (D-19)$$

The overall relationship of total work, plastic work, and increments of total work and plastic work is illustrated in Figure D-5. A diagram that helps clarify the remarks on the effects of work hardening on plastic strain and that led to Equation D-19 is given in Figure D-6.

(a)   (b)   DF 208
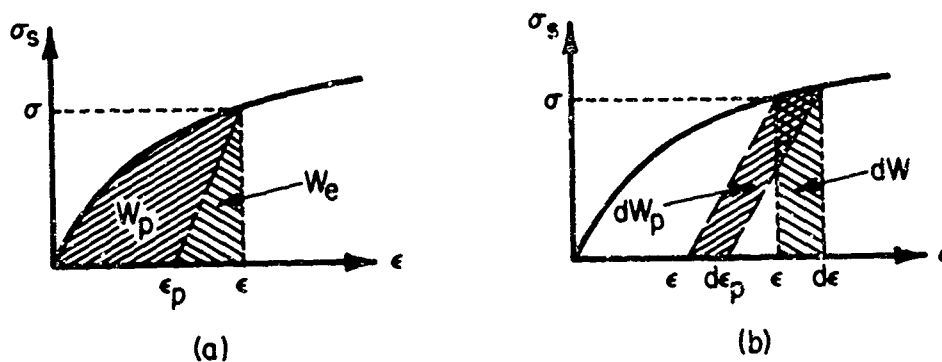
FIGURE D-5. WORK DONE DURING PLASTIC DEFORMATION

(a) W_p = plastic work, W_e = elastic work, and $W_p + W_e$ = total work at stress level σ.

(b) For added strain $d\epsilon$ at stress σ, dW = total added work, $dW_p = \sigma d\epsilon_p$ = irrecoverable plastic work.
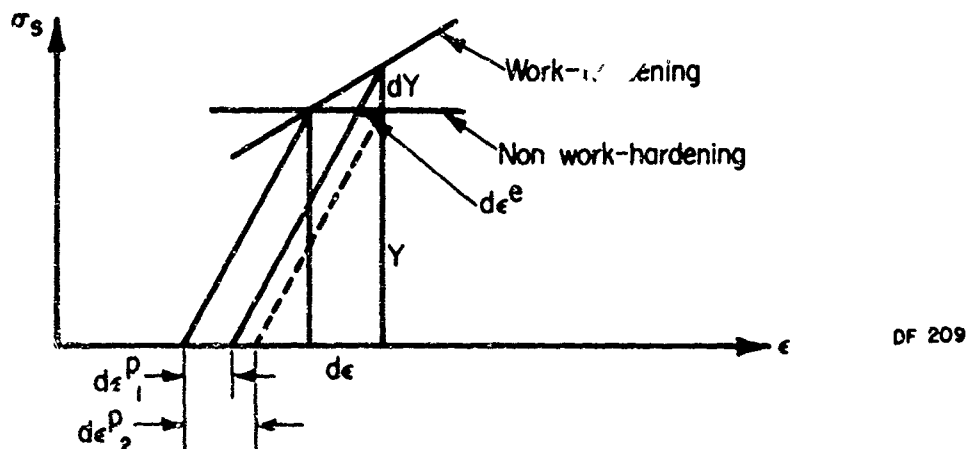
FIGURE D-6. EFFECTS OF WORK HARDENING ON THE RELATIONSHIP
BETWEEN TOTAL ELASTIC AND PLASTIC STRAIN

For work hardening, $d\epsilon_p = d\epsilon^P_1$, $d\epsilon^e = dY/E$.

If work hardening is absent, $dY = 0$, $d\epsilon^e = 0$, $d\epsilon_p = d\epsilon^P_2 = d\epsilon$.

One-Dimensional Strain. The x direction will be designated as the strain direction. The elastic relations, Equation D-11, then become

$$de_x^e = \frac{1}{E}(d\sigma_x - 2\nu\,d\sigma_y), \quad de_y^e = de_z^e = \frac{1}{E}(1-\nu)d\sigma_y - \nu d\sigma_x \; ; \qquad (D-20)$$

where the equality $d\sigma_y = d\sigma_z$, due to symmetry, has been utilized in the above. The plastic incompressibility relation, Equation D-16, becomes

$$de_x^p + 2de_y^p = 0 \; . \qquad (D-21)$$

The von Mises criterion (Equation D-15) reduces to

$$\sigma_x - \sigma_y = Y(W_p) \; . \qquad (D-22)$$

It should be recalled that the von Mises and Tresca yield criteria are identical under the conditions of uniaxial stress and uniaxial strain, as above.

Finally, the general relation for plastic work must be specialized to the present case. Thus, Equation D-14 reduces to

$$dW_p = \sigma_x de_x^p + 2\sigma_y \, de_y^p \; . \qquad (D-23)$$

However, $de_y^p = -de_x^p/2$ from Equation D-21, so that the above becomes

$$dW_p = (\sigma_x - \sigma_y)de_x^p \; . \qquad (D-24)$$

Using the yield condition, Equation D-22 thus becomes

$$dW_p = Y(W_p)de_x^p \; , \qquad (D-25)$$

which is the same as the case for one-dimensional stress.

In order to express the incremental plastic work in terms of total strain increment and work-hardening characteristics in a manner analogous to Equation D-19 for one-dimensional stress, the following relation is utilized:

$$de_x^p = d\epsilon_x - d\epsilon_x^e \; . \qquad (D-26)$$

Recall that, for the one-dimensional stress situation, the case of no work
hardening yielded $de_s^e = 0$; whereas for work hardening, $de_s^e = dY/E$ was obtained.
In the present case, from Equation D-11,

$$de_x^e = \frac{d\sigma_x'}{2\mu} + \frac{(1-2\nu)}{E} d\sigma \; ; \tag{D-27}$$

so that

$$de_x^P = de_x - \frac{d\sigma_x'}{2\mu} - \frac{(1-2\nu)}{E} d\sigma \; . \tag{D-28}$$

Expressions may be developed for $d\sigma_x'$, $d\sigma$ that make it possible to put the above
in the desired form. Thus it is observed that

$$de_{ii} = de_{ii}^P + de_{ii}^e = de_{ii}^e \tag{D-29}$$

by virtue of Equation D-16. However, $de_{ii} = de_x$, since $de_y = de_z = 0$. Then,
since $de_x^e = de_x - de^P$, Equation D-26 may be written as

$$de_{ii} = de_{ii}^e = \frac{d\sigma_{ii}'}{2\mu} + \frac{3(1-2\nu)}{E} d\sigma \; . \tag{D-30}$$

Noting that $d\sigma_x'$, $d\sigma_y'$ $(= d\sigma_z')$ are increments of the deviatoric principal stresses,
and recalling that in an earlier observation $J_1' = \sigma_1' + \sigma_2' + \sigma_3' = 0$, one finds
that $d\sigma_{ii}' = 0$. Consequently,

$$de_{ii} = de_x = \frac{3(1-2\nu)}{E} d\sigma \; . \tag{D-31}$$

It is further noted that

$$d\sigma_x' = d\sigma_x - d\sigma = d\sigma_x - \frac{1}{3} (d\sigma_x + 2d\sigma_y) = \frac{2}{3} (d\sigma_x - d\sigma_y) \; . \tag{D-32}$$

From the yield criterion, Equation D-22, $d\sigma_x - d\sigma_y = dY$ so that $d\sigma_x' = \frac{2}{3} dY$.
Substituting these results, and substituting Equation D-31 in Equation D-28, one
obtains

$$de_x^P = \frac{2}{3} \left[de_x - \frac{dY}{2\mu} \right] \; . \tag{D-33}$$

This permits expression of Equation D-25 in the desired form:

$$dW_p = \frac{2}{3} Y [d\epsilon_x - \frac{dY}{2\mu}] . \tag{D-34}$$

The next objective is to relate explicitly the stress increment, $d\sigma_x$, to the total strain increment, $d\epsilon_x$. Now, $d\epsilon_x = d\epsilon_x^e + d\epsilon_x^p$. The conditions of uniaxial strain require that $d\epsilon_y = d\epsilon_z = 0$, so that $d\epsilon_y^p = - d\epsilon_y^e$. Using this and Equation D-21, $d\epsilon_x^p = - 2d\epsilon_y^p = 2 d\epsilon_y^e$, so that the total strain increment, $d\epsilon_x$, is given by

$$d\epsilon_x = d\epsilon_x^e + 2d\epsilon_y^e . \tag{D-35}$$

Using Hooke's Law, Equation D-11, for $d\epsilon_x^e$, $d\epsilon_y^e$, one obtains

$$d\epsilon_x = \frac{(1-2\nu)}{E} (d\sigma_x + 2d\sigma_y) . \tag{D-36}$$

Now, the yield criterion may be put in the form

$$d\sigma_x + 2d\sigma_y = 3d\sigma_x - 2dY. \tag{D-37}$$

Hence, Equation D-36 becomes

$$d\epsilon_x = \frac{3(1-2\nu)}{E} (d\sigma_x - \frac{2}{3} dY). \tag{D-38}$$

From the relationships between the elastic moduli, the bulk modulus, K, is given by $K = E/3(1-2\nu)$ so that

$$d\sigma_x = K d\epsilon_x + \frac{2}{3} dY , \tag{D-39}$$

which is the desired incremental stress-strain relation. The mean stress, $d\sigma$, is given by $d\sigma = Kd\epsilon = Kd\epsilon_x$. Hence, Equation D-39 becomes $d\sigma_x - d\sigma = \frac{2}{3} dY$. This integrates to

$$\sigma_x - \sigma = \frac{2}{3} Y. \tag{D-40}$$

Thus, beyond the material yield limit, the difference between the one-dimensional strains and hydrostatic stress-strain curves is only a function of the material yield stress as a function of strain. If the material does not strain harden, $dY = 0$, $Y = Yo = $ constant, and $\sigma_x - \sigma = \frac{2}{3} Yo$.

Some of the features of the resulting stress-strain relations for one-dimensional strain are reviewed in Figure D-7.
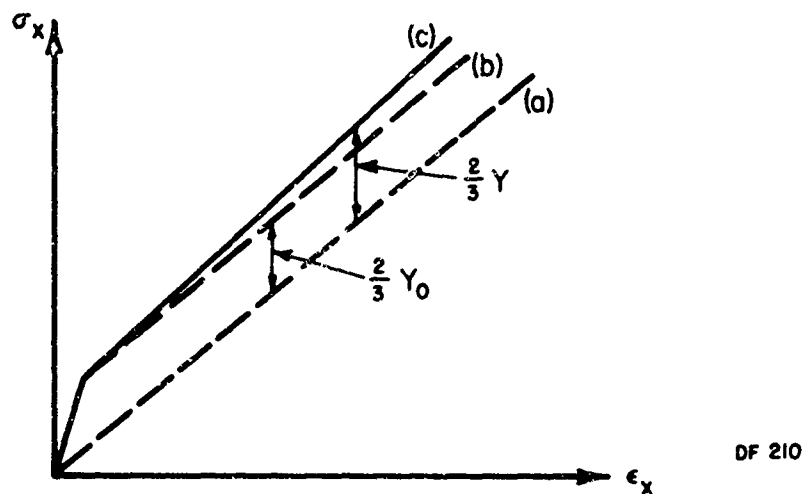

DF 210

FIGURE D-7. STRESS-STRAIN RELATION FOR
ONE-DIMENSIONAL STRAIN

(a) Material hydrostat; $d\sigma_x/d\epsilon_x = K = $ slope.

(b) Perfectly-plastic material; parallel to hydrostat but removed a distance $\frac{2}{3} Y_o$.

(c) Work-hardening material; $d\sigma_x = Kd\epsilon_x + \frac{2}{3} dY$.

It is also of interest to review the loading, unloading cycle for the one-dimensional strain case. This is shown in Figure D-8.
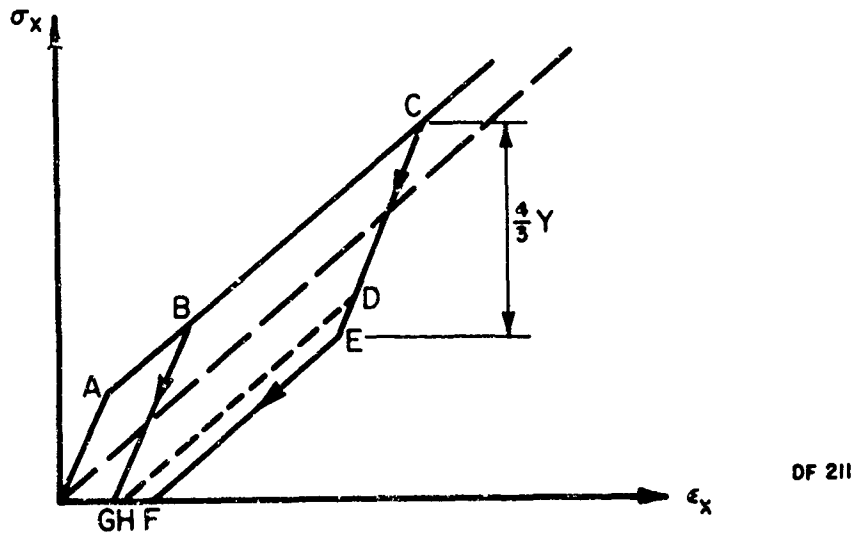
FIGURE D-8. LOADING-UNLOADING CYCLE FOR
ONE-DIMENSIONAL STRAIN

In cycle OABG, plastic yielding has occurred, but unloading has been purely elastic, BG. Cycle OACEF illustrates the reverse yielding that can occur under one-dimensional strain conditions at sufficiently high loads. Unloading from the maximum stress, C, is initially elastic, CE. At E, reverse yielding sets in, since the yield criterion is again satisfied. Further unloading, EF, is plastic and leaves a residual strain. Cycle OACDH illustrates reverse yielding with a Bauschinger effect.

The reverse yielding phenomenon during unloading represents one of the major differences between one-dimensional strain and one-dimensional stress loadings. A second major difference is the relative slopes of the stress-strain curves under the two conditions. The initial elastic portions of the two cases are given by

$$d\sigma_x/d\epsilon_x = \frac{E(1 - \nu)}{(1-2\nu) \, (1 + \nu)} = \text{one-dimensional strain}$$

and

$$d\sigma_s/d\epsilon_s = E \qquad = \text{one-dimensional stress} ,$$

and they are nearly the same for most materials. However, beyond the yield point, the slopes differ radically. Thus, for a non-work-hardening material, the slope of the one-dimensional strain case is $d\sigma_x/d\epsilon_x = K$, whereas, $d\sigma_s/d\epsilon_s = 0$. This factor will be of significance when wave-propagation velocities are considered.

The preceding development has served to delineate the major features of the stress-strain curve, such as the slopes of the curve (before and after yielding) and the relation to the hydrostat. It is evident that the parameters necessary for the construction of the curve are the elastic constants and the yield stress obtained from uniaxial stress experiments. In fact, if the stress-strain curve for uniaxial strain is to be approximated by straight line segments with an abrupt break at the yield stress, the preceding is sufficient. However, if a more detailed picture of the transition region between elastic and plastic behavior is desired, further considerations are necessary.

It is possible to obtain the desired information from uniaxial stress data, provided the comparison is made at corresponding values of strain for which the plastic work is the same. Equating increments of work, dW_p, for the two cases, as given by Equations D-19 and D-34, gives

$$\frac{2}{3} Y[d\epsilon_x - \frac{dY}{2\mu}] = Y[d\epsilon_s - \frac{dY}{E}] . \tag{D-41}$$

This simplifies to

$$d\epsilon_x = \frac{3}{2} d\epsilon_s - \frac{dY}{6K} . \tag{D-42}$$

If any variation in K with strain is neglected, the above may be integrated to give

$$\epsilon_x - \epsilon_x^o = \frac{3}{2} (\epsilon_s - \epsilon_s^o) - \frac{(Y-Y^o)}{6K} , \tag{D-43}$$

where the "o" superscript refers to initial yield values. However,

$$\epsilon_x^o = \frac{1+\nu}{E} Y^o, \epsilon_s^o = \frac{Y^o}{E} , \tag{D-44}$$

so that Equation D-43 reduces to

$$\epsilon_x = \frac{3}{2} \epsilon_s - \frac{Y}{6K} . \qquad (D-45)$$

Thus, the procedure is to calculate ϵ_x from uniaxial stress data, using Equation D-45, and to obtain σ_x, using Equation D-40 and the fact that $\sigma = K\epsilon_x$. Figure D-9 illustrates the procedure.
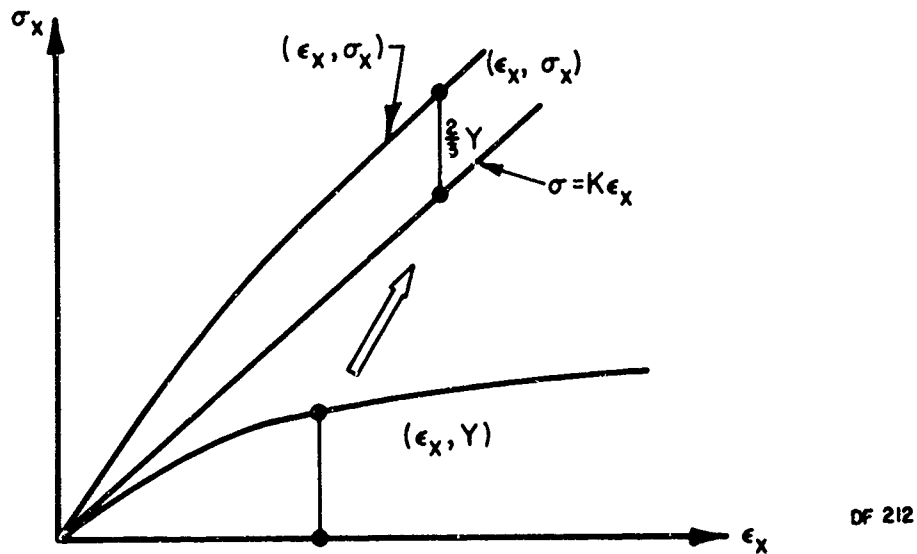
FIGURE D-9.   RELATION OF UNIAXIAL STRAIN
AND STRESS CURVES

A slightly modified procedure, described by Barker, et al,[D-4] calculates the strain offsets relative to the elastic slopes in order to establish the comparison.

At this stage, a constitutive relation between stress and strain for uniaxial strain conditions has been derived. The uniaxial stress, isothermal, quasi-static stress-strain curve has been utilized in the development. Variations in the elastic constants due to finite strain effects have been neglected.

The applicability of the resulting quasi-static relation to the dynamic situation of elastic-plastic wave propagation is, of course, open to question. Ultimately, the degree of comparison between experimental results and theoretical predictions will establish the applicability. These will be discussed in a later section in an attempt to arrive at an assessment of such items as strain rate, finite strain, thermodynamic and Bauschinger effects. For the immediate purpose of reviewing wave propagation, unobscured by the complicating effects mentioned above, the quasi-static, isothermal relation, as given by Equation D-39, will be used.

The Basic Governing Equations

The basic postulates of continuum mechanics will be applied to derive the governing equations of elastic-plastic wave propagation. The constitutive relations developed in the preceding section will be utilized and the method of characteristics will be applied to solve the equations. The development parallels that of Morland.[D-5]

Wave propagation in the x direction will be assumed, and a Lagrangian coordinate system (x,t) will be employed. Under these conditions, conservation of mass requires that

$$\rho(1 - \epsilon_x) = \rho_i \; ; \tag{D-46}$$

where ρ_i and ρ are initial and final densities, respectively; ϵ_x is the infinitesimal compressive strain defined as $\epsilon_x = - \partial u/\partial x$; and $u(x,t)$ is the particle displacement. Conservation of momentum gives

$$\frac{\partial v}{\partial t} = - \frac{1}{\rho_i} \frac{\partial \sigma_x}{\partial x} \; ; \tag{D-47}$$

where $v(x,t)$ is the particle velocity defined as $v = \partial u/\partial t$. The compressive stress is σ_x. Because uniaxial strain conditions will be assumed, there will also exist stresses σ_y and σ_z, where $\sigma_y = \sigma_z$.

Assuming the existence of a constitutive equation, $\sigma_x = \sigma_x(\epsilon_x)$, as discussed in the previous section, the above may be written as

$$\frac{\partial v}{\partial t} + c^2(\epsilon_x)\frac{\partial \epsilon_x}{\partial x} \; ; \tag{D-48}$$

where

$$c^2(\epsilon_x) = \frac{1}{\rho_i}\frac{d\sigma_x}{d\epsilon_x} \; . \tag{D-49}$$

From the definitions of strain and velocity,

$$\frac{\partial v}{\partial x} = -\frac{\partial \epsilon_x}{\partial t} \; . \tag{D-50}$$

Using Equation D-50, Equation D-48 may also be written as

$$\frac{\partial^2 u}{\partial t^2} + c^2(\epsilon_x)\frac{\partial^2 u}{\partial x^2} \; . \tag{D-51}$$

The moment-of-momentum postulate of continuum mechanics does not enter here because of the uniform normal stresses and zero shear stresses. Similarly, the energy equation does not directly influence the development. Neglecting thermodynamic effects, it would merely represent a first integral of the momentum equation.

The method of characteristics will be used to solve the system governing equations, given by Equations D-48 and D-50. The characteristics in the x - t plane for these equations are given by

$$dx/dt = \pm C(\epsilon_x), \; \text{or} \; \frac{dt}{dx} = \pm \, ^1/C(\epsilon_x) \; . \tag{D-52}$$

The invariant quantities along these characteristics are

$$\frac{dx}{dt} = + C(\epsilon_x), \; v + \int^{\epsilon_x} C(\epsilon_x)d\epsilon_x = \text{constant} = R_1 \tag{D-53}$$

and

$$\frac{dx}{dt} = - C(\epsilon_x), \; v - \int^{\epsilon_x} C(\epsilon_x)d\epsilon_x = \text{constant} = R_2; \tag{D-54}$$

where the constants (R_1, R_2) are, in general, different along different characteristics.

Further information regarding the above constants may be developed as follows: Suppose the stress pulse is propagating into a uniform region of the material, where v and ϵ_x are constant. This would correspond to the situation before arrival of the pulse, where $v = \epsilon_x = 0$. It is represented by the shaded region of the $x - t$ plane in Figure D-10.
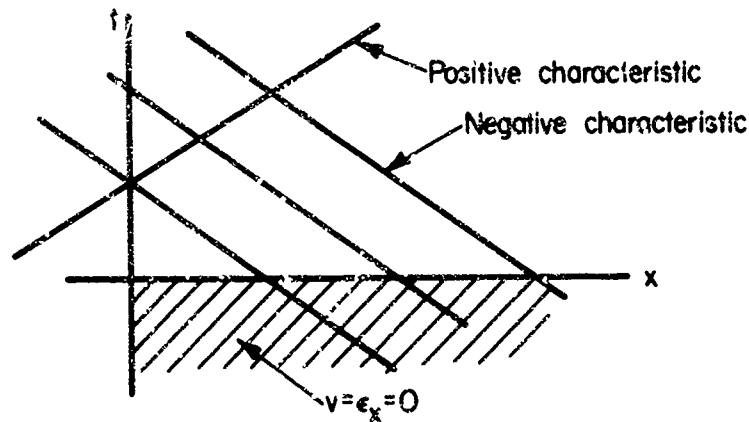
FIGURE D-10. THE $x - t$ PLANE, INCLUDING A UNIFORM
REGION OF $v = \epsilon_x = 0$

Since each negative characteristic passes through the uniform region, it may be concluded that the invariant, R_2, is the same for all characteristics and may be replaced by R. A positive characteristic is intersected at each point by a negative characteristic, so that along each positive characteristic

$$v + \int^{\epsilon_x} C(\epsilon_x)d\epsilon_x = R_1, \quad v - \int^{\epsilon_x} C(\epsilon_x)d\epsilon_x = R. \qquad (D-55)$$

Results of adding and subtracting the above are

$$v = \frac{R_1 + R}{2}, \quad \int^{\epsilon_x} C(\epsilon_x)d\epsilon_x = \frac{R_1 - R}{2}. \qquad (D-56)$$

In other words, v and $\int^{\epsilon_x} C(\epsilon_x) d\epsilon_x$ are separately constant along each positive characteristic. Further, since $C(\epsilon_x) > 0$, $\int^{\epsilon_x} C(\epsilon_x) d\epsilon_x$ is an increasing function of ϵ_x, it is concluded that c_x must remain constant along a positive characteristic if the integral is to remain constant. It follows directly that the dependent variables, $C(\epsilon_x)$, $\sigma_x(\epsilon_x)$, are also constant. A further result, useful in a later, limiting case, is obtained by integrating Equation D-47. Thus,

$$v - v_o = \frac{1}{\rho_1} \int_{t_o}^{t} \left(\frac{\partial \sigma_x}{\partial x} \right) dt \ . \tag{D-57}$$

Propagation of Elastic-Plastic Waves - General Description

The propagation of an elastic-plastic wave considered here is that initiated by a general, prescribed stress applied on the surface of a half-space. The essential features of the initial stages of propagation will be the existence of an elastic precursor or forerunner, a propagating plastic wave front lagging behind the elastic front, an elastic unloading front that is overtaking the plastic front, and finally, a possible plastic unloading front. The formation of plastic shock fronts will be considered, as well as specialized loading pulses. (However, treatment of complicated wave interactions that occur when unloading waves overtake the loading fronts will be treated in the next section.) The equations of motion and constitutive relations developed in the previous section will be utilized. Thus, complications due to strain-rate or Bauschinger effects will be avoided at this stage, as well as other subsidiary effects briefly discussed in the previous sections.

The prescribed stress pulse is shown in Figure D-11(a). Figure D-11(b) shows the associated stress-strain curve. Each stress amplitude propagates with the local slope of the stress-strain curve. The associated Lagrangian diagram is shown in Figure D-12.
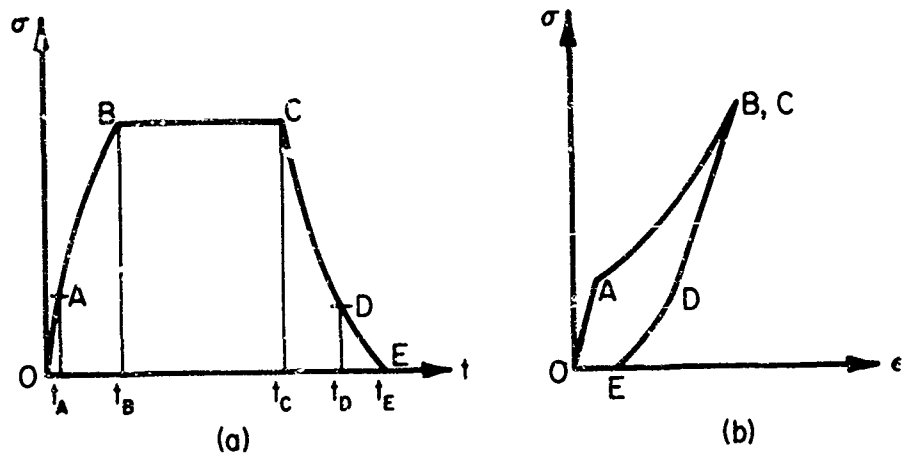
FIGURE D-11 (a). APPLIED PRESSURE PULSE
(b). STRESS-STRAIN CURVE FOR THE MATERIAL
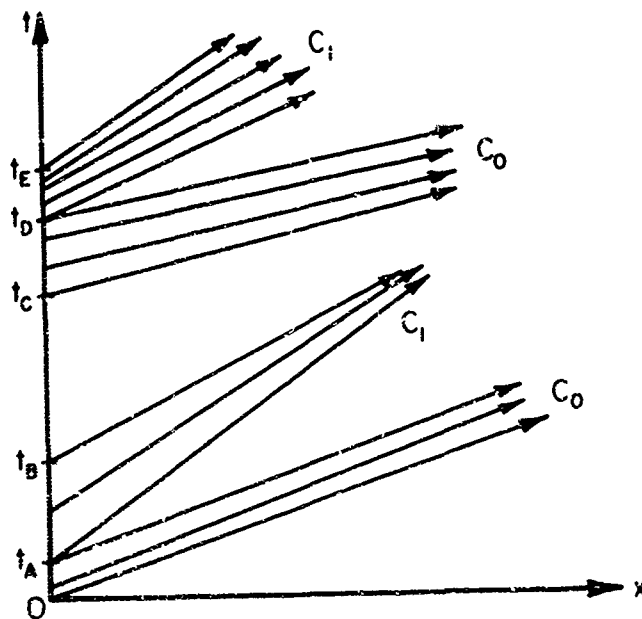
FIGURE D-12. LAGRANGIAN DIAGRAM DESCRIBING
PRELIMINARY STAGES OF ELASTIC-
PLASTIC PULSE PROPAGATION

The portion OA of the pulse propagates with the elastic velocity, C_o. These are represented on the Lagrangian diagram by the rays emanating between 0 and t_A, the time duration of the elastic portion of the pulse. The AB portion of the pulse is represented by rays from t_A - t_B of the Lagrangian diagram. The various stress levels of this portion propagate with different velocities, as indicated by the variation of slope of the stress-strain diagram in the AB region. Thus, because of the upward curvature of AB, higher values of stress propagate at higher velocities. This is indicated by the clustering together of the rays from t_A - t_B. A region of constant stress, BC, then exists from t_B to t_C.

Unloading occurs along CE. The initial stage, CD, is elastic and is indicated in the Lagrangian diagram by rays from t_C - t_D. The final stage of unloading, DE, is anelastic due to reverse yielding and has various velocities associated with the various stress levels. The rays from t_D - t_E represent this region. The divergence of this family of rays is a consequence of unloading from higher stress with associated higher velocities to lower stress with associated lower velocity levels.

It is of interest to consider the variations of pulse shape that arise from variations of wave velocity indicated in the foregoing. There would, of course, be no such variations if the loading were within the elastic region, since the stress-strain curve would have constant slope. All rays of the Lagrangian diagram would then be parallel and would indicate undistorted propagation of the stress pulse. However, variations do occur for the anelastic case, as shown in Figure D-13, where the pulse shapes at two time instants are shown. The major features of Figure D-13 are: (a) the elastic precursor or forerunner, OA; (b) the plastic wave, AB, whose front is increasingly steep due to the greater propagation velocity of the higher stress levels; (c) the region of constant stress, BC, that is diminishing because of the overtaking elastic unloading wave, CD; (d) the plastic tail, DE, that is becoming stretched out because of the slower propagation velocity of the lower stresses. Because the effects described are essentially related to the stress-amplitude dependence of the velocity, the subsequent wave distortion is referred to as amplitude dispersion.
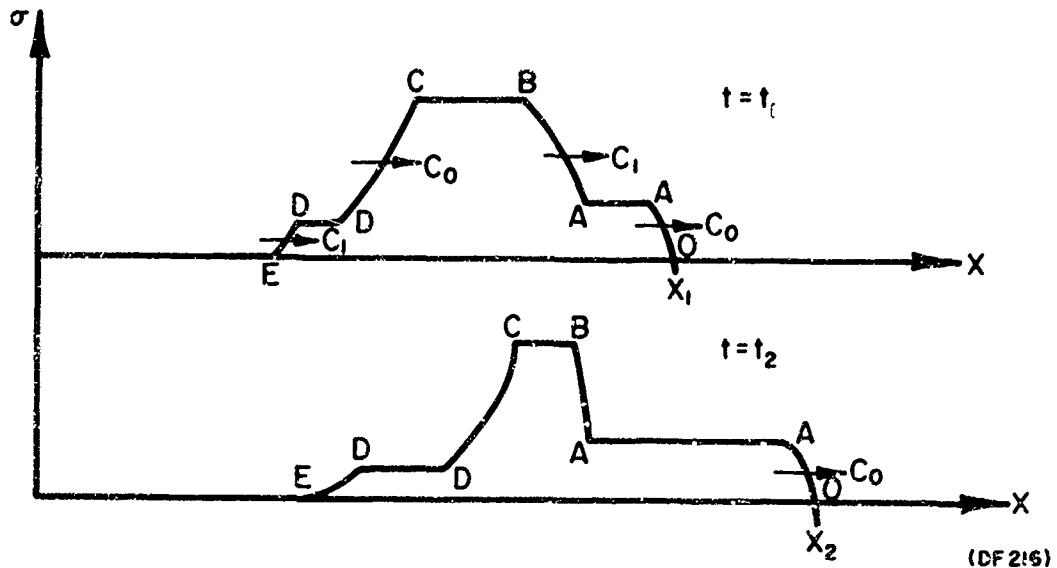
FIGURE D-13.   VARIATIONS IN STRESS PULSE AT TWO INSTANTS OF TIME

This description of the progressive variation in the wave shape has been terminated before two major events have occurred. These are the formation of a plastic shock front at AB and the overtaking of the loading front (either before or after shock formation) by the unloading front, CD. Consideration will be given to shock formation. The stages leading to this situation are shown in Figure D-14. The steepening of the front is shown for $t = t_0$, t_1, t_2.
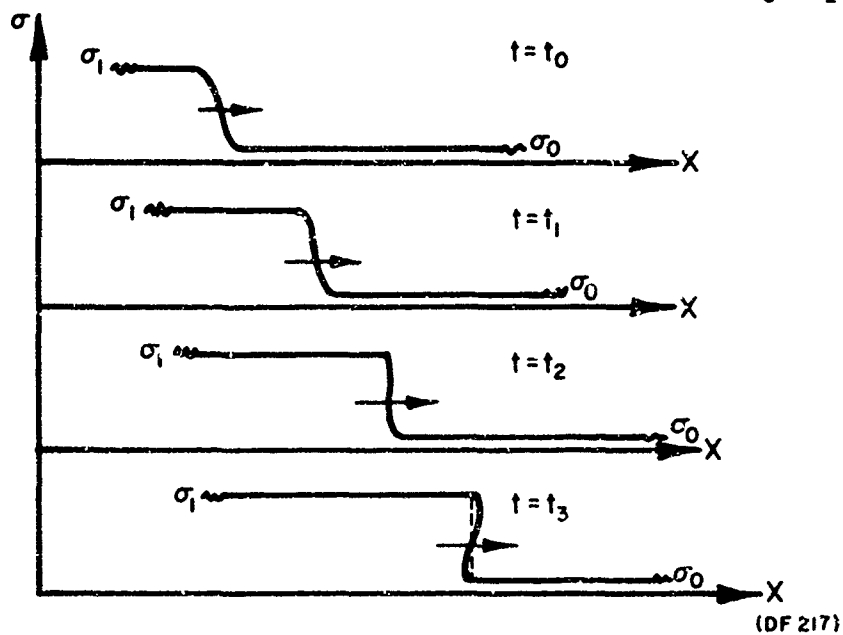
FIGURE D-14.   FORMATION OF THE PLASTIC SHOCK FRONT

At $t = t_3$, a physically unacceptable situation has arisen as the more rapidly traveling stress components have "overlapped" the slower, lower stress level portion of the wave. This situation is indicated on the Lagrangian diagram by the crossing of characteristics.

It is when the wavefront, or a portion of the wavefront, becomes vertical that the continuous plastic wave front breaks down and a discontinuous shock front is formed traveling at a shock velocity, U. Across the shock front, the variables of stress, density, velocity, and internal energy vary discontinuously as shown in Figure D-15.
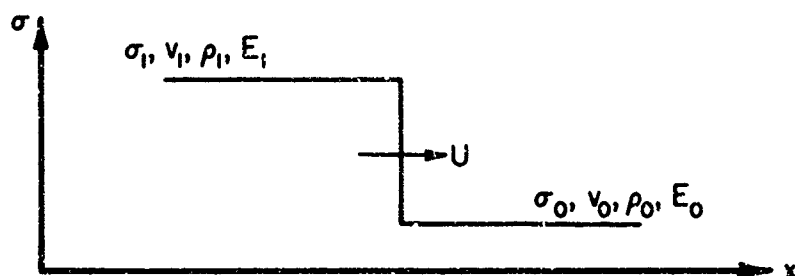
FIGURE D-15. SHOCK FRONT ACROSS WHICH MATERIAL
VARIABLES CHANGE DISCONTINUOUSLY

The equations of conservation of mass, momentum, and energy still pertain in the region separating the two states, σ_0 and σ_1. If $q_0 = v_0 - U$ and $q_1 = v_1 - U$ define the material velocities relative to the shock, the mass and momentum equations become

$$\rho_1 q_1 = \rho_0 q_0 \ , \quad \sigma_1 - \sigma_0 = \rho_0 q_0^2 - \rho_1 q_1^2 \ . \tag{D-58}$$

These may be solved to give

$$q_0^2 = \frac{\rho_1 (\sigma_1 - \sigma_0)}{\rho_0 (\rho_1 - \rho_0)}, \quad q_1^2 = \frac{\rho_0 (\sigma_1 - \sigma_0)}{\rho_1 (\rho_1 - \rho_0)} \ . \tag{D-59}$$

Conservation of energy is expressed by

$$\rho_1 q_1 E_1 - \rho_0 q_0 E_0 = \sigma_0 q_0 - \sigma_1 q_1 + \frac{1}{2} \rho_0 q_0^3 - \frac{1}{2} \rho_1 q_1^3 , \qquad (D\text{-}60)$$

where E_0, E_1 are the internal energies. When the values of q_1, q_0 given in Equation D-59 are substituted in the energy expression, one obtains

$$E_1 - E_0 = \frac{1}{2} (\sigma_1 + \sigma_0) \left(\frac{1}{\rho_0} - \frac{1}{\rho_1}\right) . \qquad (D\text{-}61)$$

This is the well-known Rankine-Hugoniot relation presented earlier in the review of hydrodynamic shock theory. By substituting for ρ in terms of E, the results for q_0, q_1 become

$$q_0 = -(1-\epsilon_0)\left[\frac{\sigma_1 - \sigma_0}{\rho_1(\epsilon_1 - \epsilon_0)}\right]^{\frac{1}{2}} , \quad q_1 = -(1-\epsilon_1)\left[\frac{\sigma_1 - \sigma_0}{\rho_1(\epsilon_1 - \epsilon_0)}\right]^{\frac{1}{2}} . \qquad (D\text{-}62)$$

Finally, by defining the particle jump velocity across the shock as v_s,

$$v_s = v_1 - v_0 = (\epsilon_1 - \epsilon_0)\left[\frac{\sigma_1 - \sigma_0}{\rho_1(\epsilon_1 - \epsilon_0)}\right]^{\frac{1}{2}} . \qquad (D\text{-}63)$$

To complete the development, it would be useful to compare the predicted velocity jump via the shock mechanism to that predicted by the continuous solution. The details of this, which require assumption of the stress-strain curve form, will not be presented here. However, Morland[D-5] has investigated this and found that the difference between the two solutions is only about 0.3%. The magnitude of the shock velocity, U, is given by

$$U = v_0 + (1 - \epsilon_0)\left[\frac{\sigma_1 - \sigma_0}{\rho_1(\epsilon_1 - \epsilon_0)}\right]^{\frac{1}{2}} . \qquad (D\text{-}64)$$

Of particular interest in Equation D-64 is the form of the square root term, which can be interpreted in terms of the chord connecting the two points on the stress strain curve connected by the shock transition. This is shown in Figure D-16.

The location of the shock front in space and time must be considered. That is, the location, x, where the shock front forms must be established, as well as the subsequent location of the front, $x_s(t)$. The details of this, which
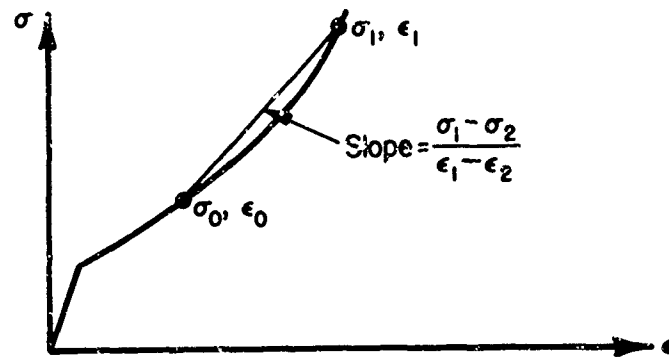
DF 219

FIGURE D-16.   SHOCK CHORD CONNECTING TWO
                STRESS-STRAIN STATES

have been developed by Morland for the general case, are somewhat involved.
However, for the case of a step-function loading, the situation is considerably
simplified as illustrated in Figure D-17. The loading pulse of magnitude, σ_m,
is shown in (a) of the figure. Since the stress rises immediately to σ_m, a
shock front immediately forms behind the elastic precursor, since none of the
lower stress level increments have had time to propagate ahead of higher stress
levels. In other words, the overtaking of stress levels, and breakdown into
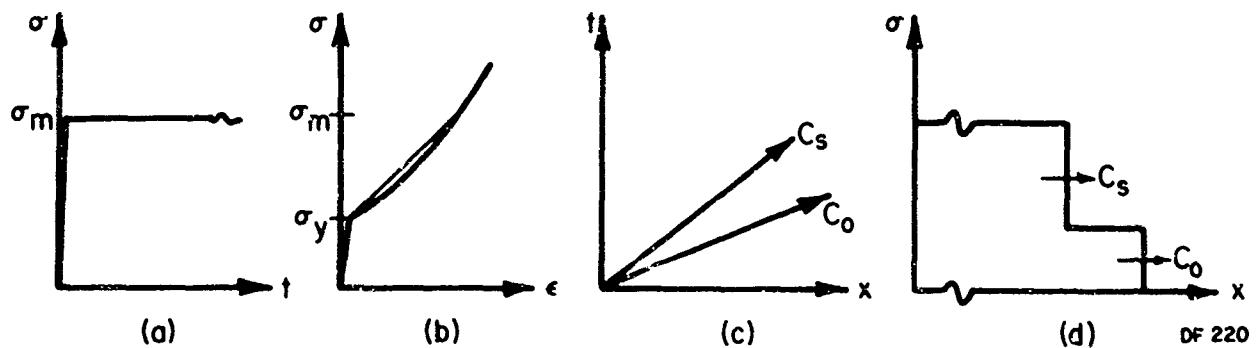
DF 220

FIGURE D-17.   SHOCK FORMATION FOR STEP-FUNCTION LOADING

shock that occurs for a smooth loading now occurs instantaneously under step loading. This is illustrated in (b) by the shock chord connecting σ_m and σ_y, and in (c) by only two rays from the origin. The resulting wave shape is shown in (d). Fortunately, the simplified case discussed is the one of greatest interest since it represents the nature of the stress pulse induced in plate-impact experiments.

Before concluding this section on shock formation, it is of interest to note other forms the elastic-plastic wave front may take due to variations in the stress-strain curve of the material. These are shown in Figure D-18, along with wave fronts characteristic of such materials.

(a)   (b)   (DF 221)
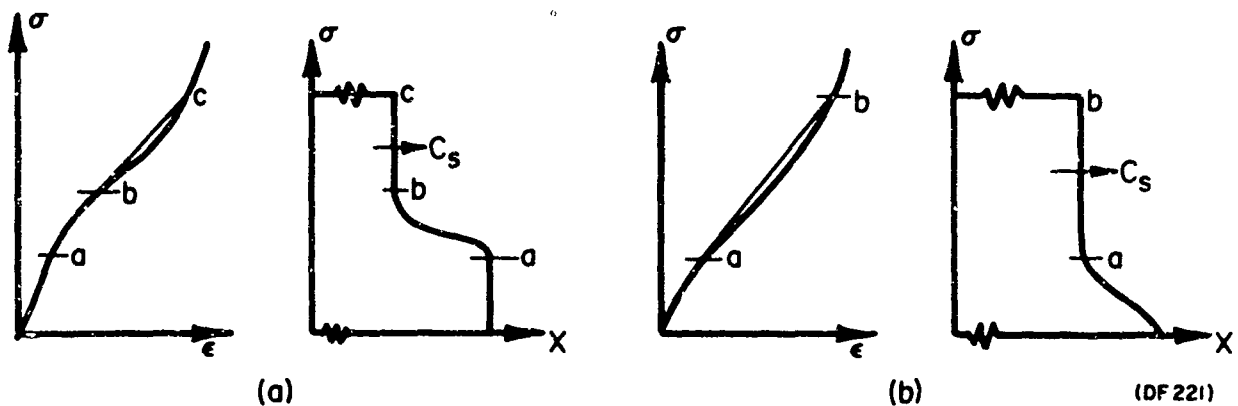
FIGURE D-18. VARIATIONS IN WAVEFORM DUE TO MATERIAL CHARACTERISTICS[D-6]
(a) Material without a well-defined yield point.
(b) Material without a linear elastic portion.

Elastic-Plastic Waves of Unloading and Reflection

The interaction between loading and unloading portions of the pulse occurs when the unloading wave overtakes the loading wave front. At this point, it is encountering a change in acoustic impedance and reflects from and transmits through this discontinuity accordingly. The general features of the reflection of elastic-plastic waves from a free surface will also be described.

The approach taken by Morland is to approximate the wave profile by a series of discontinuous steps, or stress increments, and to consider the interaction of these increments. A stress increment, $\delta\sigma$, propagating at a velocity, c, will cause a change of particle velocity, δv, and strain, $\delta\epsilon$. These quantities, which result from a discontinuous pulse, may be calculated from Equation D-57, which was developed for the continuous case by considering the limiting case of the pulse shown in Figure D-19.
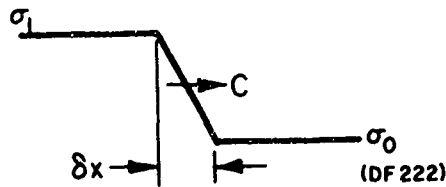
FIGURE D-19. PROPAGATING STRESS PULSE
OF LENGTH δx

Thus, in Equation D-57, it may be written that

$$\frac{\partial\sigma_x}{\partial x} = \frac{\sigma_1 - \sigma_0}{\delta x} = \frac{\delta\sigma}{\delta x} \ . \tag{D-65}$$

Noting that $\delta x = c\delta t$, it can be found that

$$\delta v = \frac{\delta\sigma}{\rho_i c\delta t} \int_{to}^{to+\delta t} dt = \frac{\delta\sigma}{\rho_i c} \ . \tag{D-66}$$

The jump in strain is found from the definition of c, i.e., $c^2 = \delta\sigma/\rho_i\delta\epsilon$. Thus,

$$\delta\epsilon = \delta\sigma/\rho_i c^2 \ . \tag{D-67}$$

Now consider the situation of an elastic unloading stress increment overtaking a plastic loading increment, as shown in Figure D-20. The dotted lines represent the point of interaction; α,β are particles on either side of this line. After interaction, a new stress, σ_3, exists at the interaction line. This may be
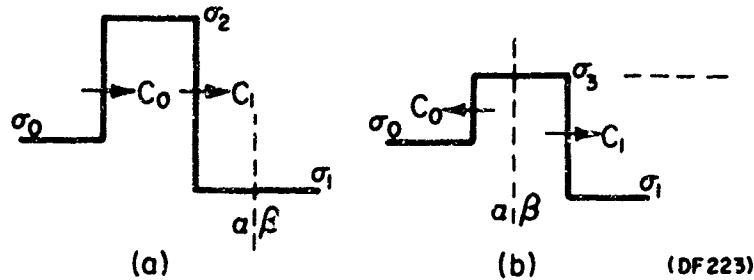
FIGURE D-20.   SITUATION BEFORE (a) AND AFTER (b) INTERACTION
BETWEEN ELASTIC-PLASTIC STRESS INCREMENTS[D-5]

determined by applying velocity continuity conditions subsequent to the interaction. Thus, it may be written for v_α, v_β that

$$v_\alpha = v_1 + \frac{\sigma_2 - \sigma_1}{\rho_i c_1} + \frac{\sigma_o - \sigma_2}{\rho_i c_o} - \frac{\sigma_3 - \sigma_o}{\rho_i c_o} , \quad v_\beta = v_1 + \frac{\sigma_3 - \sigma_1}{\rho_i c_1} . \qquad \text{(D-68)}$$

The final velocity of α is determined by the initial velocity, v_1, and the velocity increments imparted by the plastic loading wave $(\sigma_2 - \sigma_1)$, the elastic unloading wave $(\sigma_o - \sigma_1)$, and the wave resulting from the interaction $(\sigma_3 - \sigma_1)$. For β, only the latter of these three waves affects its initial velocity, v_1. Writing $v_\alpha = v_\beta$ gives

$$\sigma_3 - \sigma_o = \frac{c_o - c_1}{c_o + c_1} \Delta' , \quad \sigma_3 - \sigma_1 = \Delta - \frac{2c_1}{c_o + c_1} \Delta' ; \qquad \text{(D-69)}$$

where Δ, Δ' are the loading and unloading stress increments, respectively, given by

$$\Delta = \sigma_2 - \sigma_1 , \quad \Delta' = \sigma_2 - \sigma_o . \qquad \text{(D-70)}$$

The resulting strains, $\epsilon_\alpha, \epsilon_\beta$, may be calculated by using the incremental expression, Equation D-67. Thus,

$$\epsilon_\alpha = \epsilon_1 + \frac{\sigma_2 - \sigma_1}{\rho_i c_1^2} - \frac{\sigma_2 - \sigma_o}{\rho_i c_o^2} + \frac{\sigma_3 - \sigma_o}{\rho_i c_o^2} . \qquad \text{(D-71)}$$

$$\epsilon_\beta = \epsilon_1 + \frac{\sigma_3 - \sigma_1}{\rho_i c_1^2} .$$

From Equations D-69 and D-70, this gives

$$\epsilon_\alpha = \epsilon_1 + \frac{\Delta}{\rho_1 c_1^2} - \frac{\Delta'}{\rho_1 c_o^2} + \frac{c_o - c_1}{c_o + c_1} \frac{\Delta'}{\rho_1 c_o^2} , \qquad (D\text{-}72)$$

$$\epsilon_\beta = \epsilon_1 + \frac{\Delta}{\rho_1 c_1^2} - \frac{2c_1}{c_o + c_1} \frac{\Delta'}{\rho_1 c_1^2} .$$

Then,

$$\epsilon_\alpha - \epsilon_\beta = \frac{2c_1}{c_o + c_1} \frac{\Delta'}{\rho_1} \left(\frac{1}{c_1^2} - \frac{1}{c_o^2} \right) > 0 . \qquad (D\text{-}73)$$

This indicates that a discontinuity in strain has been introduced at the interaction line, and that it subsequently propagates at the local particle velocity.

Before the wave interaction process can be completed, the interaction of the reflected elastic loading wave, creat. y the foregoing process, and other overtaking elastic unloading waves mus. .e considered. The situation is shown in Figure D-21.

DF 224

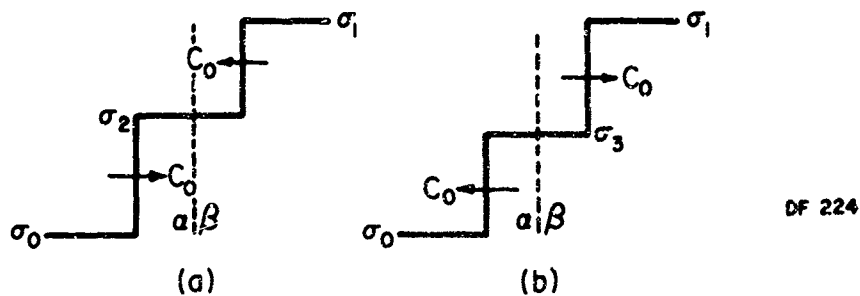FIGURE D-21.   SITUATION BEFORE (a) AND AFTER (b) INTERACTION BETWEEN ELASTIC STRESS INCREMENTS (D-5)

The particle velocities, v_α, v_β, are given by

$$v_\alpha = v_2 - \frac{\sigma_2 - \sigma_o}{\rho_1 c_o^2} - \frac{\sigma_3 - \sigma_o}{\rho_1 c_o^2} , \qquad (D\text{-}74)$$

$$v_\beta = v_2 - \frac{\sigma_1 - \sigma_2}{\rho_1 c_o^2} - \frac{\sigma_1 - \sigma_3}{\rho_1 c_o^2} .$$

Putting $v_\alpha = v_\beta$ gives

$$\sigma_3 - \sigma_o = \sigma_1 - \sigma_2 = \Delta ,$$ (D-75)

$$\sigma_1 - \sigma_3 = \sigma_2 - \sigma_o = \Delta' :$$

where Δ, Δ' are the loading and unloading increments. Calculation of $\epsilon_\alpha, \epsilon_\beta$, in the manner used for the plastic interaction, shows that $\epsilon_\alpha = \epsilon_\beta$, so that no strain discontinuity arises.

Thus, if a series of elastic unloading increments propagating at velocity c_o overtakes a plastic front propagating at c_1, the sequence of events is as follows: (1) the first unloading increment interacts with the plastic front; (2) a reduced plastic front is formed of stress σ_3 and propagates ahead at c_1; (3) an elastic loading increment of stress σ_3 is reflected at a velocity, c_o; (4) the reflected increment interacts with an oncoming elastic unloading increment; (5) the two elastic increments pass through each other, stepped to new levels; (6) the second elastic unloading increment, modified by the interaction, overtakes the plastic front and interacts with it, starting the sequence of events over again. Further consideration will be given to this process in regard to specific aspects of the plate impact.

Consideration is now extended to the reflection of waves from a free surface. For simplicity, an elastic-plastic wave having a two-front structure, as shown in Figure D-22 (a), will be considered to impinge on the free surface. By simple superposition methods, it is established that the elastic compression front reflects from the surface as a tension front and induces a change of velocity. The reflected tension, propagating to the right and annihilating the compressive elastic precursor, effectively creates an unloading wave propagating to the right, as shown in (b) of the figure. The elastic unloading wave then interacts with the oncoming plastic front, reduces the magnitude of the plastic wave, and creates a reflected elastic loading wave propagating back to the free surface ahead of the reduced plastic front (c).
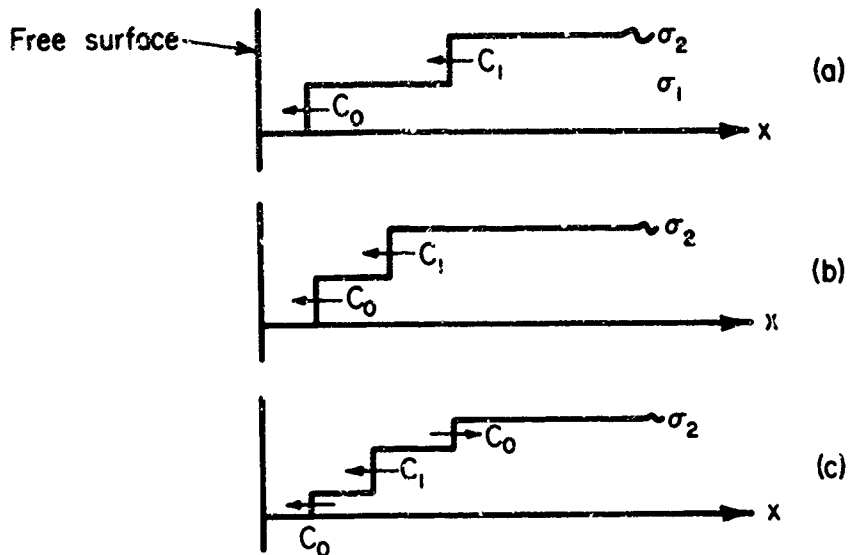
FIGURE D-22. VARIOUS STAGES OF WAVE REFLECTION AND
INTERACTION WITH A FREE SURFACE

It is, of course, evident that the above interaction process could
continue an indefinite number of times before the plastic front reaches the
surface. In actuality, the amplitude of the reverberating elastic wave is
rapidly reduced to an insignificant amount compared to the plastic stress
amplitude, and only the first reverberation is of significance. Thus, the
first reflection of the elastic front from the plastic wave will, when it
reaches the free surface, induce an additional step in velocity. The plastic
wave front will then reach the surface, stepping the velocity yet again. The
velocity and displacement profiles of the free surface motion would have the
general appearance shown in Figure D-23. Further consideration of the actual
velocity changes induced will be given in a subsequent section in which the
entire wave propagation process due to plate impact is considered.
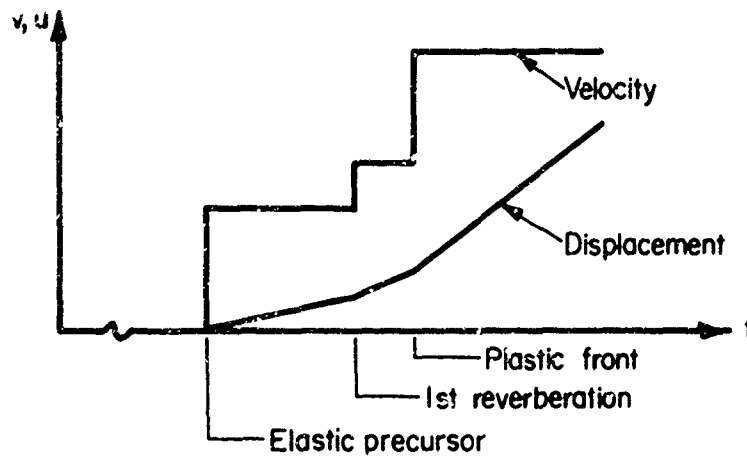
FIGURE D-23. VELOCITY AND DISPLACEMENT PROFILES
OF FREE SURFACE MOTION

Plate Impact and Determination of Material Properties

In the last three sections, various aspects of elastic-plastic wave
initiation, propagation, interaction, and reflection have been considered.
In the present section, the wave propagation problem resulting from the planar
impact of two flat plates will be reviewed. For such a problem, conditions
of uniaxial strain pertain in the interior regions of the plates until the
first rarefactions from the edges reach the center. All aspects of initiation,
propagation, etc., discussed previously, will be present. Although the
complexities of the many wave interactions will preclude extensive hand
analysis, the early stages of the process will be reviewed. A relatively simple
elastic, perfectly-plastic material model will be used so that the basic
features of the stress wave system may be easily studied. The method of
deducing the stress-strain relation of the material from the measurement of
rear surface motion will be reviewed.

An example, taken from Penning, et al,[D-7] will be used to illustrate
various aspects of the resultant stress wave system. The planar impact of a
driver plate upon a target plate, where both plates are of the same material,
will be observed. An elastic, perfectly-plastic material, having the charac-
teristics mentioned and illustrated on pages D-1 through D-17 and Figure D-8,

will be used to represent the material. The Lagrangian wave diagram will be employed to depict the wave process.

Example. Consider the case of a driver plate impacting the target plate at a velocity of 0.010 cm/μsec, inducing a compressive stress of 8.1 kbar at the plate interface. This compression will be achieved in two steps. There will be a compression to 6.33 kbar propagating into the target at the elastic velocity of 0.623 cm/μsec, followed by a further compression to 8.1 kbar propagating into the target at 0.541 cm/μsec. The former wave is the elastic precursor, and the second wave represents the plastic front. Exactly the same thing is occurring in the driver plate. This stage of the process is indicated by OA and OP on the wave diagram of Figure D-24.

The compressive waves first reach a free surface at P in the driver plate. The elastic front reflects as a decompression, or unloading wave, releasing the material from 6.33 kbar to zero stress. This front interacts with the oncoming compressive front of magnitude 1.77 kbar at point Q. The analysis of the interaction at Q follows the methods outlined on pages D-27 through D-33. The resulting stress wave system is composed of a recompression or loading wave of amplitude 1.96 kbar, propagating on to the free surface at the elastic velocity, and an unloading wave from 3.1 kbar to 1.96 kbar, propagating (at the elastic velocity) back through the driver plate. At the interaction line between these two waves, a density discontinuity or contact surface has been created. The recompression wave reflects from the driver-free surface as an unloading wave and propagates back through the driver plate leaving unstressed, unstrained material in its wake until it reaches the contact surface. Beyond the contact surface, the material is left unstressed, but with a net residual strain. Exactly the same interaction occurs in the target plate at A, only at a later time. Two stages of this interaction process are shown in Figure D-25. One occurs at $t = t_1$, subsequent to the reflection from the driver-free surface, but prior to reflection from the target surface. The other is at $t = t_2$, subsequent to the reflection from the
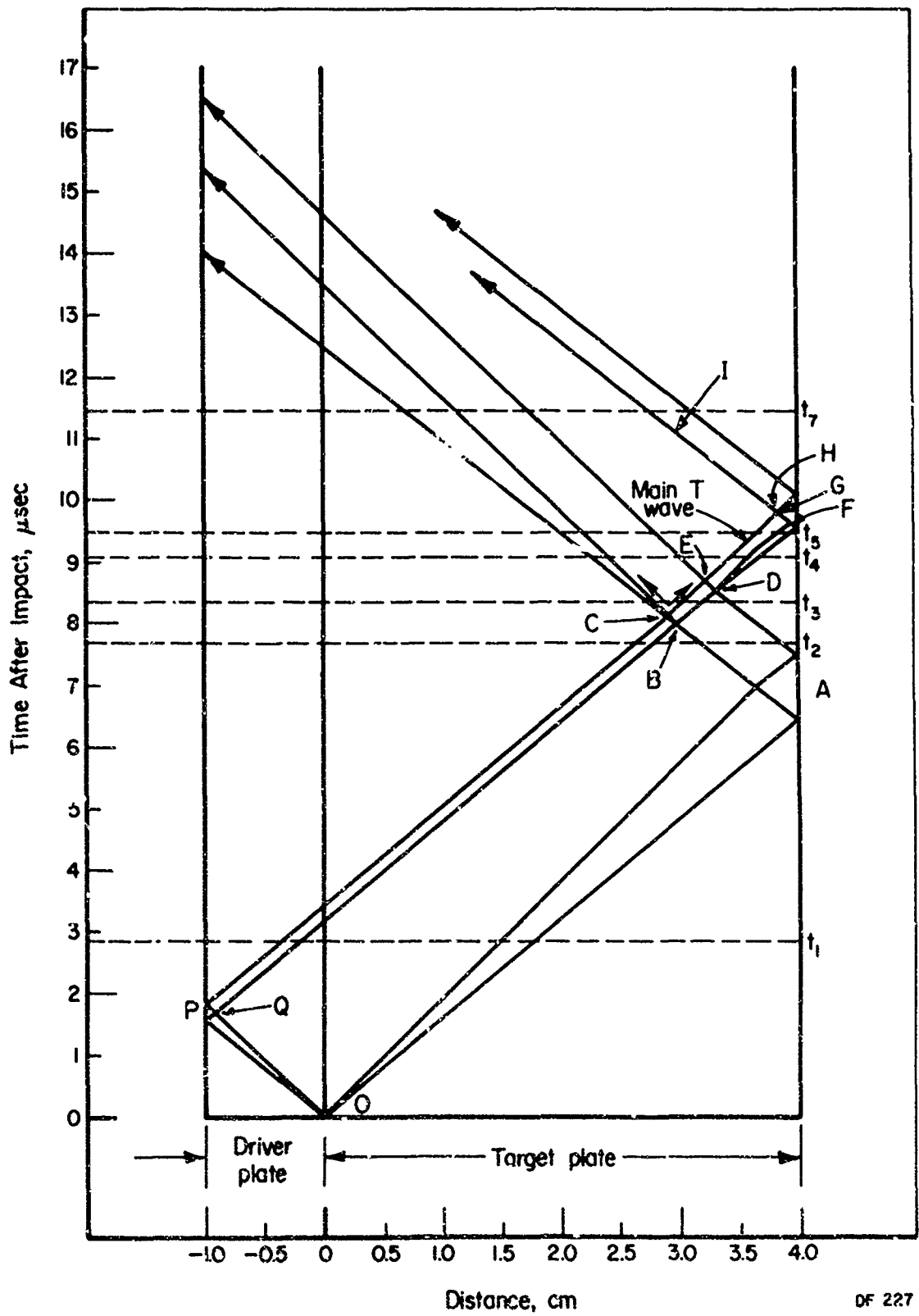
FIGURE D-24. WAVE DIAGRAM FOR AN 8.1 KBAR COMPRESSION PULSE[D-7]
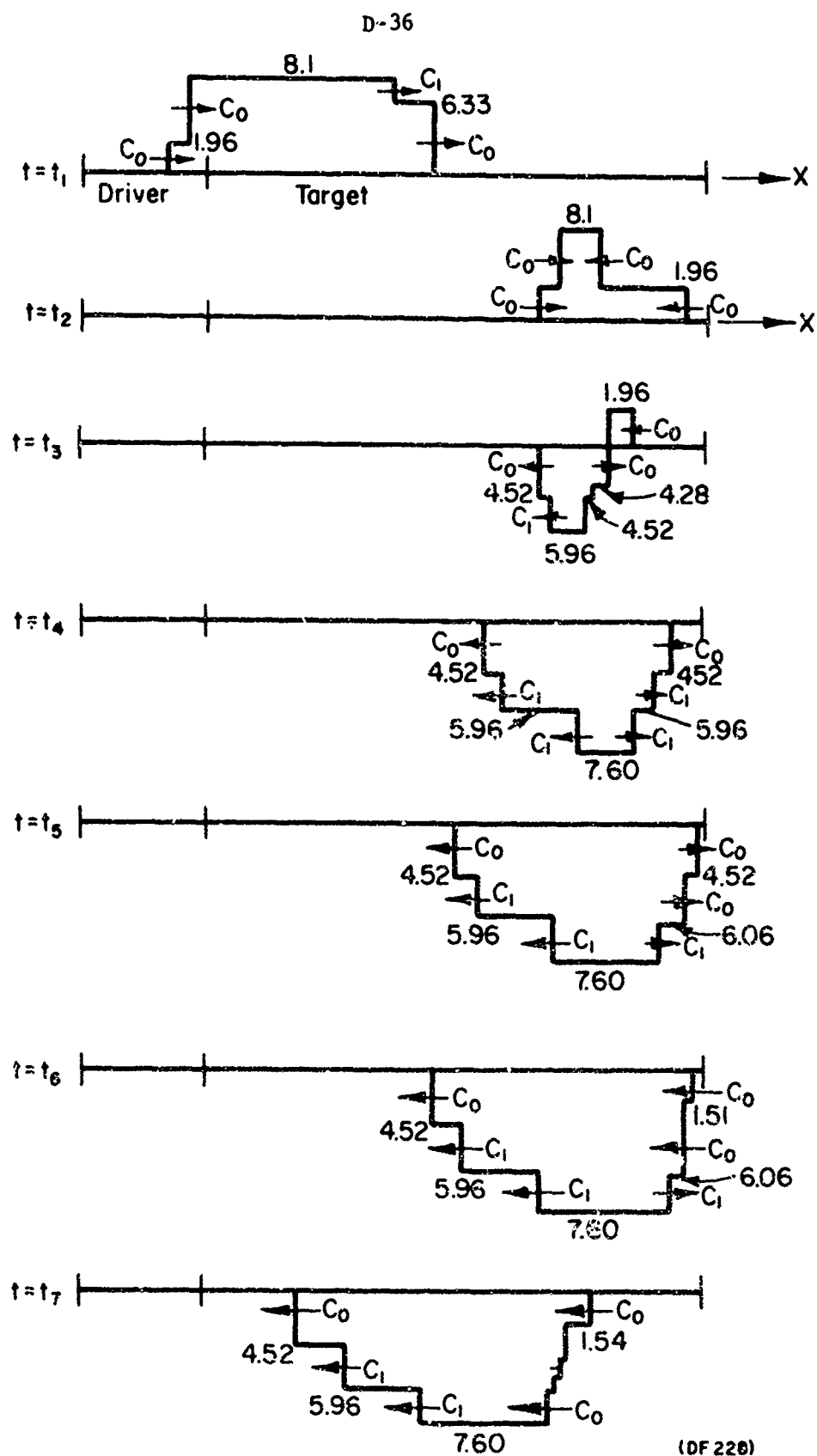
FIGURE D-25. ILLUSTRATION OF THE WAVE SYSTEMS AT VARIOUS
STAGES OF THE INTERACTION PROCESS

target surface, but prior to further interaction. These times are indicated on the Lagrangian diagram, Figure D-24, as dashed lines at $t = t_1, t_2$.

At this stage, the interaction between the unloading waves from the driver and target-free surface begins. The first interaction is between the 8.1 kbar to 1.96 kbar unloading waves, which occurs at point B of the Lagrangian diagram. This produces two oppositely-moving tension waves of magnitude -4.28 kbar propagating at the elastic velocity. These interact almost immediately with the oncoming 1.96 kbar to 0 unloading fronts (points C and D on the diagram). Each of these interactions (C and D) produces two oppositely-directed tension waves (this is illustrated for the interaction at C by the symbol $\mathsf{L}_\bullet$). Now, the tension waves produced at C are actually dual fronts; the first step takes the pressure from -4.28 kbar to -4.52 kbar (and propagates at the elastic velocity of 0.623 cm/μsec), while the second step is from -4.52 kbar to -5.96 kbar and propagates at the plastic velocity 0.541 cm/μsec. The identical situation is created at D. Lack of space on the Lagrangian diagram prevents showing all of these details. Thus, of the two dual systems from C, only the one propagating to the left shows both wave fronts (those propagating to the right from D). The resultant stress wave system is shown at an intermediate time, $t = t_3$, in Figure D-25. This is a time instant between the identical interactions at C and D described above.

Now, two of the dual systems created at C and D undergo a head-on interaction at E of the diagram. This produces a region of -7.60 kbar stress bounded by waves propagating at the plastic velocity in the opposite directions. The resulting stress situation is shown at $t = t_4$ in Figure D-25.

The next step of the process occurs when the dual wave system, emanating from D toward the target-free surface, encounters the contact surface formed from the first wave reflection off the free surface

(identical contact surfaces were formed in the driver and target
plates from the reflections and interactions at P and A). The first
step of the dual wave passes through at unchanged magnitude and speed.
When the second step encounters the surface, a very weak elastic
tension wave is reflected, moving to the left at 0.623 cm/μsec and
dropping the pressure about 0.15 kbar. This wave is neglected on
the diagram. The second step also refracts, taking on the elastic
velocity and an amplitude of -6.06 kbar. This situation is shown as
$t = t_5$ in Figure D-25.

The next stage of the process concerns the reverberation of the
-4.52 kbar tensile wave between the target-free surface and the -6.06
kbar tensile wave front. Thus, the former tensile wave reflects from
the free surface as a -4.52 kbar to 0 compressive wave at unchanged
velocity. It interacts with the second tensile wave step producing a
compression wave, from -6.06 to -1.51 kbar moving toward the driver
plate, and a tension wave, from 0 to -1.51 kbar moving toward the free
surface where it reflects as a compression wave from -1.51 to 0 kbar.
This interaction occurs in the vicinity of point F on the Lagrangian
diagram. Because of the fine detail of the wave structure at this
stage, it is not possible to show all of the rays of the diagram. Thus,
a single ray, marked G in the diagram, has been used to depict the 0
to -1.51 and -1.51 to -6.06 fronts. The situation is shown as $t = t_6$
in Figure D-25.

Meanwhile, the main tension wave (marked as "main T-wave" on the
Lagrangian diagram) encounters the previously mentioned contact surface.
In reality, this wave system, which resulted from the previously described
wave interaction at E, is a dual wave structure, although this detail is
omitted on the Lagrangian diagram (thus, only a single ray is shown
propagating to the right from E). At this stage, the interactions that
occur with the contact surfaces and with the compression fronts are too
finely spaced on the Lagrangian diagram, and too numerous to describe in
detail. The contact surface interaction is followed by wave interaction
at point H of the diagram.

After the interaction at H, waves of tensile unloading, marked I
in the diagram, propagate toward the driver, while waves of tensile
loading propagate toward the target-free surface and reflect. The
situation, after the above interactions, is shown at time $t = t_7$ in
Figure D-25. Some of the fine details of the wave structure in this
diagram are only suggested in approximate terms.

The wave system, for the example just considered, was somewhat
simplified by virtue of the magnitude of the induced stress at collision. Thus,
the impact velocity was such that the peak stress was 8.1 kbar. At this
level, the unloading that occurs when the first waves reach the free surfaces
is purely elastic (points A and P of Figure D-24). If the impact velocity
is high enough, reverse yielding occurs at unloading, creating an additional
wave front. This factor is illustrated in Figure D-26 for a 14 kbar impact
stress. At point P of that figure, the plastic front reflects as an elastic
and a plastic front, as indicated by the dual waves emanating from that point.
A similar situation holds at point A of the diagram. The subsequent wave
interactions are considerably more numerous than those described in the
lower stress level impact example. If the impact stress is still higher, the
consequent wave interactions are even more complicated due, in general, to the
reverse yielding effects which occur during unloading. This is indicated in
Figure D-27 for a 19 kbar impact stress.

The preceding discussion has been devoted to the stress history in the
interior of the material as a result of plate impact. The results have been
based on an a priori knowledge of the constitutive equation of the material and
the conditions of impact. The inverse problem, in which the material properties
are to be found from the plate-impact test, is of equal interest. Thus, assuming
that both impact conditions and experimental data on the ensuing motion of the
target-free surface are known, determination of the material constitutive
equation is desired. The procedure for this is outlined in the following.
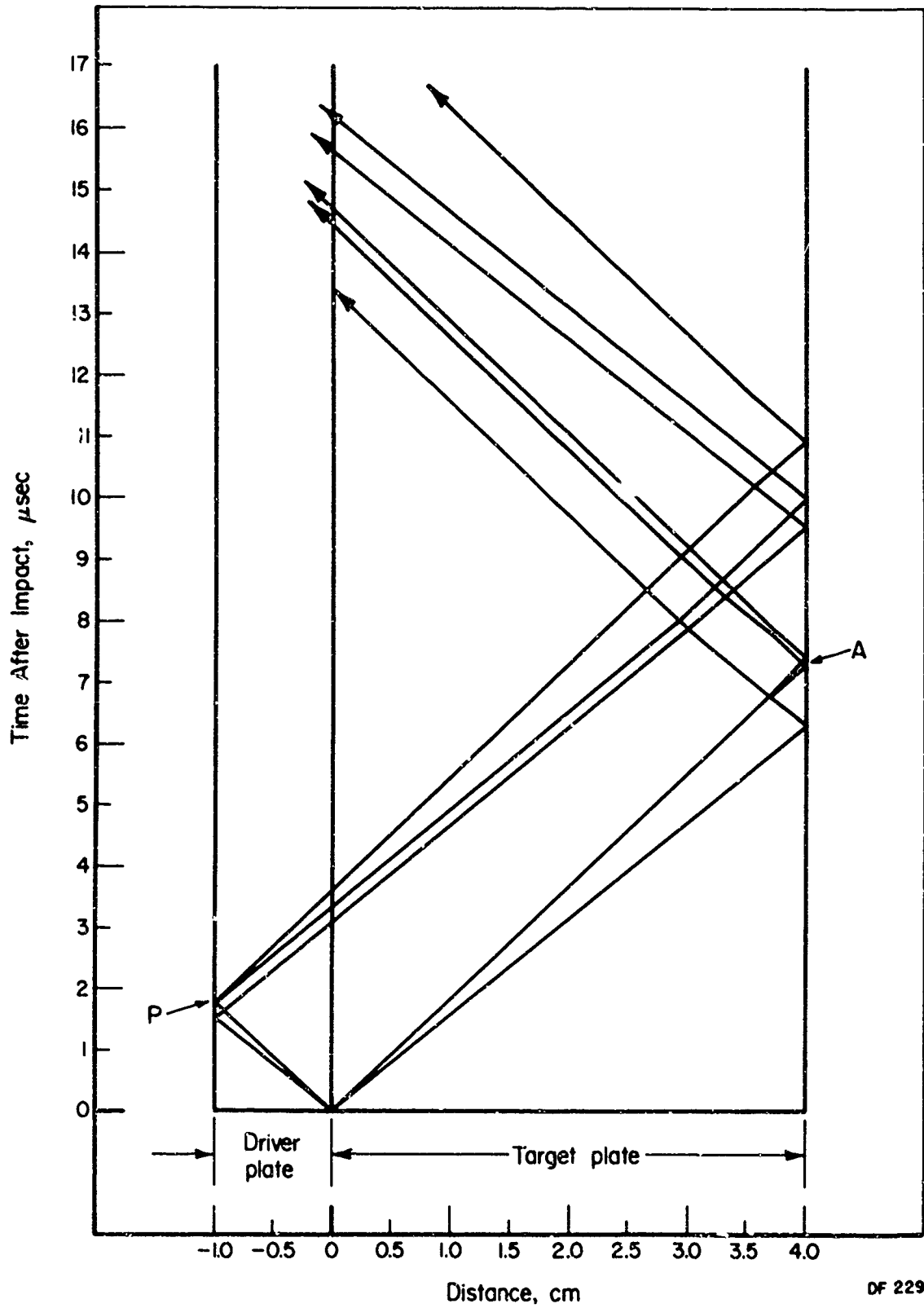
FIGURE D-26. WAVE DIAGRAM FOR A 14-KBAR COMPRESSION PULSE[D-7]
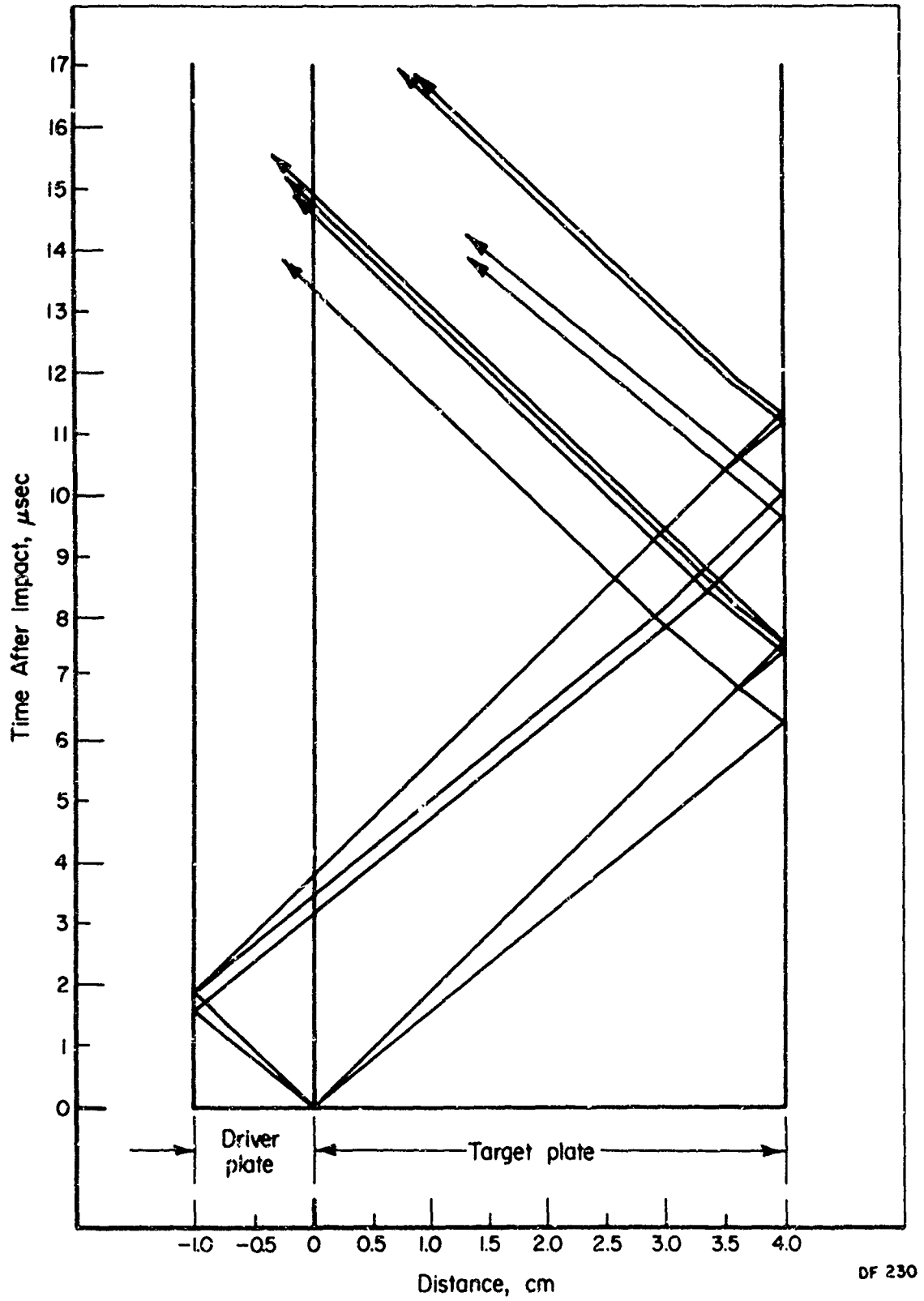
FIGURE D-27.   WAVE DIAGRAM FOR A 19-KBAR COMPRESSION PULSE[D-7]

A typical free-surface motion record from a plate-impact experiment is shown in Figure D-28. From the discussion of the last few pages, it is

DF 231
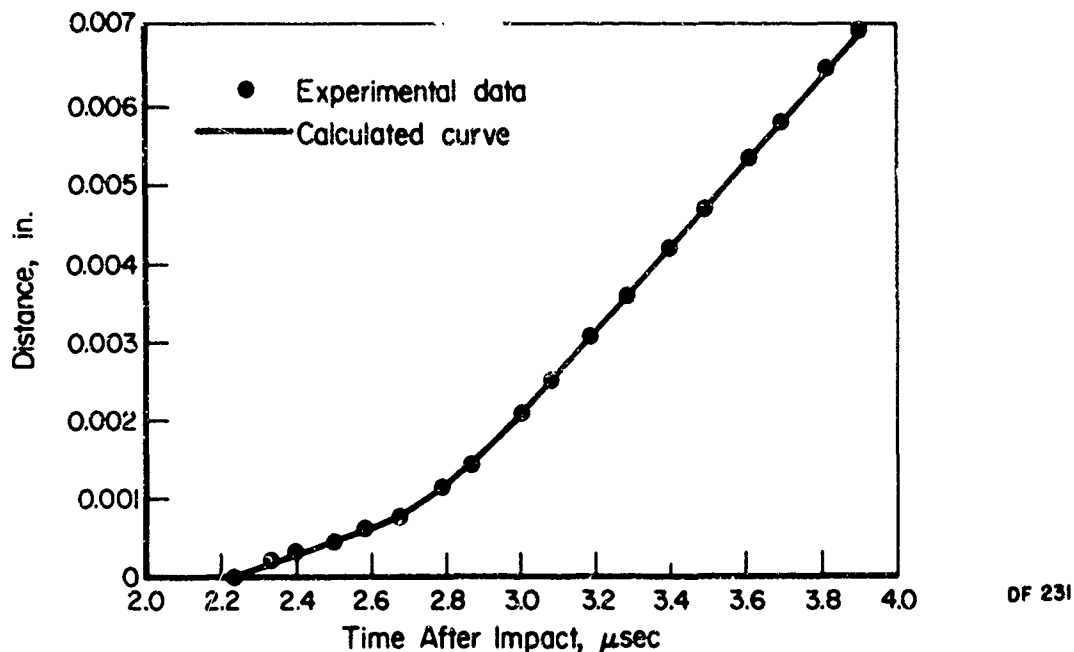
FIGURE D-28. FREE SURFACE DISTANCE-TIME PLOT FOR A
TYPICAL PLATE-IMPACT EXPERIMENT (D-8)

realized that the observed free-surface motion is a result of a rather compli-
cated system of wave interactions. A procedure for obtaining the constitutive
equation for a material from free-surface motion measurements would be to
assume a constitutive equation and then, using this relation and the impact
conditions, to solve the wave-propagation problem. Such a solution, using a
characteristics computer code, would account for all of the complex wave
interactions and would compute a predicted free-surface motion. The results
would be compared with the experimental data. If the comparison were poor, the
constitutive relation would be revised and the analysis repeated in an
iterative manner until agreement was reached. However, if the initial assumed
constitutive relation greatly deviates from the actual one, a number of itera-
tions might be required before good match between theory and experiment is
obtained. A procedure, which is described below, yields a very good approxi-
mation to the constitutive relation by neglecting many of the complex wave
interactions.

The experimentally obtained displacement-time record is approximated by a series of straight line segments. When a step-pressure pulse arrives at a free surface, it causes a step change in surface velocity which translates as a sloped straight line in the displacement-time record of the motion. If the reflection and subsequent interaction of the pressure step with the remainder of the oncoming wave is neglected, then approximation of the free-surface data by straight line segments is equivalent to representing the wave shape by a cor⁻⁻ series of discrete pressure steps, or stress jumps. The situation is ill⁻ in Figure D-29, which is intended to depict a stress wave at an arbi⁻ , t = t_n, prior to impinging on the free surface. Each stress increme⁻⁻⁻ considered to propagate with its own characteristic velocity.
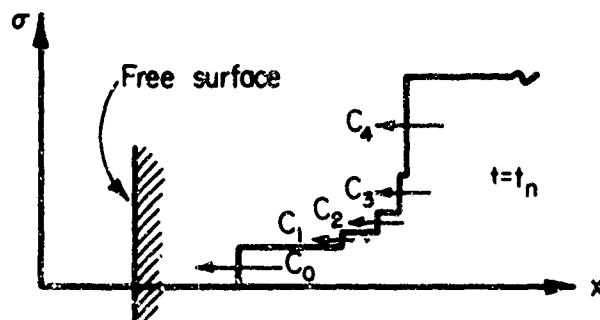
FIGURE D-29. APPROXIMATION OF A STRESS PULSE BY STRESS JUMPS

The procedure is to apply the Rankine-Hugoniot conditions across the stress jumps. Thus, the relations of interest are the momentum and mass equations which have the form

$$\Delta\sigma_x = \rho_1 U_s \Delta u_p \ , \ \frac{\rho_2}{\rho_1} = \frac{U_s}{U_s - \Delta u_p} \ ; \tag{D-76}$$

where $\Delta\sigma_x$ is the stress jump, U_s the shock velocity, Δu_p the change in particle velocity, and ρ_1, ρ_2 the densities ahead of and behind the shock, respectively. The parameters determined from the experiment are U_s, Δu_p, and ρ_1. Thus, velocity of propagation of each stress step is found merely by dividing the plate thickness by the time required for propagation from the impact surface to the free surface. The change in particle velocity is found by taking one half of the difference between successive velocity steps of the free surface. The density ahead of the shock, ρ_1, is considered as known. Thus, $\Delta\sigma_x$ and ρ_2 may

be found, which establishes points on the stress-strain curve.

An outline of a typical computation would be as follows.

Given: Target-plate thickness $= T$

Initial target density $= \rho_o$

Displacement-time data given by Figure D-30.

(DF233)
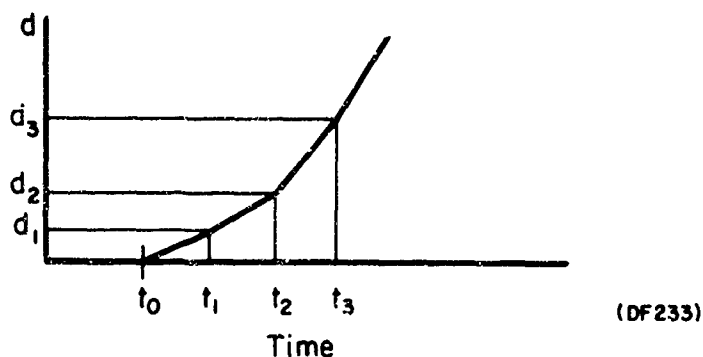
FIGURE D-30. HYPOTHETICAL DISPLACEMENT-TIME
HISTORY OF REAR SURFACE MOTION

Calculations:

(1) Velocity of first shock, $\quad U_1 = \dfrac{T}{t_o}$,

Change of particle velocity, $\quad \Delta u_1 = \dfrac{1}{2} \dfrac{d_1}{t_1 - t_o}$,

Change of stress, $\quad \Delta \sigma_x = \sigma_1 - \sigma_o = \sigma_1 = \rho_o U_1 \Delta u_1$,

Change of density, $\quad \dfrac{\rho_1}{\rho_o} = \dfrac{U_1}{U_1 - \Delta u_1}$,

Resultant strain, $\quad \epsilon_1 = 1 - \dfrac{\rho_o}{\rho_1}$.

(2) Velocity of second shock, $\quad U_2 = \dfrac{T}{t_2}$,

$$\Delta u_2 = \frac{1}{2}\left[\frac{d_2 - d_1}{t_2 - t_1} - \frac{d_1}{t_1 - t_o}\right] = \frac{1}{2}\frac{d_2 - d_1}{t_2 - t_1} - \Delta u_1 \ ,$$

$$\Delta \sigma_2 = \sigma_2 - \sigma_1 = \rho_1 U_2 \Delta u_2 \ ,$$

$$\frac{\rho_2}{\rho_1} = \frac{U_2}{U_2 - \Delta u_2} \ ,$$

$$\epsilon_{\cdot} = 1 - \frac{\rho_1}{\rho_2} \ .$$

In this way, successive pairs of points, σ_1, ϵ_1, σ_2, ϵ_2, σ_3, ϵ_3, etc., are established on the stress-strain curve and connected by straight line segments.

Having obtained an approximate stress-strain curve in this way, the results are then used in the computer program which takes into account the complex wave interactions to predict a free-surface motion. Although a number of approximations are used in generating the initial stress-strain curve, it is frequently found that the subsequent exact analysis yields predicted free-surface motion that agrees, within experimental error, with measured data and that no further iterations are required.

Nevertheless, it must be realized that the foregoing approximate procedure neglects density changes insofar as wave interactions with these changes are concerned. Also, unloading by rarefaction waves has been neglected, and the particle velocity has been approximated by one-half of the free-surface motion. This last, which holds for elastic waves, is not strictly true for the inelastic case.

APPENDIX D

REFERENCES

D-1. Fowles, C. R., "Shock Compression of Hardened and Annealed 2024 Aluminum", Journal of Applied Physics, Vol. 32, p. 1475 (1961).

D-2. Hill, R., The Mathematical Theory of Plasticity, Oxford Press, New York (1950).

D-3. Fung, Y. C., Foundations of Solid Mechanics, Prentice-Hall, Inc., New York (1965).

D-4. Barker, L. M., Lundergan, C. D. and Herrmann, W., "Dynamic Response of Aluminum", Journal of Applied Physics, Vol. 35, No. 4, pp. 1203-1212 (1964).

D-5. Morland, L. W., "The Propagation of Plane Irrotationa Waves Through an Elastic-Plastic Medium", Phil. Trans. of Roy. Soc. of London, Series A, Vol. 251, p. 341 (1959).

D-6. Ivanov, A. G., Novikov, S. A. and Sinetsyn, V. A., "Investigation o Elastic-Plastic Waves in Explosively Loaded Iron and Steel", Soviet Physics-Solid State, Vol. 5, No. 1 (July 1963).

D-7. Penning, J. R., Jr., Young, D. M. and Prindle, J. H., "Negative Equation of State and Spall Criteria", The Boeing Company, Seattle, Washington, 1963, Contract No. AF 29(601)-5363.

D-8. Butcher, B. M. and Canon, J. R., "Influence of Work-Hardening on the Dynamic Stress- in Curves of 4340 Steel", AIAA Journal, Vol. 2, pp. 2174-2179 (1964).

APPENDIX E

MATERIAL PROPERTIES EFFECTS

MATERIAL PROPERTIES EFFECTS

The propagation of elastic-plastic waves under conditions of one-dimensional strain has been considered in the past several sections. The equations governing the propagation (developed on pp D-1-D-17) were derived on the basis of certain kinematical assumptions on the deformation of the material and on a rather simple constitutive equation. For example, temperature and strain-rate effects were assumed to be negligible. From the standpoint of understanding the essential features of elastic-plastic wave propagation, it was certainly advisable to make such assumptions so that subtle material effects would not obscure the basic features of the propagation.

However, since the prediction of spallation relies on determination of the stress field in the interior of the material, it is advisable to reexamine the basic governing equations of the wave propagation since these are utilized to determine the stress field. It is important, for example, to establish whether the assumed constitutive relation accurately reflects the real behavior of the material and to assess the degree of confidence that may be placed in experimentally determined material relations. It is also important to review the current assessment of the value of strain-rate and temperature effects in describing the dynamic response of materials.

Review of Basic Equations

In order to provide a basis for the reexamination of the governing equations, the equations on pages D-17 - D-20 are restated.

Conservation of mass:

$$\rho(1 - \epsilon_x) = \rho_i$$

Conservation of momentum:

$$\frac{\partial \sigma_x}{\partial x} = - \rho_i \frac{\partial v}{\partial t} \qquad (E-1)$$

Kinematics (strain):

$$\epsilon_x = - \partial u / \partial x$$

Constitutive relation:

$$\sigma_x = \sigma_x (\epsilon_x) .$$

On the basis of elastic-plastic theory, the constitutive relation for a material under conditions of one-dimensional strain was developed on pages D-1 - D-17. Also illustrated there were the forms taken by an elastic, perfectly-plastic and an elastic, work-hardening material. How to establish the quasi-static constitutive relation directly from the results of quasi-static uniaxial stress tests was shown as well.

The order of the reexamination shall now be as follows:

(a) Thermodynamic effects

(b) Work-hardening and Bauschinger effects

(c) Strain-rate effects

(d) Finite strain effects.

Thermodynamic Considerations

Before discussing possible temperature effects on elastic-plastic wave propagation, it is desirable to review some general thermodynamic considerations of material stress-strain relations. In a propagating stress-wave system, the first physical action is generally that which compresses the material, causing a temperature rise of some magnitude. This action is followed by decompression caused by rarefaction waves. The decompression cools the material. If the process occurs rapidly enough, so that heat conduction processes do not have sufficient time to act, and if initial and final temperatures are the same indicating that a reversible action has occurred, the elastic-plastic shock-wave system would be thermodynamically described as isentropic-adiabatic. The resulting material stress-strain curve would be an isentropic relation.

However, it might be recalled that the initial development of the elastic-plastic stress-strain relations for conditions of one-dimensional strain (pages D-1 - D-17) were based on utilizing the results of quasi-static, isothermal, uniaxial stress tests. The resulting stress-strain curve for uniaxial strain conditions was, thus, an isothermal relation. Since the conditions of stress-wave propagation are more likely to be adiabatic conditions, a governing stress-strain relation based on isothermal conditions would be in error thermodynamically.

The above error may be eliminated by utilizing adiabatic data to develop the uniaxial strain relation. Thus, for materials adequately described by a simple

elastic, perfectly-plastic material model, the resulting stress-strain relation
is determined by two straight lines; one the elastic slope and the other paralleling
the hydrostat. The slopes of these lines are directly related to the elastic
constants. Hence, by establishing these con'tants under adiabatic conditions using
ultrasonic pulse-echo techniques, an adiabatic, uniaxial strain relation may be
constructed. This method has been utilized by Barker, et al,[E-1] and others.

The plate-slap experimental technique offers the possibility of estab-
lishing the material constitutive relation directly, in contrast to conversion of
uniaxial stress test data. To a certain extent, consequently, the preceding remarks
on isothermal versus adiabatic conditions must be reinterpreted. The question now
is not whether a dynamic uniaxial stress-strain relation can be derived from
isothermal or adiabatic quasi-static conditions, but can the thermodynamic condi-
tions represented by the directly obtained relation be identified? The significance
of temperature as a parameter of the material constitutive relation must, then,
be assessed.

It has been recognized that the elastic-plastic stress wave represents
an irreversible thermodynamic process. The Hugoniot relations imply that the work
of dynamically stressing a material from σ_0 to σ_1 is given by the area under the
shock chord of the stress-strain curve, which connects the two stress states
(refer to Figure D-16 on page D-26). Note that this quantity differs from the
area under the stress-strain curve itself, which applies for gradual loading. Thus,
the plastic shock introduces irreversible dissipation of additional mechanical work.
It has been shown that more than 85 percent of the work goes into heat dissipation,
and only about 15 percent into permanent changes in the microstructure. Con-
sequently, it would appear that the final stress state, σ_1, should not lie on a
continuously loaded adia' .tic curve, but on a curve modified by the additional
heat release.

Lee[E-2] has elaborated further on the above by proposing that the
extremely high pressures and finite dilatations (up to 25 percent strain at 400 kbar
for aluminum), present in one-dimensional strain experiments, introduce dominant
thermomechanical coupling effects making temperature an essential variable in the
equation-of-state. If this assessment applies to the stress-strain regir ; of
interest in the study of spall, the accuracy of stress predictions from rear
surface motion measurements would be lessened considerably.

However, other investigators have given consideration to the thermo-
dynamic aspects of the wave propagation and have developed convincing arguments
in favor of neglecting temperature effects at the lower stress levels of the
elastic-plastic regime. It will be recalled that even for the hydrodynamic shock
regime, close approximations of material behavior were possible by neglecting
temperature effects in the establishing of the Hugoniot material (Appendix C).

Considerations, similar to those in the foregoing, have been extended
to the elastic-plastic case. The basic arguments, developed by Morland, are
closely paralleled in the following presentation. Let the irreversible energy
dissipated per unit mass in a small compression, $d\epsilon$, be dQ. Conservation of work
and energy gives

$$dQ - dE - dW;$$
(E-2)

where dE is the increase in internal energy, and dW is the work done by the applied
stress. Taylor and Farren[E-4] have shown that less than 15 percent of the plastic
work goes into producing microscopic structural changes in the material, so that
heat dissipation per unit mass represents more than 85 percent of dQ.

On integrating over the full compression, the increase of E is established
from Equation D-61 as

$$E_1 - E_o = \frac{1}{2\rho_1} (\sigma_1 + \sigma_o) (\epsilon_1 - \epsilon_o) .$$
(E-3)

The work increment per unit mass is

$$dW = \frac{1}{\rho_1} \sigma d\epsilon .$$
(E-4)

Hence, the total applied work, ignoring the factor $1/\rho$, is the area under the
corresponding stress-strain curve. The area under the shock chord represents the
increase in E; the difference represents Q, the energy dissipated.

Referring again to Figure D-16, it is evident that the area between the
stress-strain curve and the shock chord will, in general, be quite small if the
stress jump is small and the upward curvature of the hydrostat is negligible, or
if work-hardening effects are absent or linear with increasing load. An estimate
of Q may be found by assuming that the stress-strain relation through the plastic
shock is the adiabatic stress-strain curve. A stress-strain relation of the
following form is assumed:

$$\frac{d\sigma}{d\epsilon} = \frac{1}{3} \alpha \beta [1 + d_1\epsilon + d_2\epsilon^2 + d_3\epsilon^3 + \ldots] ;$$
(E-5)

where α, β, d_1, d_2 ... are determined from Bridgeman's formula fitting hydrostatic material data. Integrating the above between the yield point, σ_Y, and the arbitrary upper stress level gives

$$\sigma - \sigma_Y = \frac{1}{3} \alpha \beta \left[\epsilon + \frac{1}{2} d_1 \epsilon^2 + \frac{1}{3} d_2 \epsilon^3 + \dots\right]_{\epsilon_Y}^{\epsilon} . \qquad (E\text{-}6)$$

Then,

$$\frac{1}{2}(\sigma_1 + \sigma_o) = \left\{\sigma_Y - \frac{1}{3} \alpha \beta \left[\epsilon_Y + \frac{1}{2} d_1 \epsilon_Y^2 + \dots\right]\right\} + \frac{1}{3} \alpha \beta \left\{\frac{1}{2} (\epsilon_1 + \epsilon_o) + \frac{1}{4} d_1 (\epsilon_1^2 +$$

$$\epsilon_o^2) + \dots\right\} . \qquad (E\text{-}7)$$

Also,

$$\int_{\epsilon_o}^{\epsilon_1} \sigma d\epsilon = (\epsilon_1 - \epsilon_o)\left\{\sigma_Y - \frac{1}{3} \alpha \beta \left[\epsilon_Y + \frac{1}{2} d_1 \epsilon_Y^2 + \dots\right]\right\} + \frac{1}{3} \alpha \beta \left\{\frac{1}{2}\left(\epsilon_1^2 - \epsilon_o^2\right) + \frac{1}{6} d_1\right.$$

$$\left.\left(\epsilon_1^3 - \epsilon_o^3\right) + \dots\right\} . \qquad (E\text{-}8)$$

Neglecting terms of ϵ^4 or higher gives

$$Q = \frac{\alpha\beta}{3\rho_1} \frac{d_1}{12} (\epsilon_1 - \epsilon_o)^3 .$$

Using reasonable values for aluminum, Morland establishes that for $\epsilon_1 - \epsilon_o < 0.05$, the shock change is virtually adiabatic (i.e., $dQ \cong 0$), so that the material behind the shock will satisfy the original adiabatic stress-strain relation.

The thermodynamic considerations, reviewed in the foregoing, establish the validity of assuming that the elastic-plastic wave process is adiabatic. However, the importance of temperature on the wave propagation has yet to be assessed. Thus, the fact that the process is essentially adiabatic indicates that a temperature rise occurs under the action of the shock front. The resulting interaction of the temperature on the stress field--the coupled thermomechanical problem--has not yet been solved for the plastic wave case. In fact, only slight progress has been made in the case of thermoelastic wave propagation. It is not known, for example, whether thermo-plastic effects might be confused for strain-rate effects in materials. The general procedure has been to assume that the propagating stress field is unaffected by the temperature changes.

Recently, Lee and Liu[E-5] and Lee and Wierzbicki[E-6] have generalized elastic-plastic theory to include finite strain and temperature effects. Although only the governing equations were developed, with numerical solutions yet to be

obtained, application of their theory to specific stress-wave problems may soon yield a more definite assessment of the importance of temperature on the elastic-plastic wave problem.

Work-Hardening and Bauschinger Effects

As was evident in the review of elastic-plastic wave propagation in Appendix D, the structure of the propagating stress wave is a function of the material stress-strain relation. This relation will be characterized, in the absence of strain-rate effects, by the nature of its loading and unloading. Does the material have a sharp or ill-defined yield point? Does work hardening occur? Is curvature of the hydrostat significant? Is a Bauschinger effect present?

If, by experimental methods, the precise shape of the stress-strain curve is known, no assessment of the above effects is required to complete the analytical process of computing the interior stress field in a plate-impact test. Yet, in the earlier study of the wave propagation and interior stress field (Appendix D, pages D-33-D-45), even the use of a simple material model (elastic, perfectly-plastic) led to a complicated wave structure due to many wave interactions. However, the availability of computer codes for analyzing the stress-wave propagation, including all of the wave front and interface interactions, removes the analytical difficulties resulting from complexities in the material stress-strain relation. Hence, the presence or absence of the aforementioned effects, which serve to distinguish various materials, presents no fundamental difficulty in solving the stress-wave problem.

The preceding remarks are presupposed on the basis of knowing the material stress-strain relation. However, if inexactitude exists in the experimental methods for establishing the stress-strain relations, there will be a consequent uncertainty as to the interior stress field. The present method for establishing the stress-strain relation (reviewed on pages D-33-D-45) is to measure the rear surface motion in a plate-slap experiment and, by trial-and-error solution of the stress-wave problem, to deduce a stress-strain curve that will yield a theoretical prediction of the rear surface motion in accord with the experiment. It, therefore, becomes important to assess the accuracy of the stress-strain relation obtained from the plate-slap experiment itself.

The first remark to be made in this context concerns the sensitivity of the stress-strain relation to erroneous measurement of surface motion. In this regard, it has been pointed out by Butcher and Canon[E-7] that errors in the measurement of surface velocity, when converted to material velocity, cause data points to move along the dynamic stress-strain curve rather than, say, parallel to the stress or strain axis. This means that errors in surface motion measurement are reflected as much smaller errors in the determination of the stress-strain curve.

Further assessment may be divided into consideration of the experimentally obtained loading and unloading information about the material. There is, in fact, basis for confidence in the rear surface motion measurement approach to establishing the loading characteristics of the stress-strain curve. Thus, the magnitude of the elastic precursor establishes the material yield point. The propagation velocity of the plastic front establishes the shock chord on the stress-strain curve, and, by performing several experiments at differing plate-impact velocities, several stress-strain points on the loading curve may be determined. The elastic-plastic compression waves that establish the above data are the first waves to arrive at the free surface, and they have done so with a minimum of self-interaction (see pages D-33-D-45 for the discussion of the interactions that have occurred).

However, the deduction of the unloading characteristics of a material from rear surface measurements is less certain. Thus, the unloading information appearing in the form of rear surface motion is due to waves reflecting from the back surface of the projectile-target combination. These waves arrive at the rear surface only after traveling as compression, then release, and finally as tension, undergoing numerous interactions in the process. Barker, et al,[E-1] discuss the necessity for performing tests using various target-projectile thickness ratios. Use of various ratios would help to establish unique unloading information, which is difficult to acquire because of multiple reflections and interactions. The necessity for performing multiple experiments, and resultant indirectness in establishing the stress-strain curve, casts doubt on the accuracy of unloading and reverse loading information established by rear surface motion measurements.

Until recently, the primary method for determining material properties
was by inference from rear surface motion measurements. Refinements in measuring
technique, utilizing laser velocity interferometers, have been reported
[Karnes[E-8]]. However, Barker[E-9] has recently reported on measurements of
material particle velocities in the interior of a shocked solid wherein the laser
interferometer was used in conjunction with a transparent quartz window on the
specimen to obtain the interior data. ~' 'ransparent window, of similar mechanical
impedance as the shocked material (alu·   s attached to the specimen. The
interface motion was obtained with the in..   ·meter and was assumed to depict the
motion of a truly interior point of the material. Although the complete validity
of the technique has not been established, since questions of slight impedance
mismatch effects and the light transmission characteristics of quartz under dynamic
loads remain, it does, apparently, enable the elastic-plastic wave structures to
be established directly, before wave reflections and interactions have occurred.
As a consequence of this development, direct information on the unloading charac-
teristics of materials is now available.

In Figure E-1, the data obtained by Barker on the particle velocity-
time history at an interior surface is shown for three different tests. Consider,
in the figure, the general nature of the loading portion of the wave and of the
unloading portion. It is to be noted that at the higher stress level shots
(Nos. 926 and 927), the plastic front is discontinuous, but the low stress level
of Shot 922 yields a rather smooth stress variation. This is cited by Barker as
evidence of a strain-rate effect and is discussed later. The unloading portion
of the wave, not heretofore directly measured, exhibits considerable lack of
structure. This also has been partially attributed to a strain-rate effect. How-
ever, comparing predicted and observed results, it is evident that considerably
more release wave structure was predicted by some material models.

In order to obtain comparable experimental and theoretical results,
Barker found it necessary to postulate a pronounced Bauschinger effect for aluminum.
Two other material models did not include this effect. The simplified model,
identified as $Y = 2.4$ kbar model in Figure E-1 (i.e., a constant yield strength of
2.4 kbar), postulated no Bauschinger effect and no work hardening. Although the
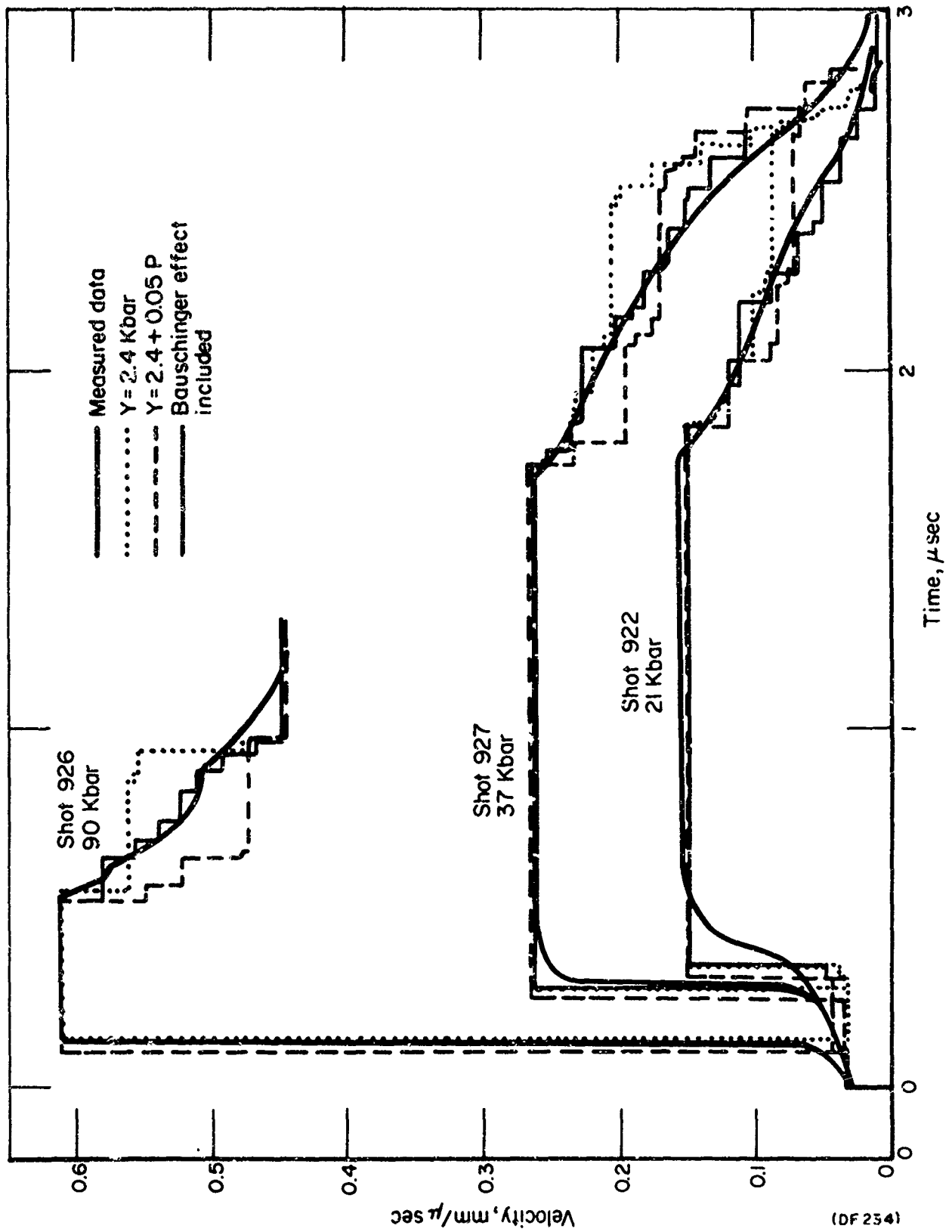loading behavior predicted by this model is as satisfactory as the more complicated

FIGURE E-1. MEASURED VELOCITY HISTORIES AND COMPARISONS WITH COMPUTER PREDICTIONS (E-9)

(DF 234)

models, considerable deviation from the observed data is predicted on unloading.
A second model, without a Bauschinger effect but including work hardening
(Y = 2.4 + 0.05P, P = hydrostatic stress), also has significant discrepancies in
the predicted unloading.

In order that the predicted release wave take on the observed form, it
was necessary for the rev · yield strength on unloading to be initially small,
then to increase--at first rapidly and later more slowly. This amounted to the
pronounced Bauschinger effect. The mathematical expression for this effect was
given by describing the tensile yield strength, Y_T, as a function of plastic
strain, ϵ_p, according to the form

$$Y_T = 4[1 - \exp(-800 \epsilon_p)]. \tag{E-9}$$

In addition, a work-hardening model, slightly different than the one previously
given, was used for the loading behavior. It was assumed that the compressive
yield strength increased from 2.4 kbar to 3.0 kbar. The resulting wave predic-
tion is shown as the dark line in Figure E-1. It is seen that considerably better
agreement between theory and test exists. Of course, the fine structure of the
predicted wave shape is a result of the numerical analysis which uses the method
of characteristics. This breaks a stress pulse into stress increments or steps,
as discussed in earlier sections of this report, and of necessity leads to a pre-
dicted wave shape possessing definite structure. The three stress-strain models
used are compared in Figure E-2.

By observing Figures E-2 and E-1, it is possible to assess, at least
qualitatively, the effect of uncertainty in the stress-strain curve on stress
pulse prediction. It is seen that all of the models accurately predict the maximum
stresses, and that at the highest stress level (Shot 926 of Figure E-1), all of
the models adequately predict the loading behavior in general. At the lower
stresses (particularly in Shot 922), discrepancies in the plastic shock front
occur, and these are thought to be due to strain-rate effects. Thus, at lowest
stress level, none of the models properly depict the nature of the plastic com-
pression front.

Considering the unloading portions of the various waves, it is seen that
significant discrepancies occur in the material models that do not contain
Bauschinger effects. Thus, fairly significant differences occur between measured
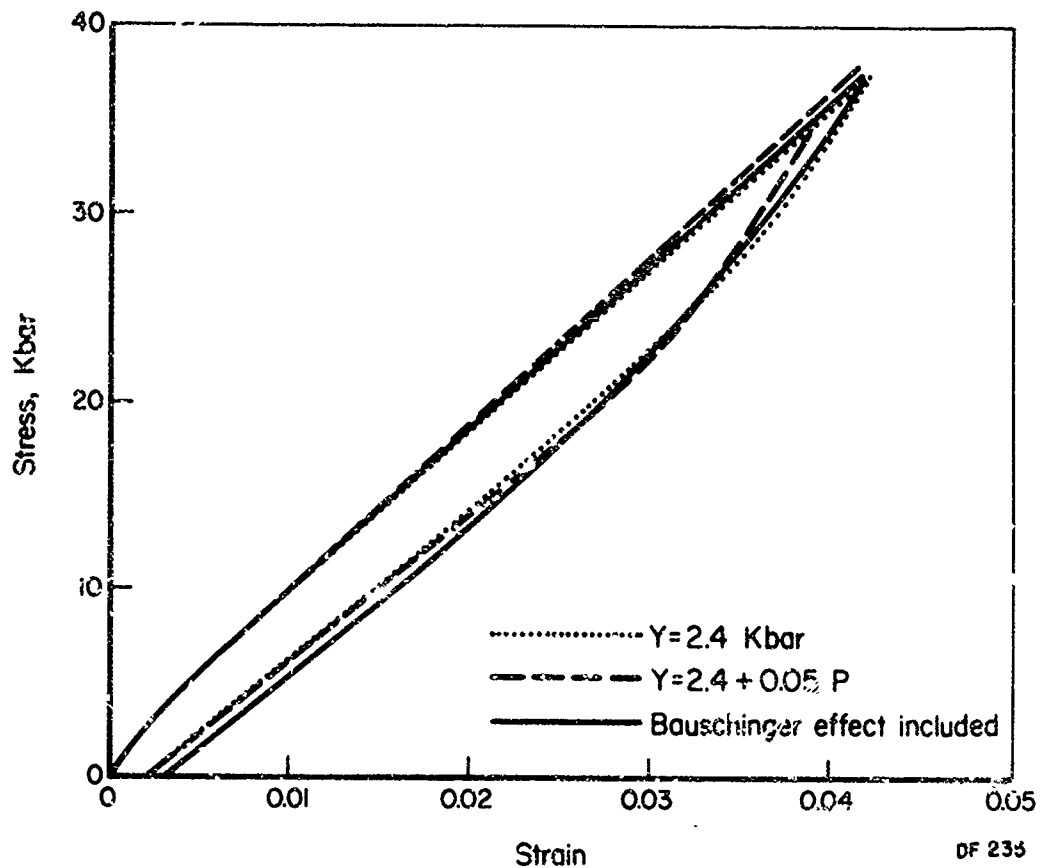
FIGURE E-2. LOADING AND UNLOADING STRESS-STRAIN PATHS
FOR SHOT 927 ACCORDING TO THREE MODELS OF
MATERIAL BEHAVIOR[E-9]

and predicted unloading at all three stress levels for the constant yield model
(Y = 2.4 kbar) and the work-hardening model (Y = 2.4 + 0.05 P). The inclusion
of the Bauschinger effect, in the manner indicated by Equation E-9, yields close
agreement between the predicted and measured results. Yet, referring to Figure
E-2, it is apparent that the percentage differences among all three models is
quite small. This suggests that the stress history within the material,
particularly the unloading history, is a sensitive function of the stress-strain
relation. Since the resultant spall-producing tensile wave is a result of inter-
action between unloading waves, it becomes important to have an accurate knowledge
of the unloading behavior of a material to be able to predict spall.

S :rain-Rate Effects

In the previous sections, some statements, at least qualitative, were possible on Bauschinger or work-hardening effects and material response. In fact, rather than actually assessing the effects, it was a matter of establishing the presence or absence of the effects by experimental methods and incorporating them into the resultant material constitutive relation. The situation is much less certain in the case of strain-rate effects. At present there is considerable controversy regarding the degree of strain-rate sensitivity of materials. More basic than this is the controversy aroused by the question of whether strain rate is even a parameter of the constitutive relation for some materials.

Nevertheless, it is a fact that wave-propagation experiments in rods and thick plates have yielded results, all details of which cannot be explained by a strain-rate independent theory. For example, in the review of elastic-plastic wave propagation (Appendix D), particularly the part referring to Figure D-25, it is indicated that sharply discontinuous plastic shock fronts are expected from a strain-rate-independent theory. However, Barker, et al,[E-1] have indicated that their experimental results were a consequence of stress waves having the general configuration shown in Figure E-3. Worthy of note in Figure E-3 is the lack of a sharp plastic front, with the strain gradually attaining its maximum value as though a relaxation process were operative. Referring also to Figure E-1, which showed Barker's results, it is evident that sharp discontinuities are absent, particularly at the lower loadings.
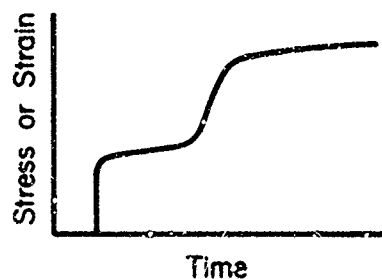

DF 236

FIGURE E-3. QUALITATIVE DRAWING OF A WAVE SHAPE WHICH INDUCED THE OBSERVED FREE SURFACE MOTION[E-1]

The presence of a strain-rate effect in terms of a general viscoplastic relaxation mechanism would tend to explain qualitatively the results obtained. This may be illustrated by considering a material that exhibits the characteristics

of a simple Voigt viscoelastic model, shown in Figure E-4. Thus, it is seen that the application of a sudden, step-function-type stress to the material would result in a delayed strain response, with the strain approaching its final value only gradually.
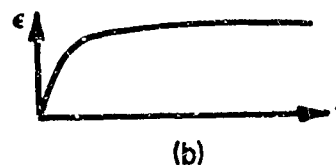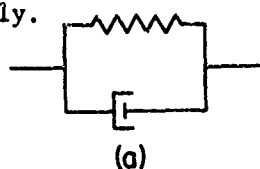
FIGURE E-4 (a). SIMPLE VOIGT VISCOELASTIC MODEL
(b). STRAIN RESPONSE TO STEP LOADING

Although certain experimental results indicate strain-rate sensitivity in materials, and the operation of certain viscoplastic mechanisms could account for some of the observations, considerable controversy still attaches to this subject. In fact, interest in this matter arose with the earliest developments of elastic-plastic theory by von Karman,[E-10] Taylor,[E-11] and Rakhmatulin.[E-12] Thus, these earlier developments pertained to a strain-rate-independent theory of elastic-plastic waves in rods and succeeded in predicting the essential features of such wave propagation, e.g., the existence and magnitude of an elastic precursor and the existence of a plateau of constant strain behind the wave front. The theory also predicted that superimposed stress increments would propagate at the plastic-wave velocity given by the local tangent modulus of the stress-strain curve. However, experiments by Bell[E-13] and others showed the increments to propagate at the elastic velocity. In addition, the theory failed to account f the increase in yield strength noted for some materials, such as iron, under dynamic loading.

In an effort to remove the apparent anomalies of the theory, Malvern[E-14], [E-15] developed a strain-rate-dependent theory where the basic constitutive equation took the form,

$$E\dot{\epsilon} = \dot{\sigma} + g(\sigma, \epsilon) ; \tag{E-10}$$

where ϵ is the total strain, σ is stress, and E is Young's modulus. The function $g(\sigma,\epsilon)$ is related to the plastic strain rate $\dot{\epsilon}_p$ by

$$E\dot{\epsilon}_p = g(\sigma,\epsilon) . \tag{E-11}$$

Although some of the anomalies were removed by this theory, the constant strain plateau predicted by the rate-independent theory and observed experimentally was not predicted by the rate-dependent theory.

In tne ensuing years, there have apparently developed "schools" of thinking regarding the sensitivity of materials to strain rate. Bell and his co-workers have been the principal proponents of the strain-rate-independent behavior of materials; Lindholm,[E-16] Malvern, and others have suggested that materials are strain-rate sensitive to one degree or another. Unfortunately, the experimental techniques used by the various investigators to arrive at their differing conclusions on dynamic materials properties have been different. Thus, the difficulty of assessing the importance of strain-rate effects is increased. Bell, for example, has utilized his unique diffraction grating technique for studying elastic-plastic wave propagation in long rods. Lindholm and others of the rate-dependent school have used the split Hopkinson bar method. Although members of each school have developed impressive arguments tending to show the experimental methods of the other school at fault, a definitive set of comparative experiments has not been conducted to settle this matter.

It has been suggested that, in fact, both schools may be correct--under the proper conditions. Dorn and Hauser[E-17] have postulated that, under proper conditions, certain materials may be essentially strain-rate independent; and other materials, under proper conditions, may be quite sensitive to rate effects. Of course, there exist intermediate regions of varying degrees of sensitivity. The factors differentiating the degrees of sensitivity were postulated to be the dislocation activation mechanisms. Thus, strain-rate-sensitive materials were postulated to be those whose dislocation mechanisms of deformation could be thermally activated, whereas rate insensitive materials had mechanisms that were athermally or stress activated.

Although the above postulation of intermediate position between the strain-rate schools certainly appears reasonable, the problem of establishing the physical classifications of materials, including the various subtle transition regions, has not yet been solved.

Accepting the existing uncertain state of affairs regarding strain-rate sensitivity of materials, it is instructive to consider the recent work of Butcher and Karnes[E-18] on strain-rate effects in metals. In their work, the strain-rate theory of Malvern was applied to the one-dimensional strain configuration of the

plate-slap experiment. Predicted stress-strain curves were determined and found to be more in accord with experimental results than rate-independent theory. Thus, the Malvern theory, which yielded some anomalous results in the one-dimensional stress application (no constant strain plateau), successfully predicted the essential features of the experimentally observed response in the one-dimensional strain situation. However, it was also pointed out by Butcher and Karnes that certain experimental factors, in particular a slight lack of planarity between the impacting plates, were capable of producing results resembling strain-rate effects. It was also indicated that increased distance of travel tended to decrease rate effects in the wave front, permitting the wave to be treated as essentially strain-rate independent. Although future study of strain-rate effects utilizing the plate-slap configuration will certainly be done, the general conclusions reached by Butcher and Karnes appeared to be that strain-rate effects were rather slight under plate-slap conditions and that, furthermore, the presence or plate tilt and propagation distance effects was capable of obscuring rate effects.

The basis for the relative insensitivity of the one-dimensional strain configuration (in comparison to the one-dimensional stress situation) to strain-rate effects has been discussed by Barker, et al. (E-1) In this configuration, the majority of the strain is dilatational and not deviatoric. However, it is the deviatoric, or shearing-type deformation, that causes dislocation motion and the consequent strain-rate effect. It follows that strain-rate effects will be considerably less significant in such configurations.

Despite the considerable research that has been directed toward ascertaining the sensitivity of materials to rate effects, it appears that material constitutive relations, including these effects and accounting for the various experimental observations, have not been established although many have been postulated. Thus, in contrast to the previously discussed Bauschinger and work-hardening effects, where explicit inclusion of these effects in the stress-strain relation became possible on the basis of experimental observations, similar developments have not been made in regard to rate effects.

Nevertheless, when one-dimensional strain considerations govern, it has been indicated in the previous discussion that strain-rate effects appear to be of little significance in predicting the essential features of the wave

propagation. Although, as is evident from Barker's work, some detail of the wave structure is lost, the essential features of the waves, such as stress amplitude, are predictable by a strain-rate-independent theory.

Finite Strain Effects

The final topic of discussion regarding various subsidiary effects pertains to the kinematic description of the deformation. The theoretical development of elastic-plastic theory reviewed in this report utilized a description of the Lagrangian strain as $\epsilon_x = \partial u / \partial x$. Such a representation is the infinitesimal strain definition and neglects quadratic terms in the displacement gradients. Yet, under plastic deformation, large strains may exist and, thus, may require the more accurate kinematical description of strain. Lee,[E-2] for example, has suggested the necessity of including finite strain effects in the theory, since strains of 25 percent are evidently obtained in some tests. The basis for using the infinitesimal definition should be reviewed.

If, in fact, strains of the magnitude indicated above were typical of those attained in the low pressure regions of interest in elastic-plastic theory, the question of finite strain effects would need to be examined with considerable care. However, such large strains are associated more often with pure hydrodynamic shock-type loading where extremely high pressures are attained, whereas, the stress regions of interest in elastic-plastic wave propagation are of the order 10-50 kbar, and the associated strains are 2-4 percent. Under these conditions, the squares of the displacement gradient are negligible compared to the displacement gradient. It might be noted further that, under strains greatly in excess of the 2-4 percent level, the differences in the principal stresses becomes quite small compared to the stresses themselves. Consequently, the elastic-plastic theory becomes little more than a small, superimposed correction to a hydrodynamic model of the material. Hence, where it becomes necessary to include the more complicated finite strain effects, a corresponding simplification may be made in the nature of the constitutive relation.

On the basis of qualitative arguments, it appears safe to neglect finite strain effects on the elastic-plastic wave propagation. It is instructive to explore this topic further to see if a more precise assessment may be attached

to finite strain effects. It should first be noted that, in general, when the deformation of a body becomes sufficiently large, it can no longer be suitably characterized in terms of either "engineering" or "true" strain. This is due to the fact that these measures of deformation are not inherently tensor quantities and are inappropriate for the establishment of a constitutive relationship that is to be independent of the choice of coordinates. In addition, if Lagrangian coordinates are being used, the Eulerian stress tensor of linear elasticity theory must be distinguished from and replaced by a Lagrangian or Kirchhoff stress tensor based on predeformation geometry.

For the case of wave propagation in uniaxial strain, there is no need to distinguish between Eulerian and Lagrangian normal-to-surface stresses. Also, as far as stress and displacement wave propagation is concerned, it makes no difference whether the dynamic stress-strain relationship is given in terms of the components of a finite strain tensor or engineering strain.

To see this, consider a material with dynamic stress versus finite-strain curve defined by

$$\sigma_x = \sigma_x(E) ; \tag{E-12}$$

where

σ_x = stress normal to the direction of wave propagation,

E = finite strain normal to the direction of wave propagation (the only nonzero component of the strain tensor).

Suppose, also, that the finite-strain component, E, and the engineering strain component, ϵ_x, are related by

$$E = E(\epsilon_x) ; \tag{E-13}$$

where ϵ_x is the previously defined infinitesimal strain, given by

$$\epsilon_x = \frac{\partial u}{\partial x} . \tag{E-14}$$

u = particle displacement in the direction of wave propagation,

x = Langrangian coordinate in the direction of wave propagation.

The expressions for conservation of mass and momentum are, respectively,

$$\rho_0 = \rho(1 + e_x), \quad \rho_0 \frac{\partial^2 u}{\partial t^2} = \frac{\partial \sigma_x}{\partial x} . \tag{E-15}$$

Now assuming continuous first derivatives,

$$\frac{\partial \sigma_x}{\partial x} = \frac{\partial \sigma_x}{\partial E} \frac{\partial E}{\partial x} = \frac{\partial \sigma_x}{\partial E} \frac{\partial E}{\partial \epsilon_x} \frac{\partial \epsilon_x}{\partial x} \quad . \tag{E-16}$$

However, $\dfrac{\partial \sigma_x}{\partial E} \dfrac{\partial E}{\partial \epsilon_x} = \dfrac{\partial \sigma_x}{\partial \epsilon_x}$, so that

$$\frac{\partial \sigma_x}{\partial x} = \frac{\partial \sigma_x}{\partial \epsilon_x} \frac{\partial \epsilon_x}{\partial x} = \frac{\partial \sigma_x}{\partial \epsilon_x} \frac{\partial^2 u}{\partial x^2} \quad . \tag{E-17}$$

Consequently, the governing equation reduces to that which would be obtained if only engineering strain were considered, i.e.,

$$\frac{\partial^2 u}{\partial t^2} = c^2 \frac{\partial^2 u}{\partial x^2} \quad ; \tag{E-18}$$

where

$$c^2 = \frac{1}{\rho_o} \frac{\partial \sigma_x}{\partial e} \quad . \tag{E-19}$$

Thus, while the stress versus finite-strain and stress versus engineering-strain relationships may be of entirely different form, the spatial derivative of σ_x and, hence, the governing equation of motion is unchanged.

In order to illustrate the above comments further, it will be instructive to consider wave propagation in two rather ideal materials. For the purpose of this discussion, the Lagrangian strain tensor will be used. The only nonvanishing component of this tensor will be E, the strain normal to the direction of wave propagation. For uniaxial strain,

$$E = \epsilon_x + \frac{1}{2} \epsilon_x^2 = \frac{\partial u}{\partial x} + \frac{1}{2} \left(\frac{\partial u}{\partial x}\right)^2 \quad . \tag{E-20}$$

First, consider a material that is linearly elastic with respect to engineering strain, ϵ_x; i.e.,

$$\sigma_x = K^* \epsilon_x \quad , \tag{E-21}$$

where K* is the effective dynamic modulus in uniaxial strain. Expressing ϵ_x in terms of E gives

$$\epsilon_x = +\sqrt{1 + 2E} - 1, \quad (\epsilon_x > -1, \ E > -1/2). \tag{E-22}$$

The stress versus finite-strain relationship becomes

$$\sigma_x = K^* \left(+\sqrt{1 + 2E} - 1\right). \tag{E-23}$$

Now

$$\frac{\partial \sigma_x}{\partial E} = + \frac{K*}{\sqrt{1 + 2E}} = + \frac{K*}{1+\epsilon_x} \qquad \text{(E-24)}$$

and

$$\frac{\partial E}{\partial x} = \frac{\partial^2 u}{\partial x^2} + \left(\frac{\partial u}{\partial x}\right) \frac{\partial^2 u}{\partial x^2} = (1 + \epsilon_x) \frac{\partial^2 u}{\partial x^2} . \qquad \text{(E-25)}$$

Hence,

$$\frac{\partial \sigma_x}{\partial x} = \frac{\partial \sigma_x}{\partial E} \frac{\partial E}{\partial x} = \frac{K*}{(1+\epsilon_x)} (1 + \epsilon_x) \frac{\partial^2 u}{\partial x^2} = K* \frac{\partial^2 u}{\partial x^2} . \qquad \text{(E-26)}$$

Thus, the equation of motion is the same as it would have been if finite strain were not considered, i.e.,

$$\frac{\partial^2 u}{\partial t^2} = c^2 \frac{\partial^2 u}{\partial x^2}, \quad c^2 = \frac{K*}{\rho_0} . \qquad \text{(E-27)}$$

Now consider a material that is linearly elastic with respect to finite strain. Rubber-like materials can often be described in this way. Let the stress versus finite-strain relationship be given by

$$\sigma_x = \overline{K} E , \qquad \text{(E-28)}$$

where $\overline{K}$ is an effective dynamic modulus in uniaxial strain. Now

$$\frac{\partial \sigma_x}{\partial x} = \overline{K} \frac{\partial E}{\partial x} = \overline{K} (1 + \epsilon_x) \frac{\partial^2 u}{\partial x^2} , \qquad \text{(E-29)}$$

and the equation of motion becomes

$$\frac{\partial^2 u}{\partial t^2} = c^2 \frac{\partial^2 u}{\partial x^2} , \qquad \text{(E-30)}$$

where

$$c^2 = \frac{\overline{K} (1 + \epsilon_x)}{\rho_0} = \frac{\overline{K}}{\rho} . \qquad \text{(E-31)}$$

The interesting and perhaps surprising result is that, in this type of material, large tensile disturbances propagate at a higher velocity than small tensile disturbances, and large compressive disturbances propagate at a lower velocity than small compressive disturbances. Such behavior has even been

observed experimentally. Kolsky,[E-19] for example, reports that the propagation velocity of small tensile pulses in neoprene filaments increased by a factor of ten when the filament was prestretched to six times its original length.

This behavior is not so surprising if it is realized that a material, linearly elastic with respect to finite strain, is not linear with respect to engineering strain. Using the Lagrangian definition of finite strain, the stress-engineering-strain curve would have the parabolic form shown in Figure E-5. The "sound" speed for a material with this type of stress-engineering-strain relationship is given by

$$c^2 = \frac{1}{\rho_0} \frac{\partial \sigma_x}{\partial \epsilon_x} = \frac{\overline{K}(1 + \epsilon_x)}{\rho_0} . \tag{E-32}$$

This is identical to the sound speed obtained previously with the stress-finite-strain relationship (Equation E-31).

$$\sigma = \overline{K}E = \overline{K}\left(e + \tfrac{1}{2} e^2\right)$$
$$\sigma = \overline{K}e$$
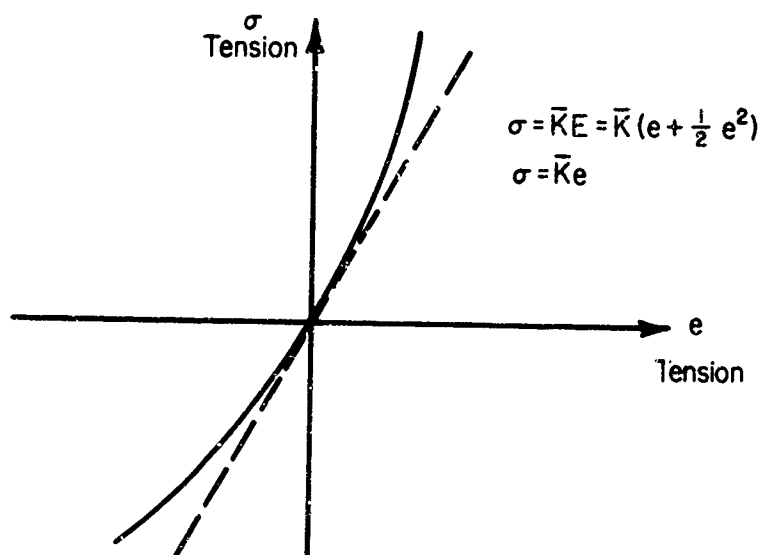
DF 238

FIGURE E-5. NONLINEAR AND ENGINEERING
STRESS-STRAIN CURVES

From the discussion above, it may then be concluded that if the stress versus engineering-strain relationship for uniaxial strain is known, there is no need to add a finite strain correction for large values of strain since the equation governing displacements would be unchanged. The magnitude or amplitude of the strain pulse, however, does change according to how strain is defined; i.e., the Lagrangian strains are always larger than the engineering strains. But these quantities are not generally of interest. It should perhaps also be emphasized

that the magnitude of the stress pulse does not change. Since the use of a stress
finite-strain relationship was shown to have no effect on the equation governing
displacement wave propagation, application of the Rankine-Hugoniot jump conditions
to determine stress from shock and particle velocity measurements would be no less
valid than it was when only engineering strain was considered. Thus, although
$E(x,t) \neq \epsilon_x(x,t)$, the stress calculated as a function of E and the stress
calculated as a function of ϵ_x are equal because of the different moduli involved.

APPENDIX E

REFERENCES

E-1. Barker, L. M., Lundergan, C. D. and Herrmann, W., "Dynamic Response of Aluminum", Journal of Applied Physics, Vol. 35, No. 4, pp. 1203-1212 (1964).

E-2. Lee, E. H., "Elastic-Plastic Waves of One-Dimensional Strain", Proceedings Fifth U. S. National Congress of Applied Mechanics, pp. 405-420 (1965).

E-3. Morland, L. W., "The Propagation of Plane Irrational Waves Through an Elasto-Plastic Medium", Phil. Trans. of Roy. Soc. of London, Series A, Vol. 251, p. 341 (1959).

E-4. Taylor, G. I. and Farren, W. S., "The Heat Developed During Plastic Extension of Metals", Proc. Roy. Soc. of London, Series A, Vol. 107, p. 422 (1925).

E-5. Lee, E. H. and Liu, D. T., "Finite-Strain Elastic-Plastic Theory with Applications to Plane-Wave Analysis", Journal of Applied Physics, Vol. 38, No. 1, pp. 19-27 (1967).

E-6. Lee, E. H. and Wierzbicki, T., "Analysis of the Propagation of Plane Elastic-Plastic Waves at Finite Strain", Journal of Applied Mechanics, pp. 931-936 (December 1967).

E-7. Butcher, B. M. and Canon, J. R., "Influence of Work-Hardening on the Dynamic Stress-Strain Curves of 4340 Steel", AIAA Journal, Vol. 2, pp. 2174-2179 (1964).

E-8. Karnes, C. H., "The Plate Impact Configuration for Determining Mechanical Properties of Materials at High Strain Rates", paper presented at Symposium on the Mechanical Behavior of Materials Under Dynamic Loads, San Antonio, Texas (1967).

E-9. Barker, L. M., "Fine Structure of Compressive and Release Wave Shapes in Aluminum Measured by the Velocity Interferometer Technique", paper presented at Symposium on High Dynamic Pressure, Paris, France (September 11-15, 1967).

E-10. von Karman, T., "On the Propagation of Plastic Deformation in Solids", NDRC Report No. A-29, OSRD No. 3651, 1942.

E-11. The Scientific Papers of G. I. Taylor, Volume 1 - Mechanics of Solids, Edited by G. K. Batchelor, Cambridge University Press, New York (1958), "The Plastic Wave in a Wire Extended by an Impact Load", (Taylor, G. I.), pp. 467-479.

REFERENCES (Continued)

E-12. Rakhmatulin, Kh. A., "On Propagation of the Unloading Wave", Prik. Mat. i Mek., Vol. 9, pp. 91-100 (1945).

E-13. Behavior of Materials Under Dynamic Loading, American Society of Mechanical Engineers, New York (1965), "The Dynamic Plasticity of Metals at High Strain Rates: An Experimental Generalization", (Bell, J. F.), pp. 19-41.

E-14. Malvern, L. E., "Plastic Wave Propagation in a Bar of Material Exhibiting a Strain-Rate Effect", Quart. Appl. Math., Vol. 8, p. 405 (1951).

E-15. Malvern, L. E., "The Propagation of Longitudinal Waves of Plastic Deformation in a Bar of Material Exhibiting a Strain-Rate Effect", Journal of Applied Mechanics, Vol. 18, pp. 203-208 (1951).

E-16. Behavior of Materials Under Dynamic Loading, American Society of Mechanical Engineers, New York (1965), "Dynamic Deformation of Metals", (Lindholm, U. S.), pp. 42-61.

E-17. Dorn, J. E. and Hauser, F. E., "Dislocation Concepts of Strain-Rate Effects", paper presented at Symposium on Structural Dynamics Under High Impulsive Loading, Dayton, Ohio (1962), pp. 175-202.

E-18. Butcher, B. M. and Karnes, C. H., "Strain-Rate Effects in Metals", Journal of Applied Physics, Vol. 37, No. 1, p. 402 (1966).

E-19. Proceedings of the Fifth National Congress of Applied Mechanics, American Society of Mechanical Engineers, New York (1966), "Experimental Studies in Stress Wave Propagation", (Kolsky, H.).

DOCUMENT CONTROL DATA - R&D

(Security classification of title, body of abstract and indexing annotation must be entered when the overall report is classified)

1 ORIGINATING ACTIVITY (Corporate author)	2a REPORT SECURITY CLASSIFICATION
Battelle Memorial Institute	Unclassified
Columbus Laboratories	2b GROUP
Columbus, Ohio 43201	

3 REPORT TITLE

Spall Fracture and Dynamic Response of Materials

4. DESCRIPTIVE NOTES (Type of report and inclusive dates)

Summary Report

5. AUTHOR(S) (Last name, first name, initial)

Oscarson, John H., and Graff, Karl F.

6. REPORT DATE	7a. TOTAL NO OF PAGES	7b. NO. OF REFS
March 21, 1968	115	63

8a CONTRACT OR GRANT NO.	9a. ORIGINATOR'S REPORT NUMBER(S)
DA-49-083 OSA-3176	BAT-197A-4-3
b. PROJECT NO.	
c.	9b. OTHER REPORT NO(S) (Any other numbers that may be assigned this report)
d.	

10. AVAILABILITY/LIMITATION NOTICES

Distribution of this document is unlimited.

11. SUPPLEMENTARY NOTES	12 SPONSORING MILITARY ACTIVITY
	Advanced Research Projects Agency
	Department of Defense
	Washington, D. C. 20301

13. ABSTRACT

This report describes the time-dependent fracture, or spalling, of materials as a result of dynamic response to shock-wave or impulse loading. From stress-wave and fracture-mechanics theory and assuming knowledge of the dynamic properties of the material, theories are developed to predict the stress at the spall plane. The cumulative, energy, stress-rate, and bond-breaking models for the prediction of spall fracture are described, along with the basic criteria of each model.

	LINK A		LINK B		LINK C	
	ROLE	WT	ROLE	WT	ROLE	WT
fracture	8,7		0			
spall, spalling	8,7		0			
dynamic	0					
shock wave	0,10,6					
impulse	0					
loading	10,6					
stress wave			0			
fracture mechanics			0			
model			8,10,9			
stress rate			0			
bond-breaking			0			
computation, calculation			8			
stress			2			